STUDY OF VORTICITY, DIRECTED FLOW AND FREEZE-OUT IN HEAVY-ION COLLISIONS AT ENERGIES OF NICA
18-02-40085

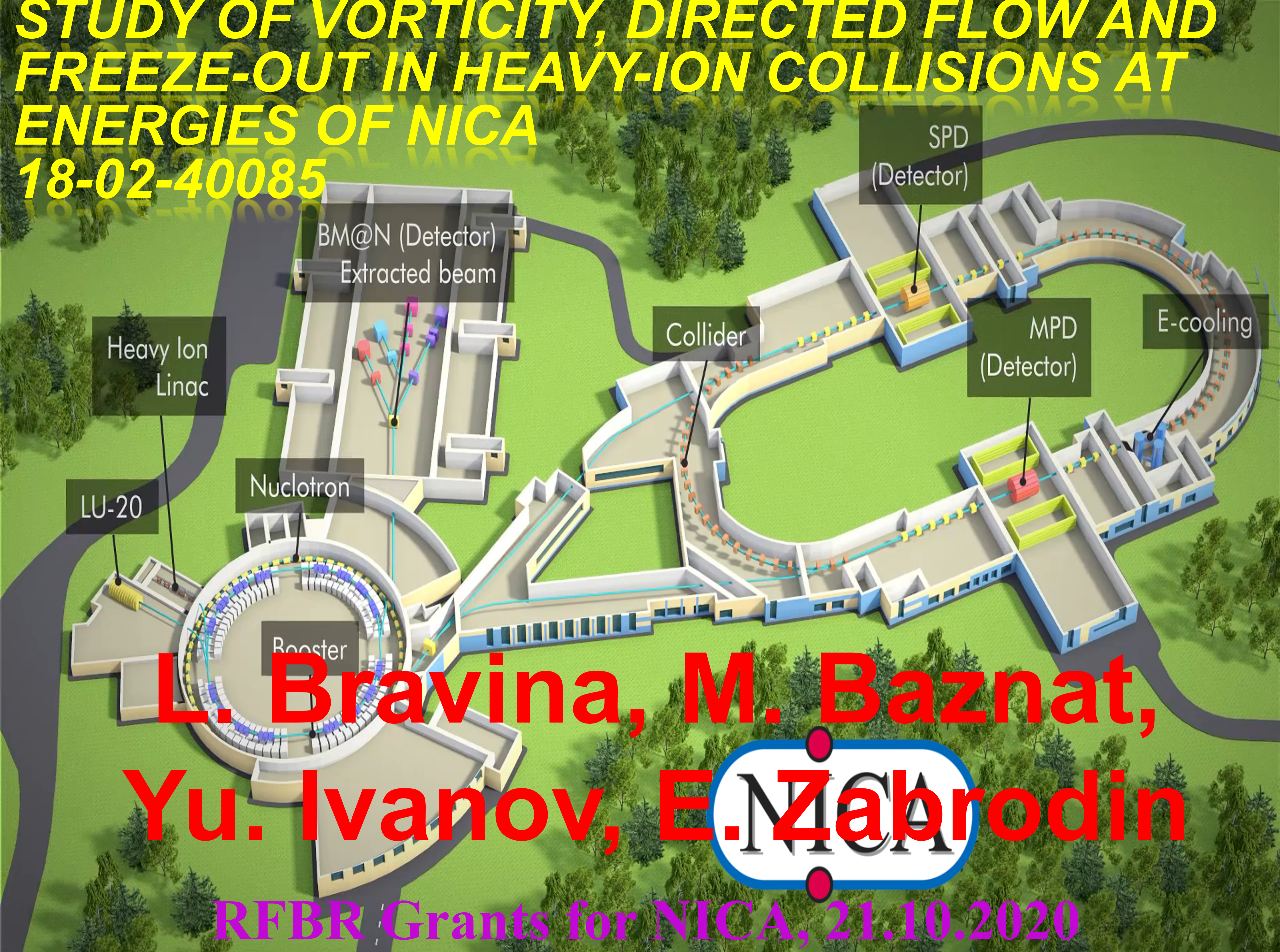

L. Bravina, M. Baznat,
Yu. Ivanov, E. Zabrodin

RFBR Grants for NICA, 21.10.2020

Outline

I. Motivation

II. Freeze-out of main hadron species

Chemical and Thermal

III. Spatial separation of different spieces :

- in Thermal Model predictions of yields
- directed flow for different particles
- Thermal Vorticity
- in Lambda-anti Lambda polarization

IV. Spacial Freeze-out and R_{long}, R_{site} and R_{out}

V. 3FD-Hydro and Polarization

See more in the talk of Yu. Ivanov, 22.10.2020

VI. Results

Dynamic Regimes

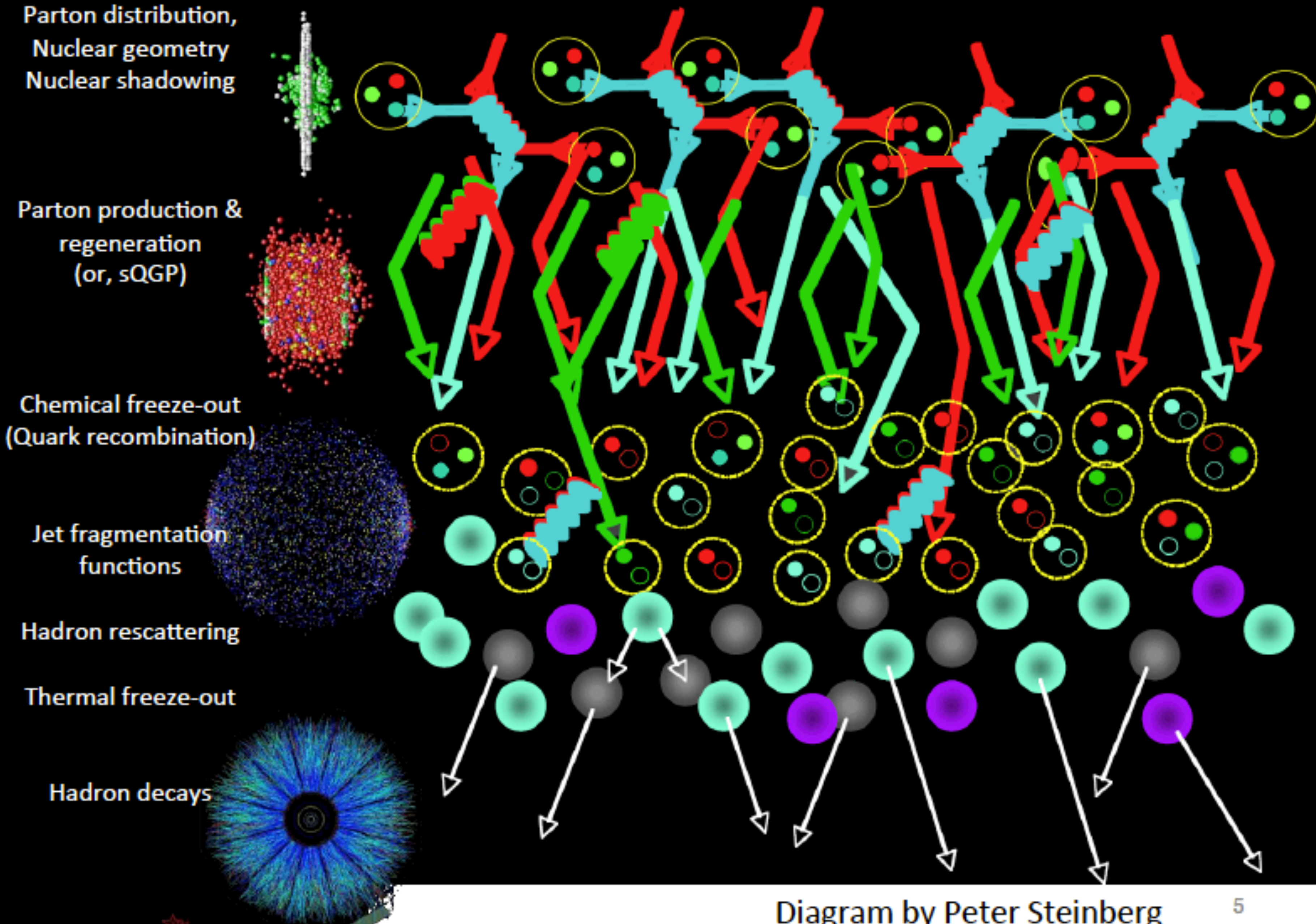

Diagram by Peter Steinberg

Motivation

1. Flavor dependent Freeze-out temperatures in A+A collisions at RHIC and LHC
In the crossover region of QCD phase diagram.
F.A. Flor, G. Olinger, R. Bellwied ArXiv: 2009.14781
T_u,d = 150 MeV, T_s= 165 MeV

2. Tom Reichert, Gabriele Inghirami and Marcus Bleicher :
Probing chemical freeze-out criteria in relativistic
nuclear collisions with coarse grained transport simulations EPJ (2020)
arXiv:2007.06440 The average chemical break-up time remains constant
at t ≈ 7 fm above √sNN = 7.7 GeV

3. Gabriele Inghirami, Paula Hillmann, Boris Tomášik, Marcus Bleicher
Temperatures and chemical potentials at kinetic freeze-out in relativistic heavy
ion collisions from coarse grained transport simulations arXiv:1909.00643

Motivation

1. Flavor dependent Freeze-out temperatur
In the crossover region of QCD phase diagra
F.A.Flor, G.Olinger, R Bellwied ArXiv: 2009.1
T u,d = 150 MeV, T s= 165 MeV

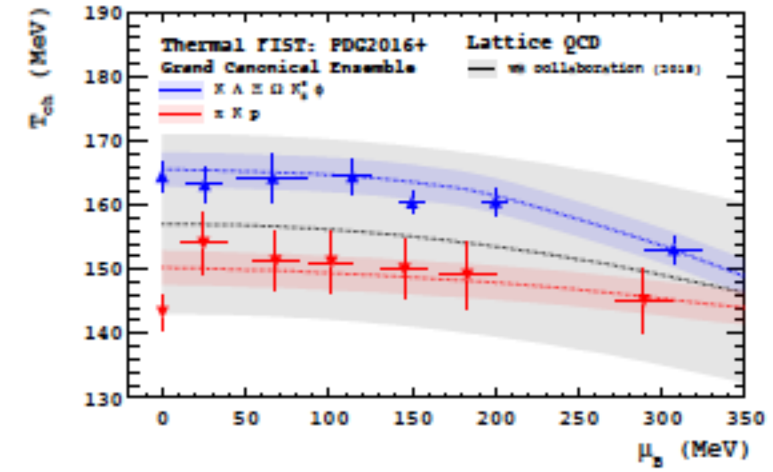

FIG. 2: *Strange* (blue points) and *light* (red points) GCE fits to STAR and ALICE data measured at collision energies ranging from $\sqrt{s_{NN}}$ = 11.5 GeV to 5.02 TeV (0 - 10%) via The FIST using the PDG2016+ hadronic spectrum.

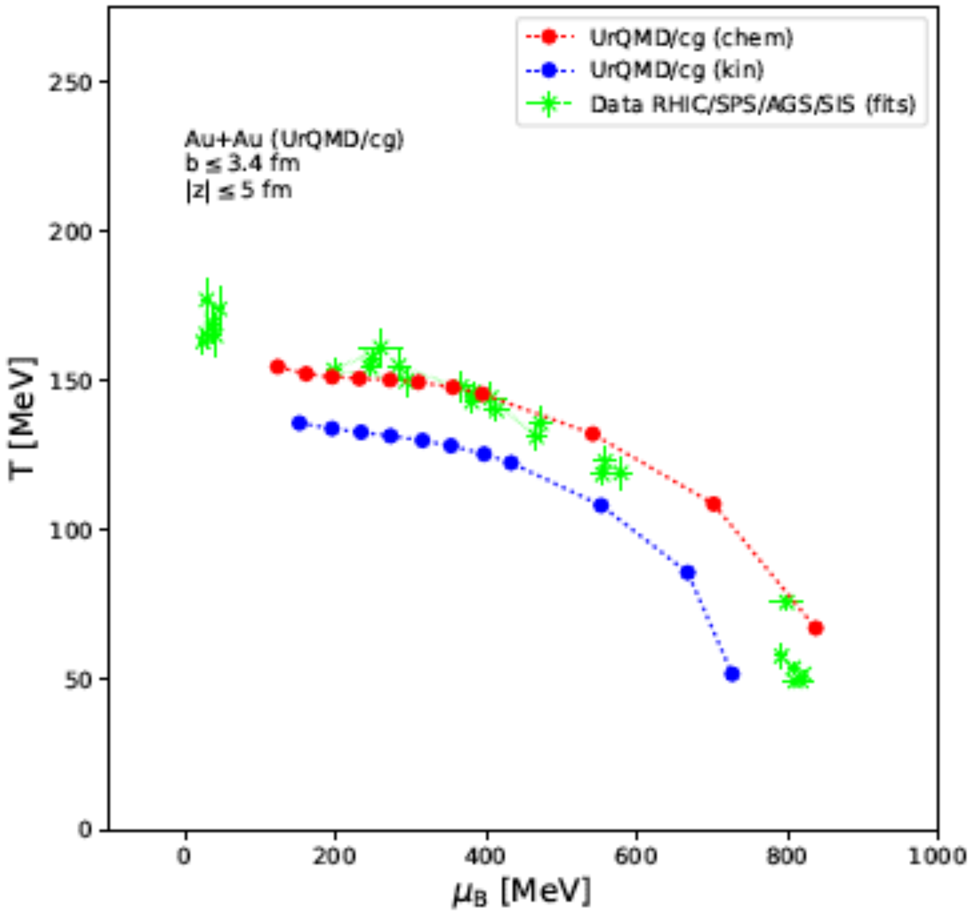

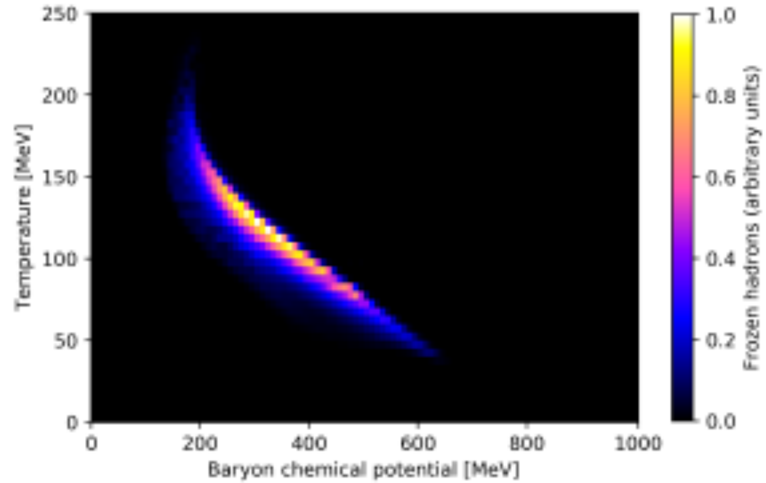

Figure 12. (Color online) Profile of the kinetic freeze-out temperature and baryon chemical potential at $|y| < 0.2$ for Au+Au collisions at $\sqrt{s_{NN}} = 19.6$ GeV.

Motivation

Au+Au at $E_{lab} = 40$A GeV and $b = 0$ fm within UrQMD

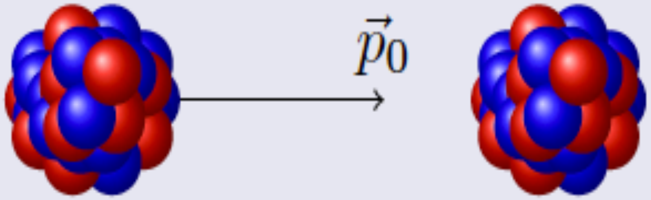

- To do the analysis of the spatio-temporal evolution of all particles in the $T - \mu_B$, $T - \mu_S$ plane and the analysis of the finally emitted particles in $x - t$ plane.
- See the spatial separation of strange particles from non strange (and of mesons from baryons).
- Find average T, μ_B, μ_S of different particles at freeze-out time.

Identified hadron yields

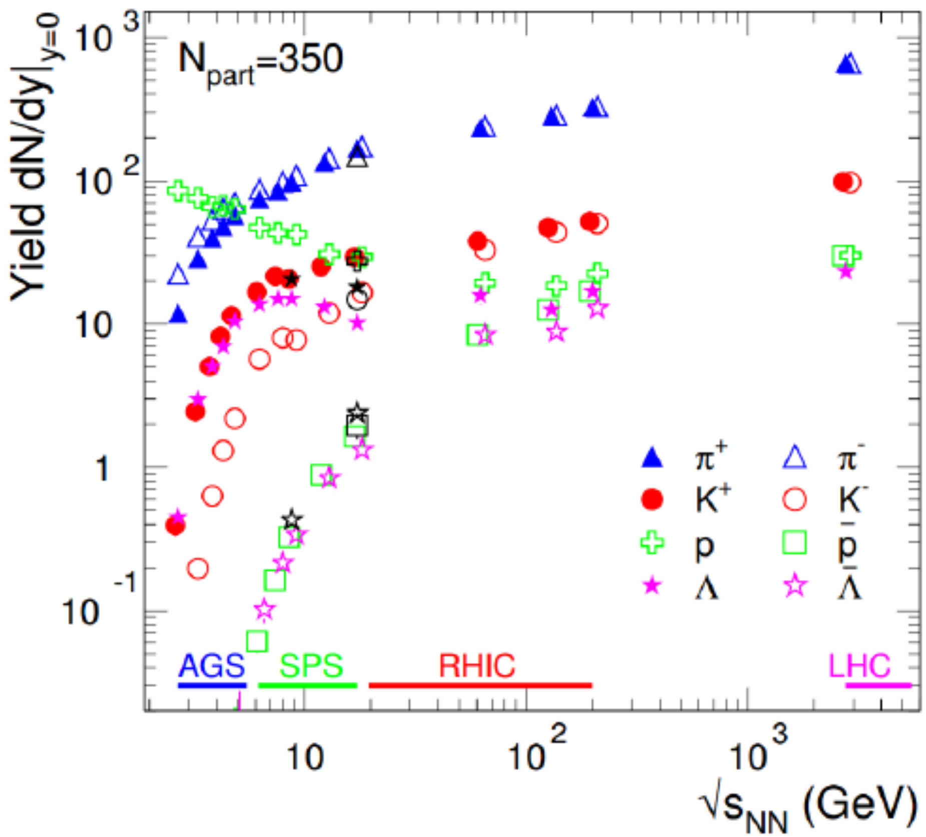

- Lots of particles, most newly created from the excited gluon fields ($E=mc^2$)
- Large variety of species:

  $\pi^\pm(u\bar{d},d\bar{u})$, m=140 MeV

  $K^\pm(u\bar{s},s\bar{u})$, m=494 MeV

  p(uud), m=938 MeV

  Λ(uds), m=1116 MeV

  also: Ξ(dss), Ω(sss), …
- Abundancies follow mass hierarchy, except at low energies where remnants from the incoming nuclei are significant
- What do we learn?

Grand Canonical Ensemble

$$\ln Z_i = \frac{V g_i}{2\pi^2} \int_0^\infty \pm p^2 dp \ln(1 \pm \exp(-(E_i - \mu_i)/T))$$

$$n_i = N/V = -\frac{T}{V}\frac{\partial \ln Z_i}{\partial \mu} = \frac{g_i}{2\pi^2} \int_0^\infty \frac{p^2 \, dp}{\exp((E_i - \mu_i)/T) \pm 1}$$

$$\mu_i = \mu_B B_i + \mu_S S_i + \mu_{I_3} I_i^3$$

for every conserved quantum number there is a chemical potential μ
but can use conservation laws to constrain:

- Baryon number: $V \sum_i n_i B_i = Z + N \quad \rightarrow V$
- Strangeness: $V \sum_i n_i S_i = 0 \quad \rightarrow \mu_S$
- Charge: $V \sum_i n_i I_i^3 = \frac{Z - N}{2} \quad \rightarrow \mu_{I_3}$

This leaves only μ_b and T as free parameter when 4π considered

for rapidity slice fix volume e.g. by dN_{ch}/dy

Fit at each energy provides values for T and μ_b

Chemical freeze-out

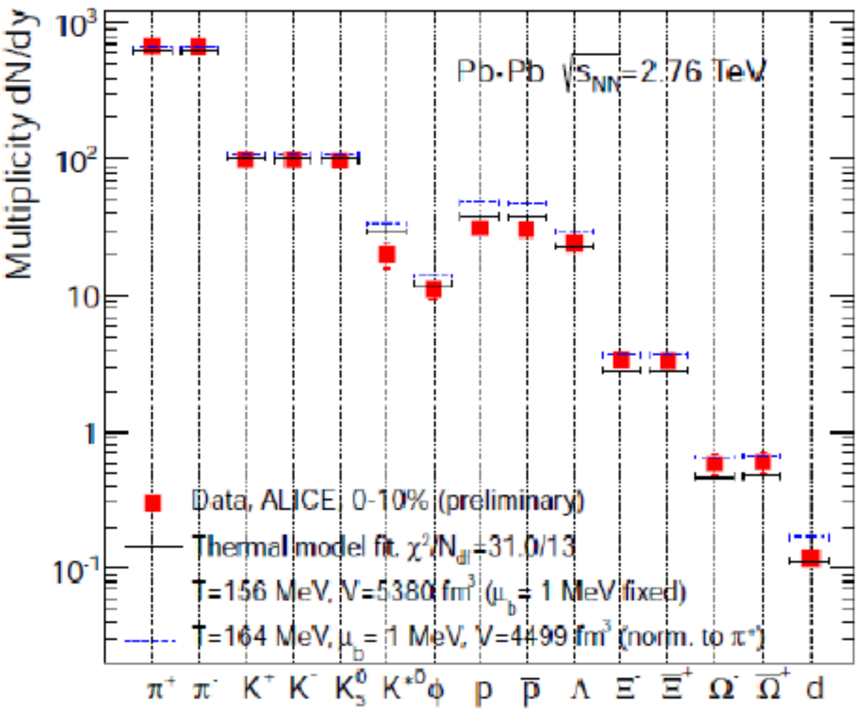

- Thermal fits of hadron abundancies:

$$n_i = N_i/V = -\frac{T}{V}\frac{\partial \ln Z_i}{\partial \mu} = \frac{g_i}{2\pi^2}\int_0^\infty \frac{p^2 \mathrm{d}p}{\exp[(E_i-\mu_i)/T] \pm 1}$$

- Quantum numbers conservation

  $\mu=\mu_B B+\mu_{I3} I_3+\mu_S S+\mu_C C$

- Hadron yields N_i can be obtained using only 3 parameters: (T_{chem}, μ_B, V)

- The hadron abundancies are in agreement with a thermally equilibrated system

  T_{chem}=155-165 MeV

  μ_B~0

Central cell:

Relaxation to (local) equilibrium

Equilibration in the Central Cell

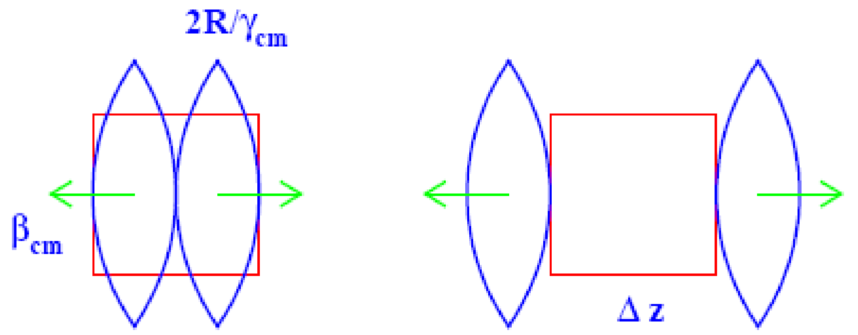

$t^{cross} = 2R/(\gamma_{cm}\,\beta_{cm})$ $\qquad$ $t^{eq} \geq t^{cross} + \Delta z/(2\beta_{cm})$

Kinetic equilibrium:

Isotropy of velocity distributions

Isotropy of pressure

Thermal equilibrium:

Energy spectra of particles are described by Boltzmann distribution

L.Bravina et al., PLB 434 (1998) 379; JPG 25 (1999) 351

$$\frac{dN_i}{4\pi p E dE} = \frac{V g_i}{(2\pi\hbar)^3} \exp\left(\frac{\mu_i}{T}\right) \exp\left(-\frac{E_i}{T}\right)$$

Chemical equlibrium:

Particle yields are reproduced by SM with the same values of $(T,\ \mu_B,\ \mu_S)$:

$$N_i = \frac{V g_i}{2\pi^2\hbar^3} \int_0^\infty p^2 dp \exp\left(\frac{\mu_i}{T}\right) \exp\left(-\frac{E_i}{T}\right)$$

Statistical model of ideal hadron gas

input values output values

$$\varepsilon^{\mathrm{mic}} = \frac{1}{V}\sum_i E_i^{\mathrm{SM}}(T,\mu_{\mathrm{B}},\mu_{\mathrm{S}}),$$

$$\rho_{\mathrm{B}}^{\mathrm{mic}} = \frac{1}{V}\sum_i B_i \cdot N_i^{\mathrm{SM}}(T,\mu_{\mathrm{B}},\mu_{\mathrm{S}}),$$

$$\rho_{\mathrm{S}}^{\mathrm{mic}} = \frac{1}{V}\sum_i S_i \cdot N_i^{\mathrm{SM}}(T,\mu_{\mathrm{B}},\mu_{\mathrm{S}}).$$

Multiplicity

$$N_i^{\mathrm{SM}} = \frac{V g_i}{2\pi^2\hbar^3}\int_0^\infty p^2 f(p,m_i)dp,$$

Energy

$$E_i^{\mathrm{SM}} = \frac{V g_i}{2\pi^2\hbar^3}\int_0^\infty p^2\sqrt{p^2+m_i^2}\, f(p,m_i)dp$$

Pressure

$$P^{\mathrm{SM}} = \sum_i \frac{g_i}{2\pi^2\hbar^3}\int_0^\infty p^2 \frac{p^2}{3(p^2+m_i^2)^{1/2}}\, f(p,m_i)dp$$

Entropy density

$$s^{\mathrm{SM}} = -\sum_i \frac{g_i}{2\pi^2\hbar^3}\int_0^\infty f(p,m_i)\,\left[\ln f(p,m_i)-1\right]\, p^2 dp$$

Kinetic Equilibrium

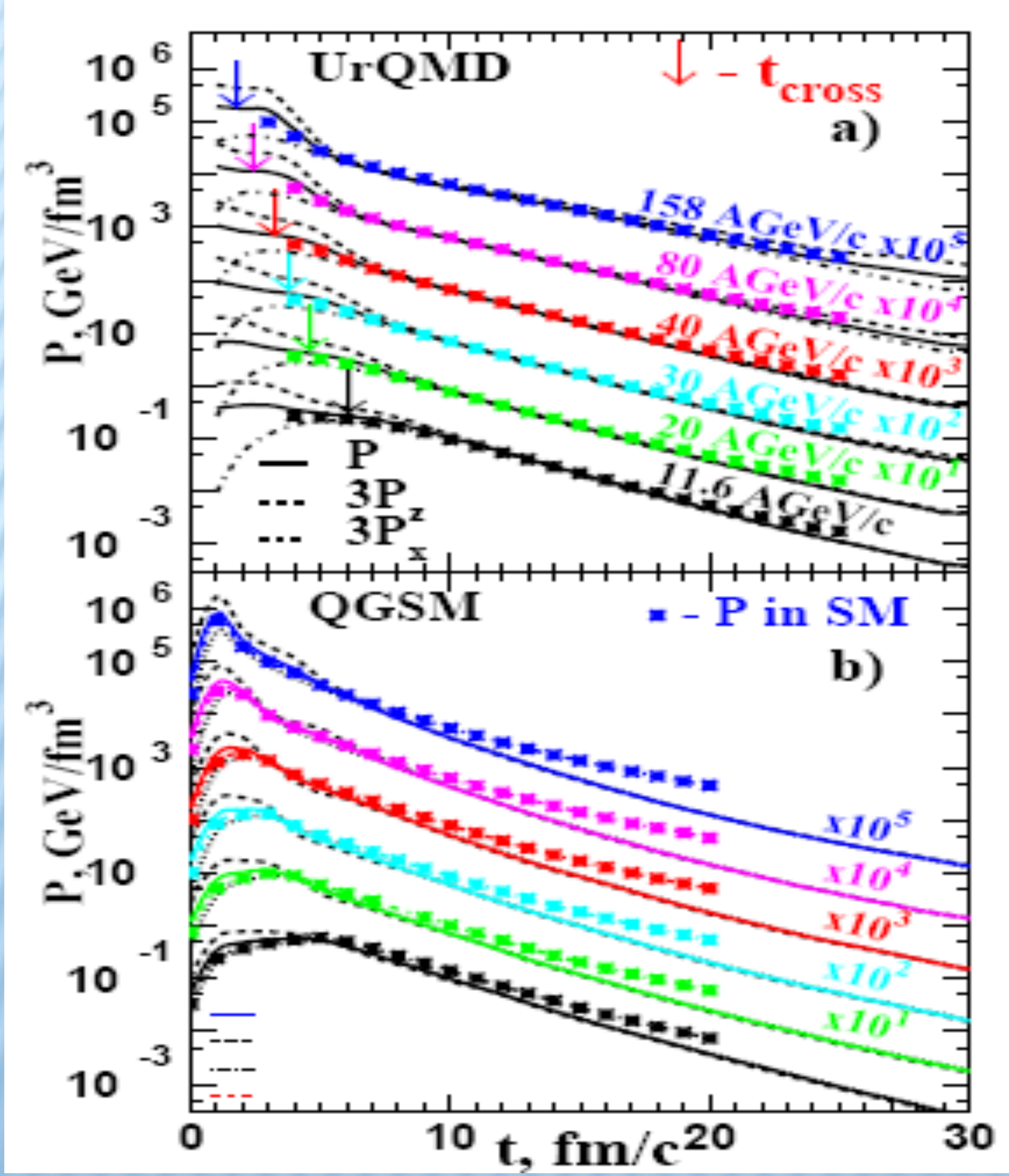

Isotropy of pressure

L.Bravina et al., PRC 78 (2008) 014907

Pressure becomes isotropic for all energies from 11.6 AGeV to 158 AGeV

NEGATIVE NET STRANGENESS DENSITY

Net strangeness density in the central cell at 11 to 80 AGeV

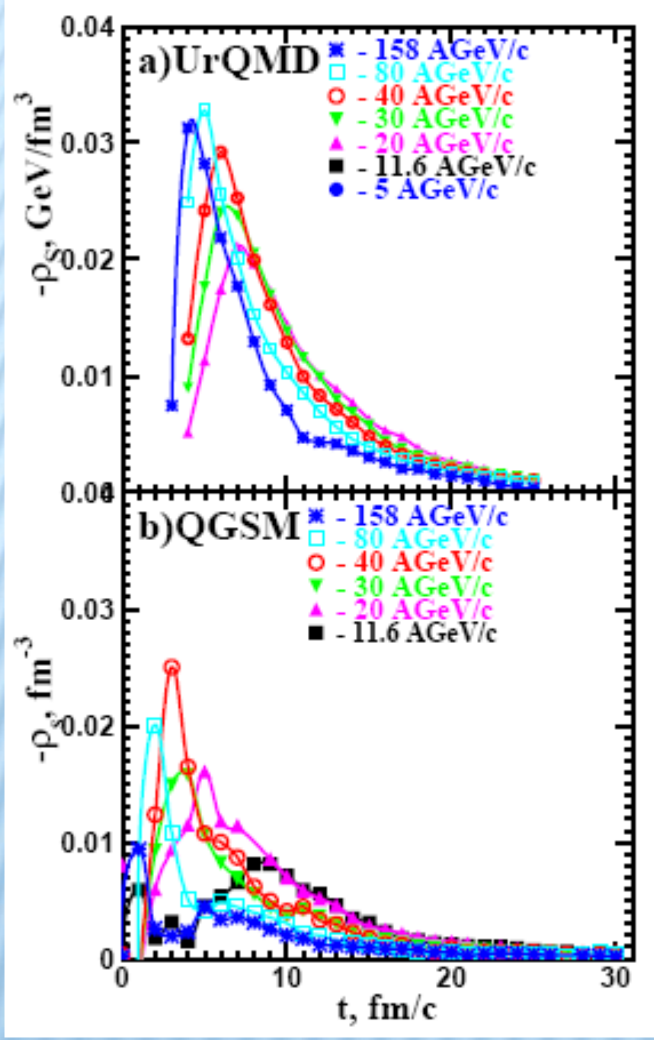

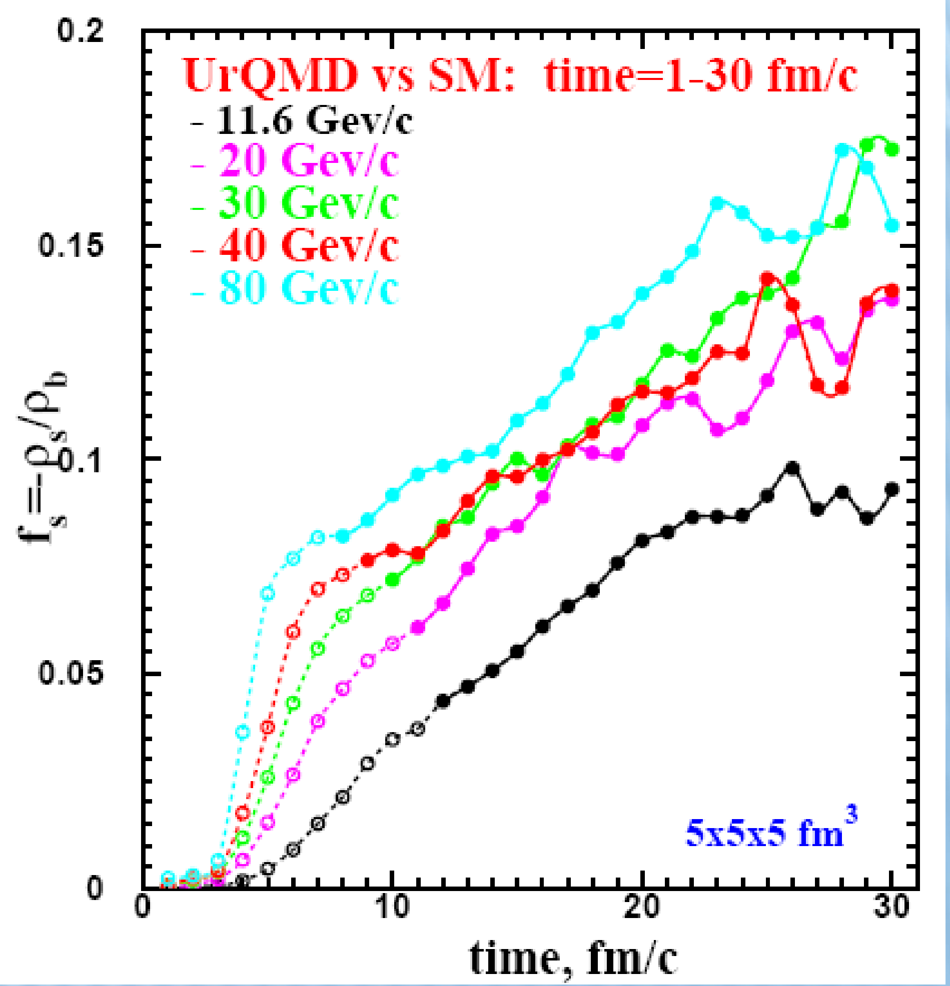

Net strangeness in the cell is negative because of different interaction cross sections for Kaons and antiKaons with Baryons

THERMAL AND CHEMICAL EQUILIBRIUM

Boltzmann fit to the energy spectra

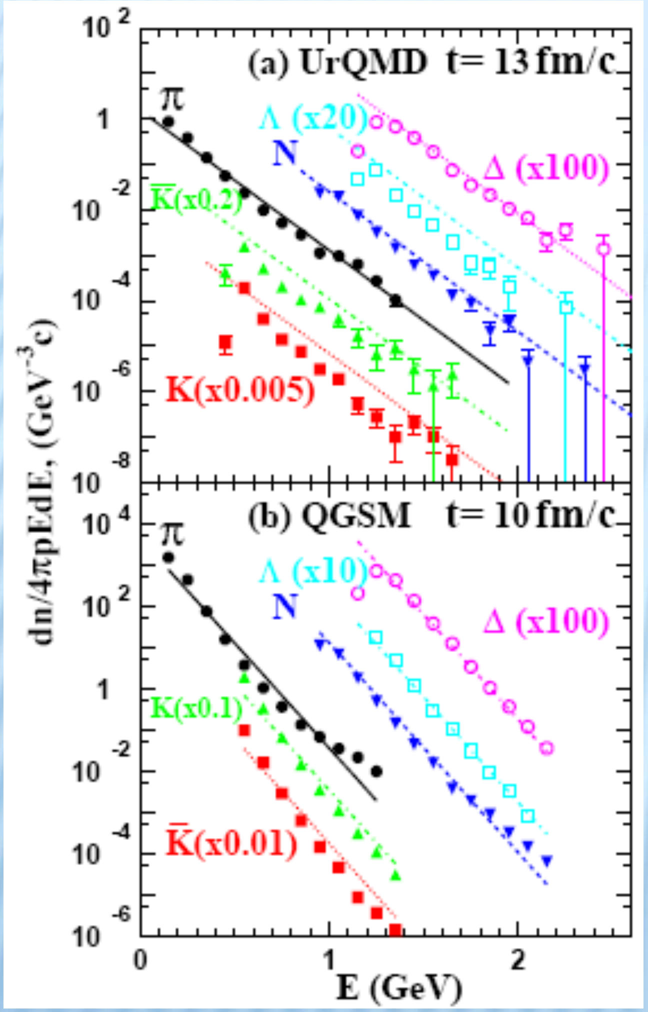

Particle yields

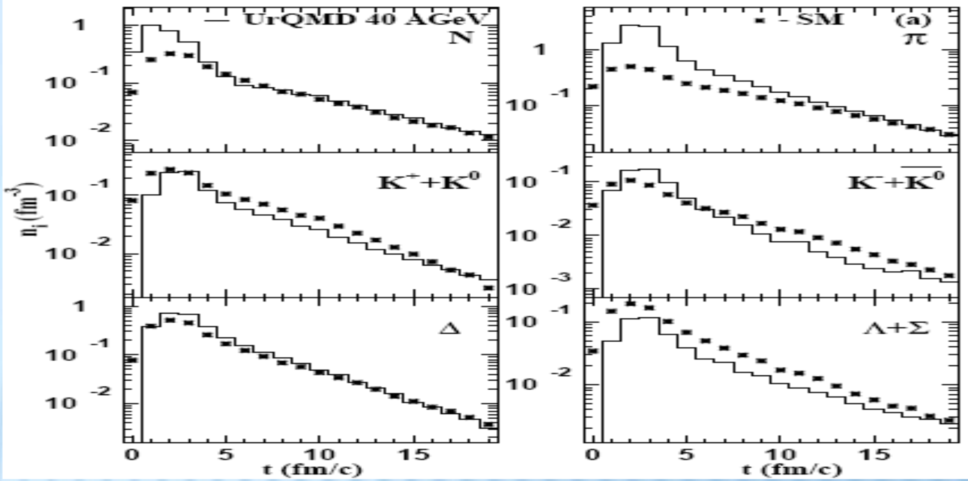

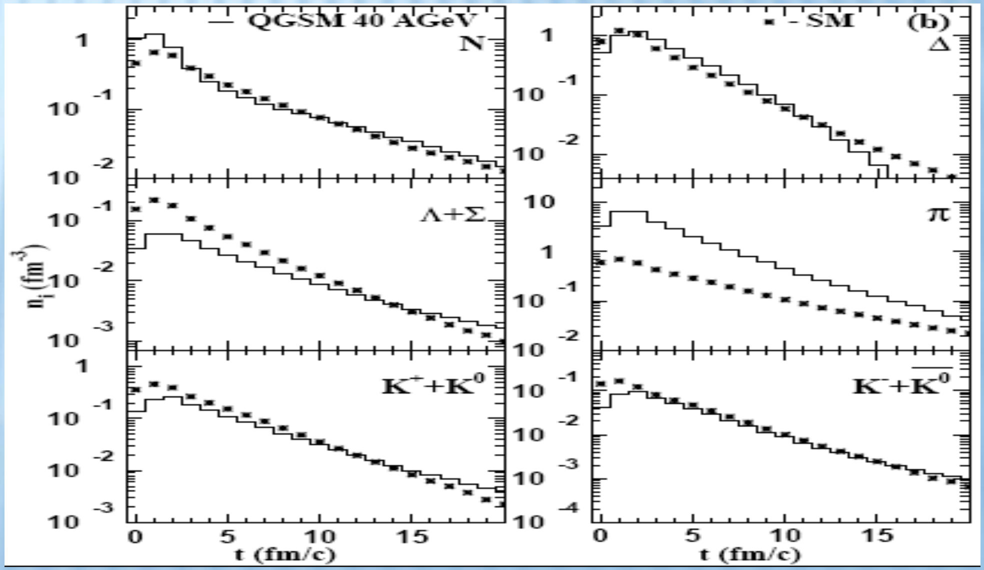

PRC 78 (2008) 014907

Thermal and chemical equilibrium seems to be reached

HOW DENSE CAN BE THE MEDIUM?

PRC 78 (2008) 014907

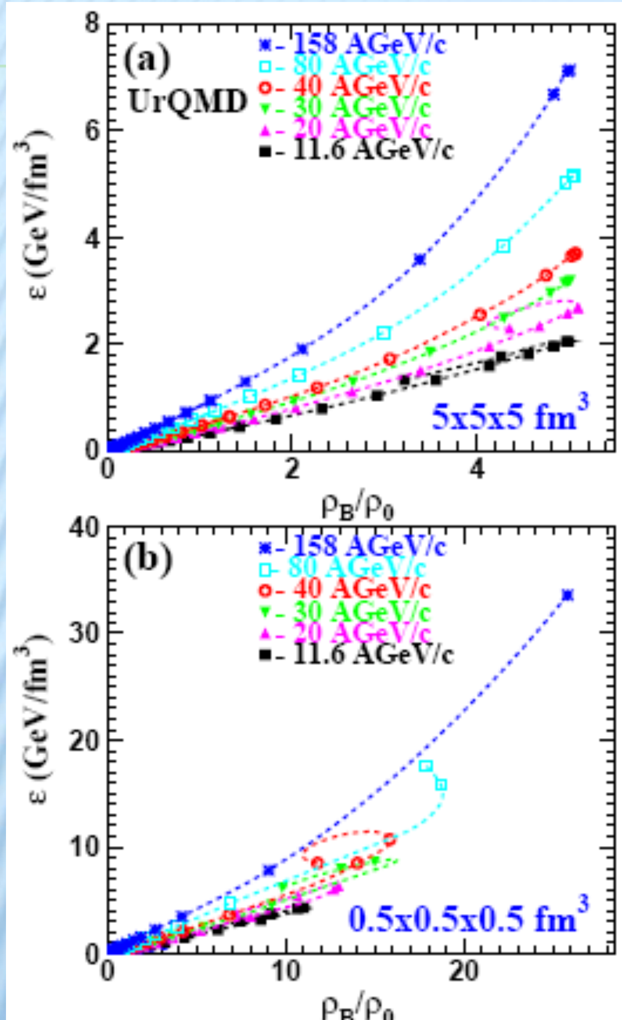

"Big" cell (V = 5x5x5 fm^3)

"Small" cell (V => 0)

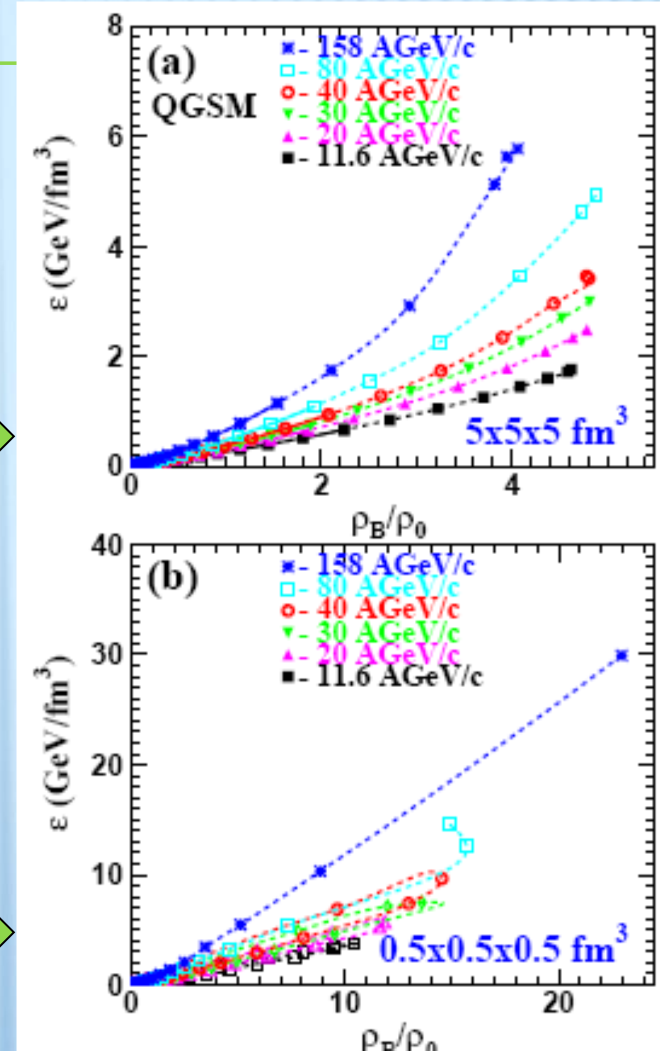

Dramatic differences at the non-equilibrium stage; after beginning of kinetic equilibrium the energy densities and the baryon densities are the same for "small" and "big" cell

COMPARISON BETWEEN MODELS

The phase trajectories at the center of a head-on Au+Au collisions

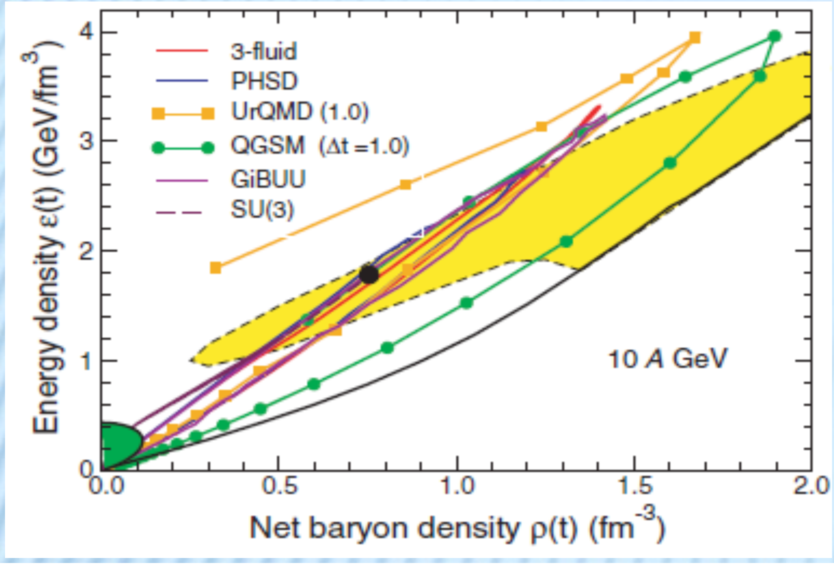

I. Arsene et al., PRC 75 (2007) 034902

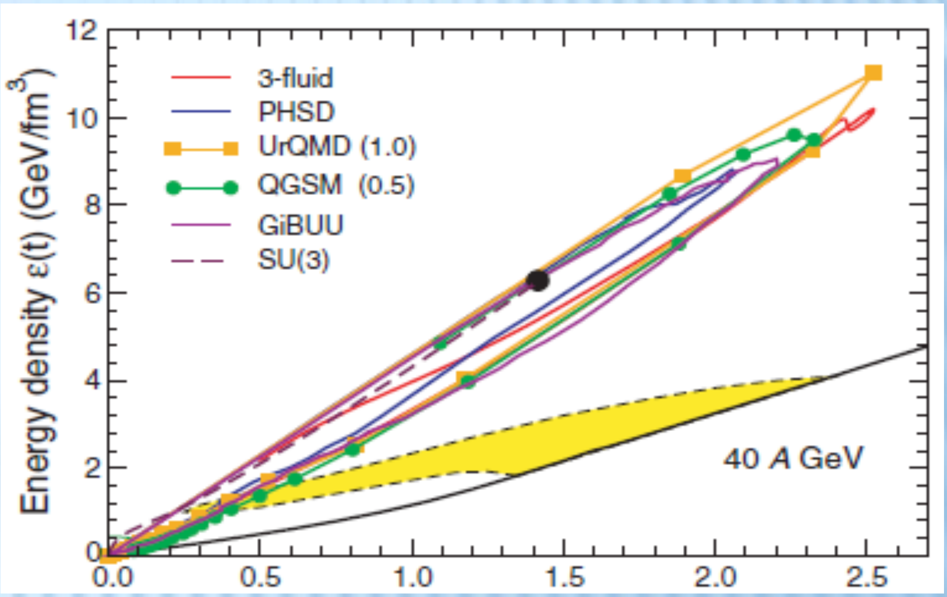

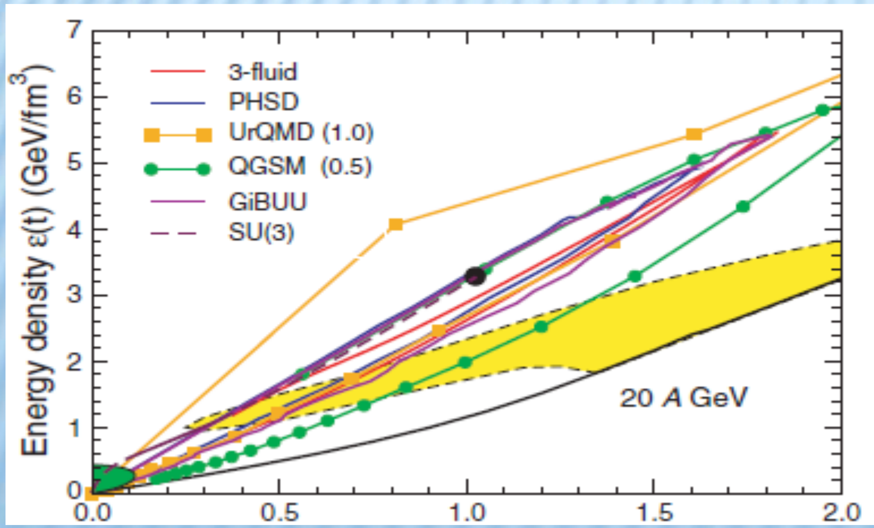

Green area : freeze-out region;
Yellow area : the phase coexistence region from schematic EOS that has a critical point at final density

Different models exhibit a large degree of mutual agreement

Infinite hadron gas:

a box with periodic boundary conditions

BOX WITH PERIODIC BOUNDARY CONDITIONS

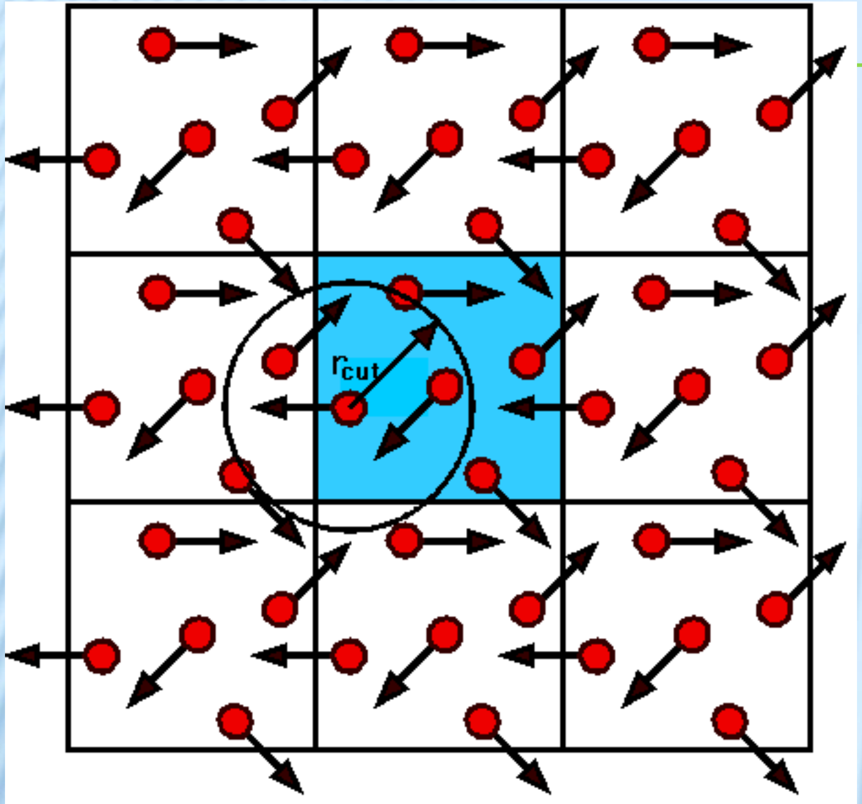

M.Belkacem et al., PRC 58, 1727 (1998)

Model employed: UrQMD
55 different baryon species
(N, Δ, hyperons and their resonances with
$m \leq 2.25\ \mathrm{GeV}/c^2$),
32 different meson species
(including resonances with
$m \leq 2\ \mathrm{GeV}/c^2$) and their respective antistates.
For higher mass excitations a string mechanism is invoked.

Initialization: (i) nucleons are uniformly distributed in a configuration space;
(ii) Their momenta are uniformly distributed in a sphere with random radius and then rescaled to the desired energy density.

Test for equilibrium: particle yields and energy spectra

BOX: PARTICLE ABUNDANCES

M.Belkacem et al., PRC 58, 1727 (1998)

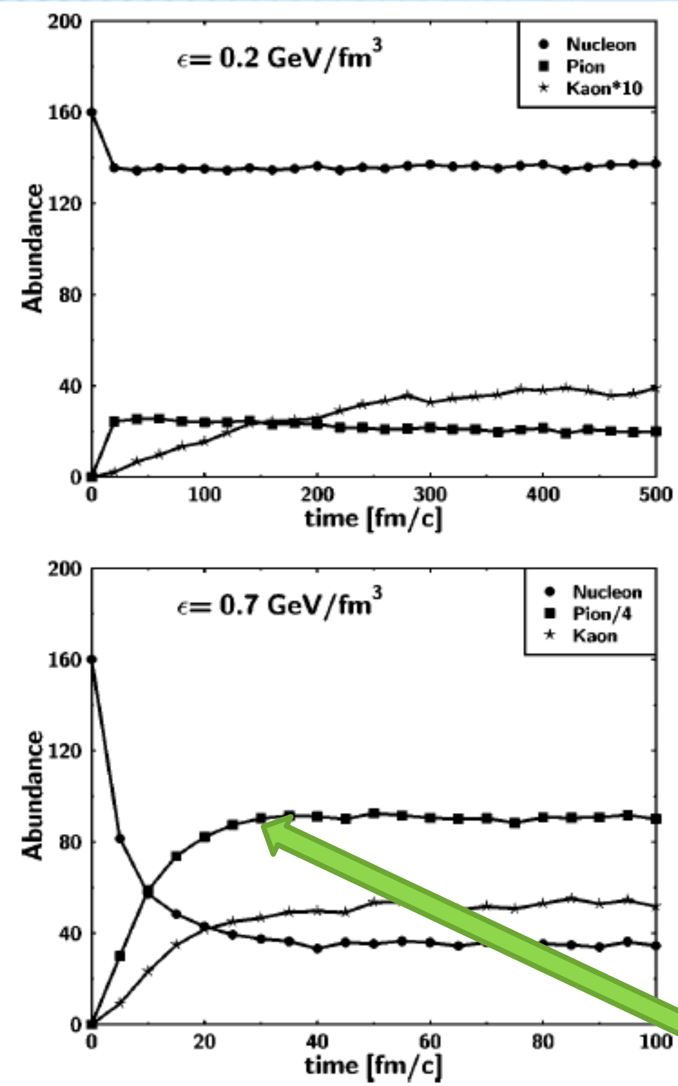

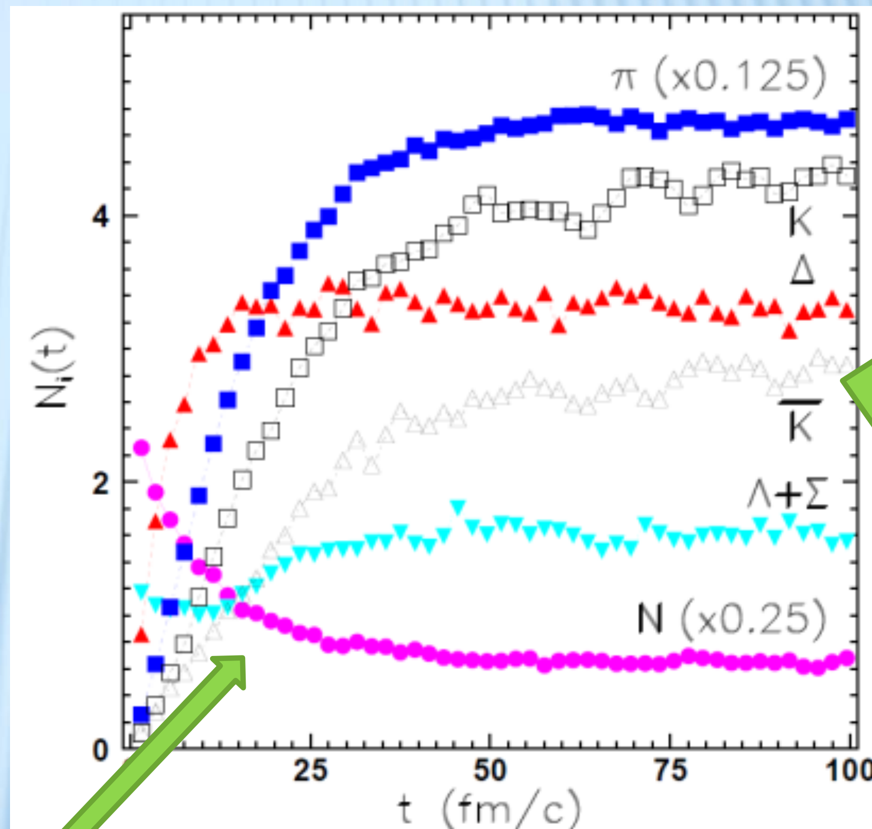

L.Bravina et al., PRC 62, 064906 (2000)

Saturation of yields after a certain time. Strange hadrons are saturated longer than others .

BOX: ENERGY SPECTRA AND MOMENTUM DISTRIBUTIONS

Fit to Boltzmann distributions ~exp(-E/T)

Fit to Gaussian distributions ~exp(-p^2/2mT)

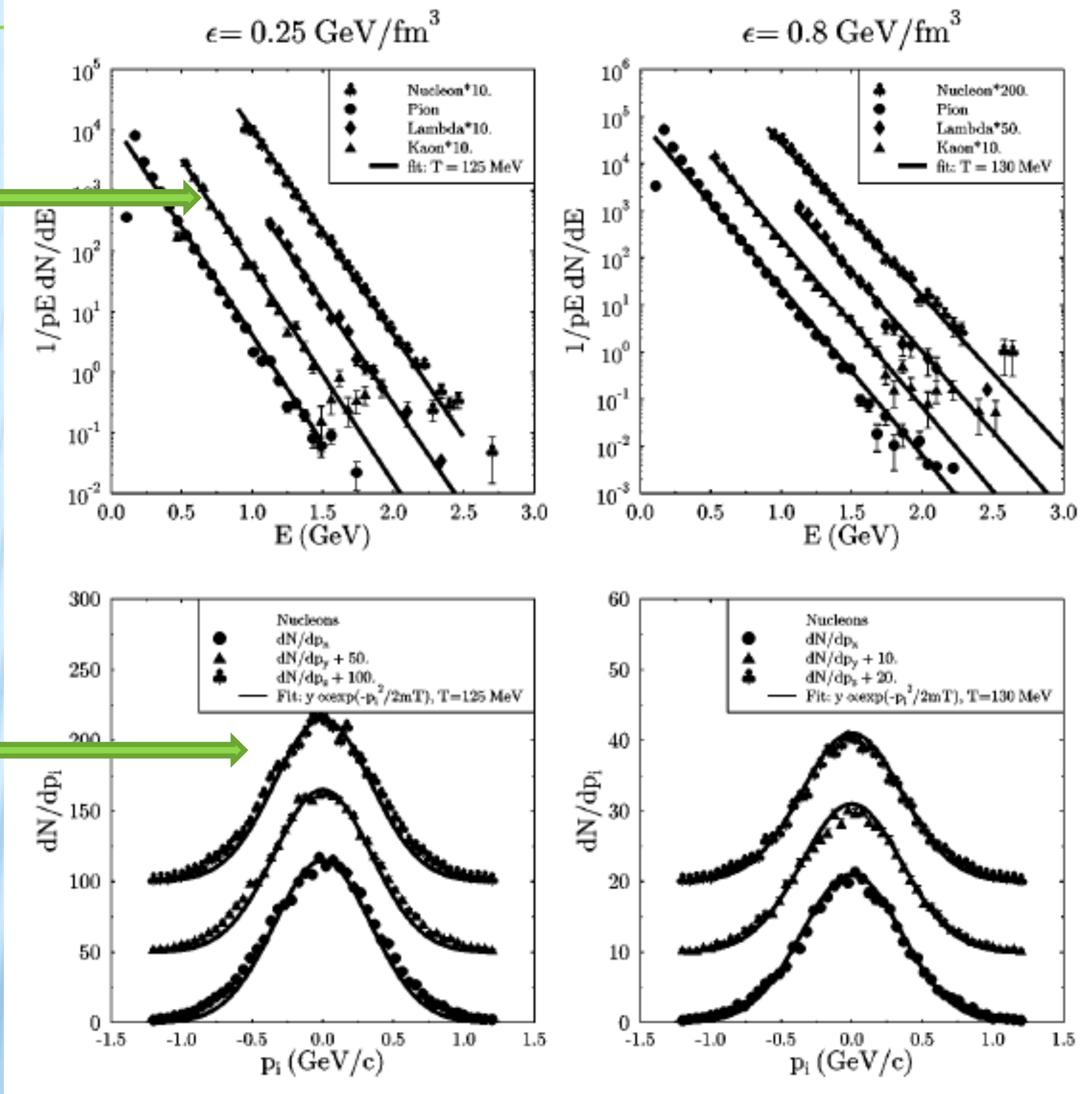

M.Belkacem et al., PRC 58, 1727 (1998)

Nearly the same temperature and complete isotropy of dN/dp$_T$

BOX: HAGEDORN-LIKE LIMITING TEMPERATURE

M.Belkacem et al., PRC 58, 1727 (1998)

HSD

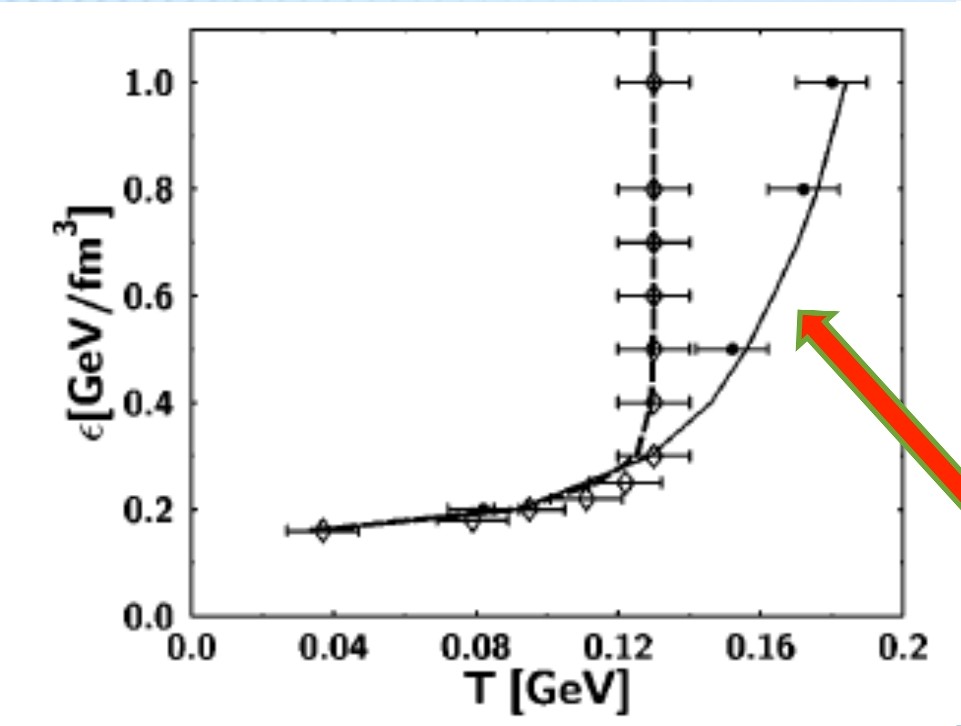

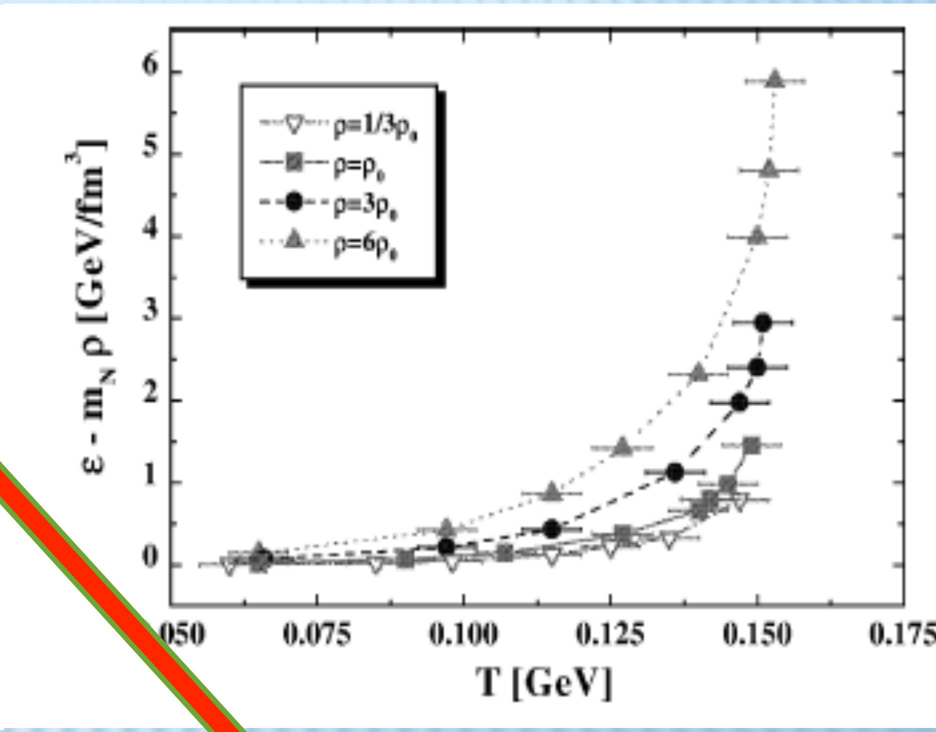

E.Bratkovskaya et al., NPA 675, 661 (2000)

UrQMD

A rapid rise of T at low ε and saturation at high energy densities. Saturation temperature depends on number of resonances in the model. W/o strings and many-N decays – no limiting T is observed.

Freeze-out of main hadron species

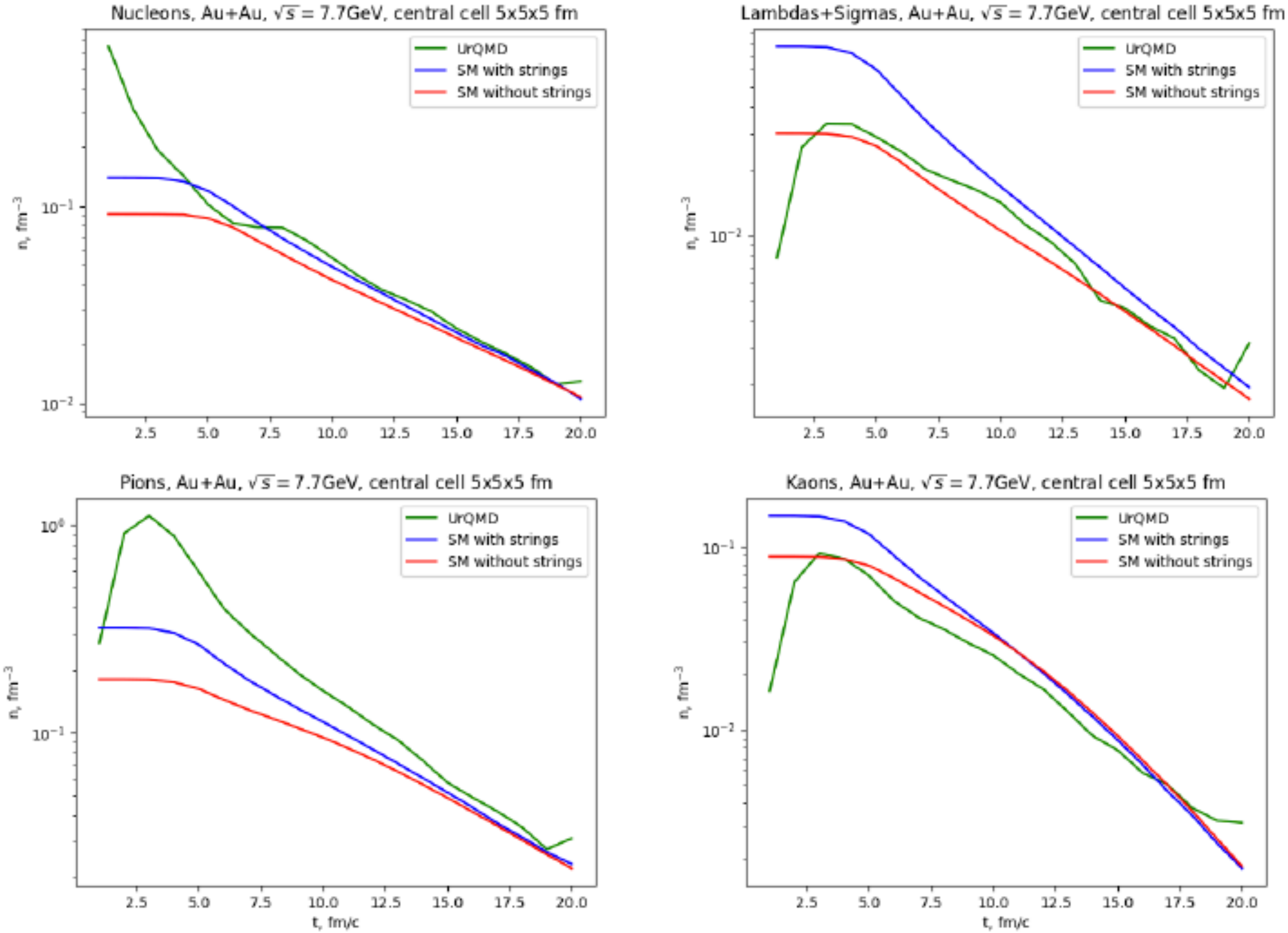

Figure 1: Particle densities in the central cell at times 1 – 20 fm/c.

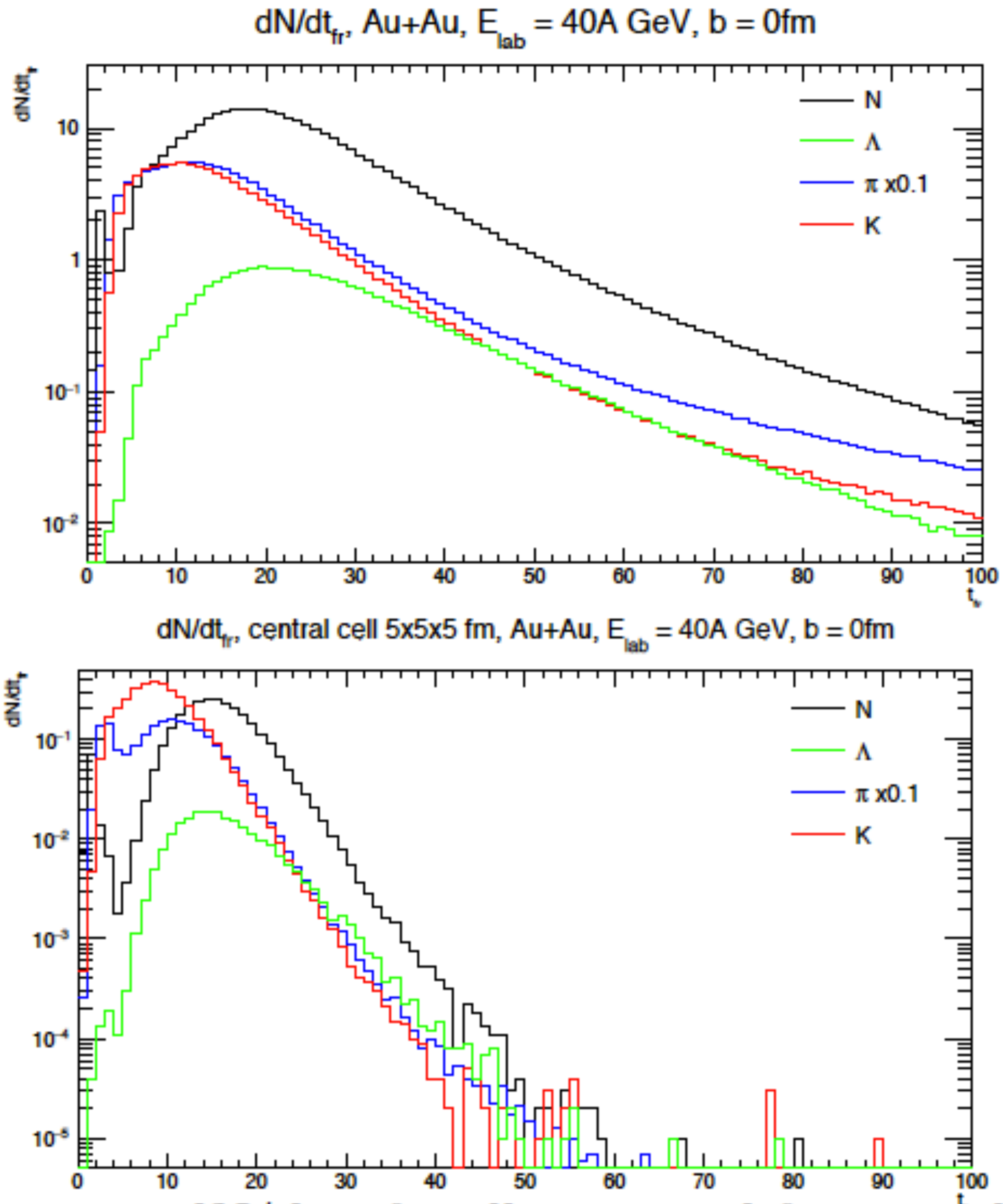

Figure 3: dN/dt_{fr} for all space and for central cell.

Different particles
are frozen at different space -
times
with different values of
T-μ_B-μ_S

Au+Au, E_{lab}=10A GeV, b = 0 fm, all space

	All y						$\|y\| < 1$					
	t, fm/c	$\|x\|,\|y\|$, fm	$\|z\|$, fm	T, MeV	μ_b, MeV	μ_s, MeV	t, fm/c	$\|x\|,\|y\|$, fm	$\|z\|$, fm	T, MeV	μ_b, MeV	μ_s, MeV
All	18.0	4.7	6.4	112.4	473.1	72.1	18.1	4.9	5.3	110.6	492.3	70.8
p	19.7	4.7	7.2	108.6	478.1	63.0	19.6	4.9	5.7	101.9	524.5	72.5
$\overline{p}$	19.1	5.9	7.8	109.0	459.1	64.5	18.3	6.4	5.8	106.1	462.1	66.6
Λ	24.6	5.5	8.1	90.4	539.8	50.4	24.4	5.7	7.1	92.2	532.3	49.4
$\overline{\Lambda}$	23.3	6.6	8.6	98.2	487.0	58.0	22.7	6.8	7.2	96.4	497.4	54.1
Σ	20.4	4.7	6.4	105.0	496.4	56.8	20.3	4.8	5.7	101.9	524.5	72.5
$\overline{\Sigma}$	20.0	5.5	7.5	106.3	472.7	62.3	19.5	5.7	6.4	104.0	489.4	62.4
π	16.9	4.7	6.1	116.8	448.5	69.0	17.0	4.9	5.1	114.6	471.2	73.4
K	14.4	3.7	4.4	128.1	457.4	83.5	14.4	3.9	3.8	124.8	486.1	93.8
$\overline{K}$	20.9	5.3	7.1	102.9	486.2	59.9	20.8	5.5	6.1	101.0	500.6	64.8

Table 1: Average coordinates of freezeout and T, μ_b, μ_s at this coordinates.

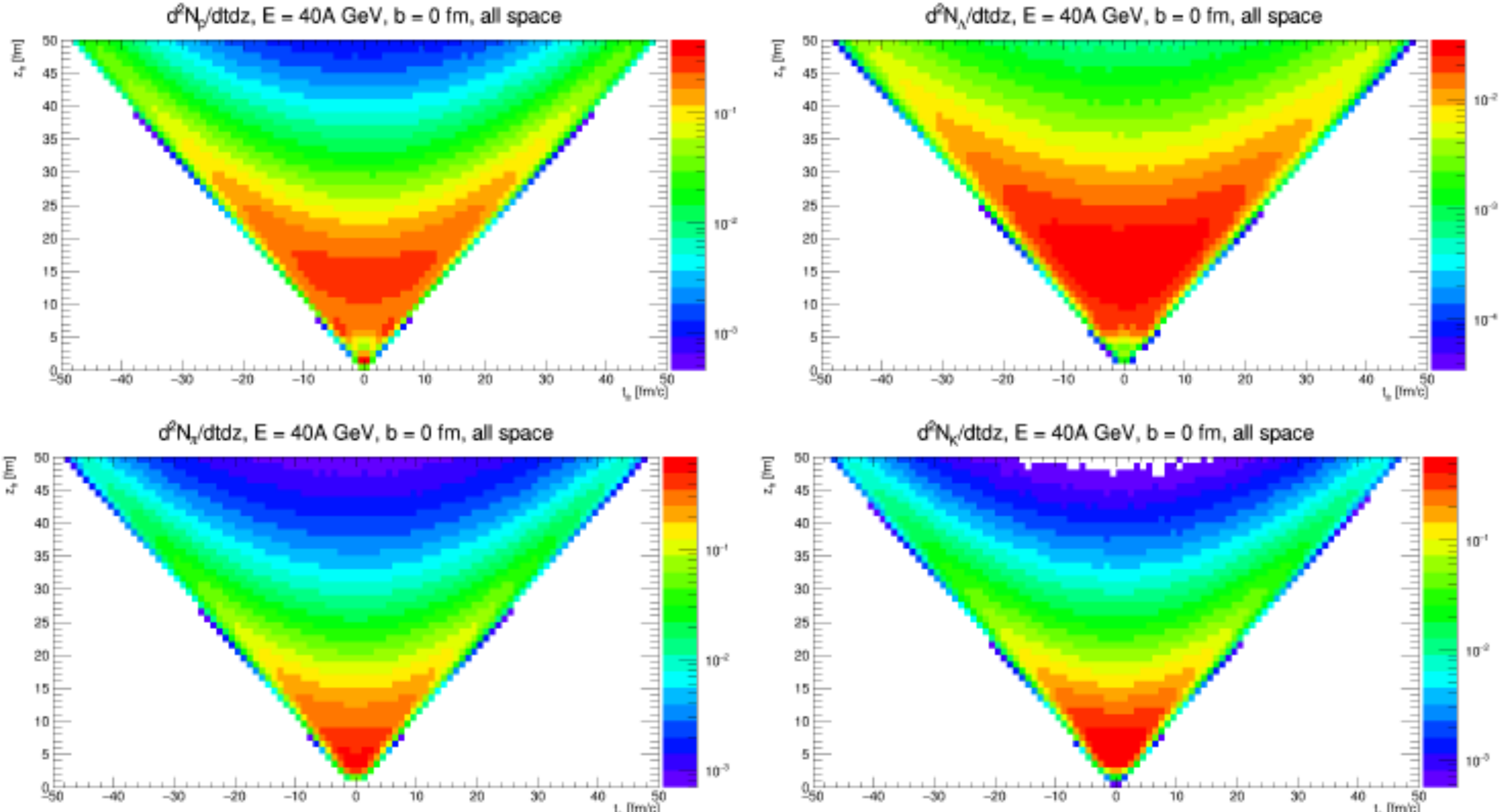

Figure 4: $d^2N/dtdz$ for protons, lambdas, pions and kaons.

Freeze-out

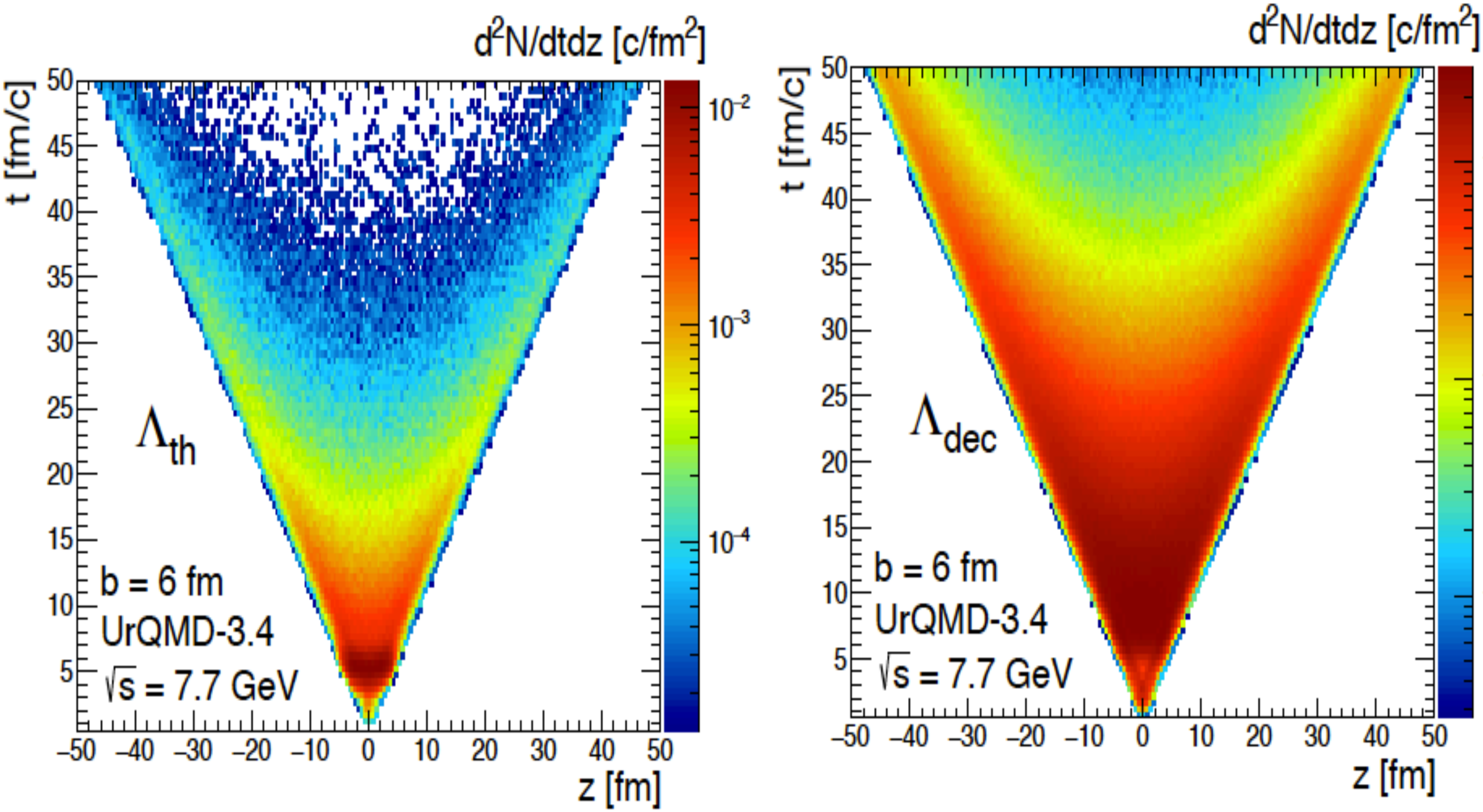

$d^2N/dtdz$ distribution of the final state hadrons over their formation point in (t, z) plane at $\sqrt{s} = 7.7\ GeV$ (left), $\sqrt{s} = 19.6\ GeV$ (right), $b = 6\ fm$.

Freeze-out

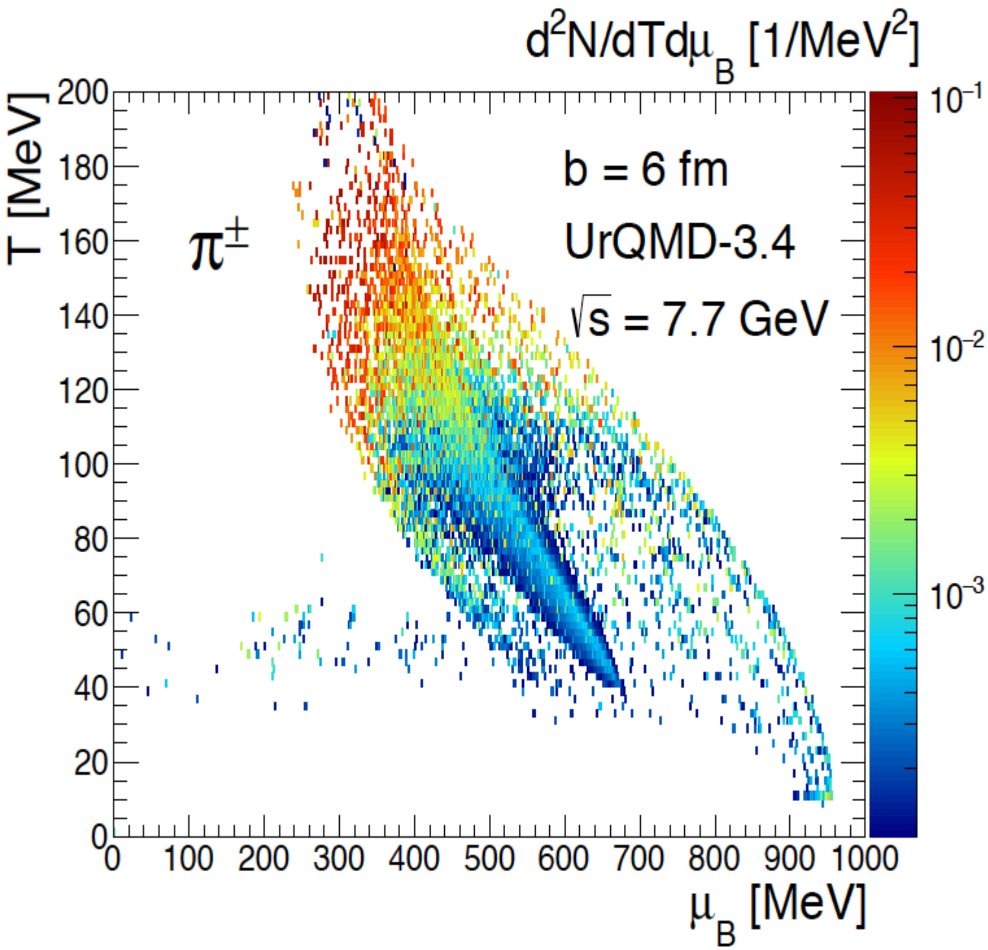

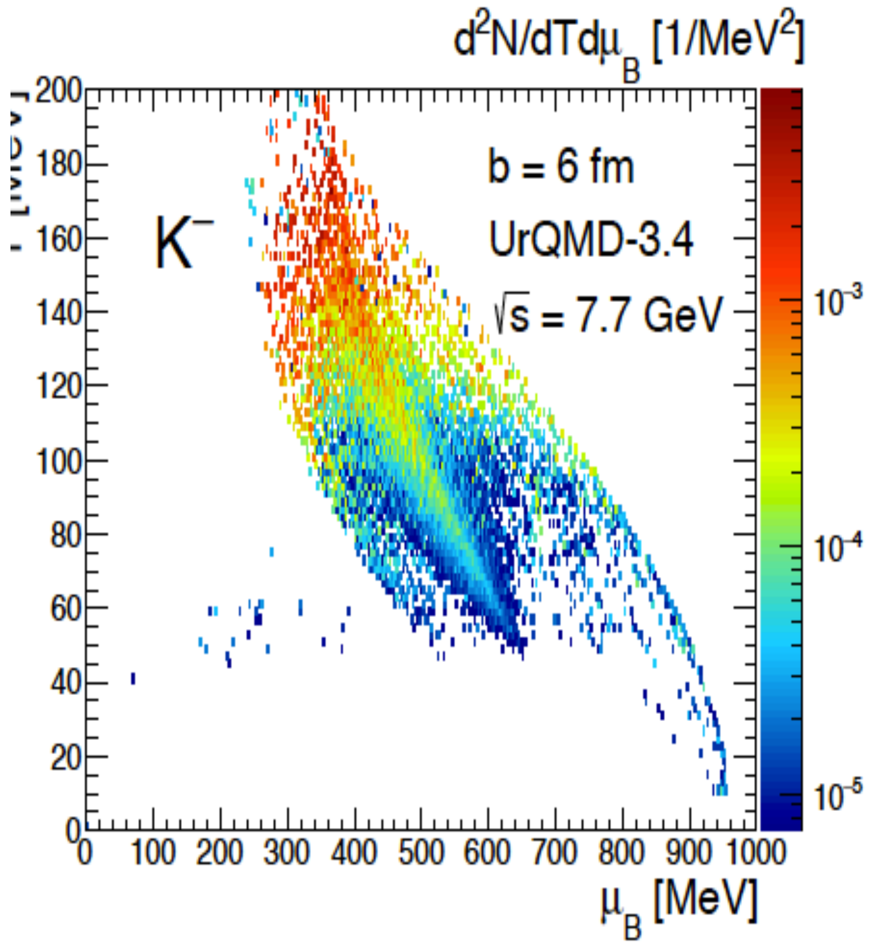

$d^2N/dTd\mu_B$ distribution of the final state hadrons over their formation point in (T, mu_B) plane at $\sqrt{s} = 7.7\ GeV,\ b = 6\ fm$.

Freeze-out

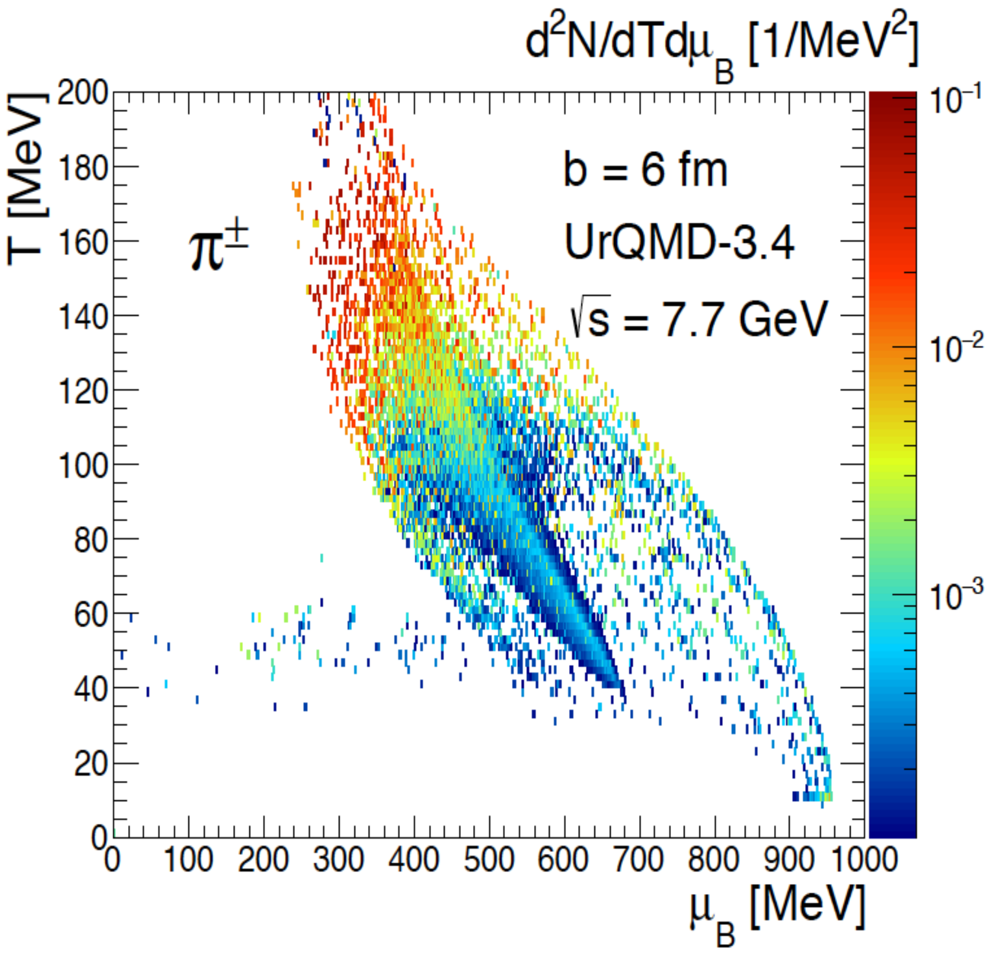

$d^2N/dTd\mu_B$ distribution of the final state ha
(T, mu_B) plane at $\sqrt{s} = 7.7\ GeV,\ b = 6\ fm.$

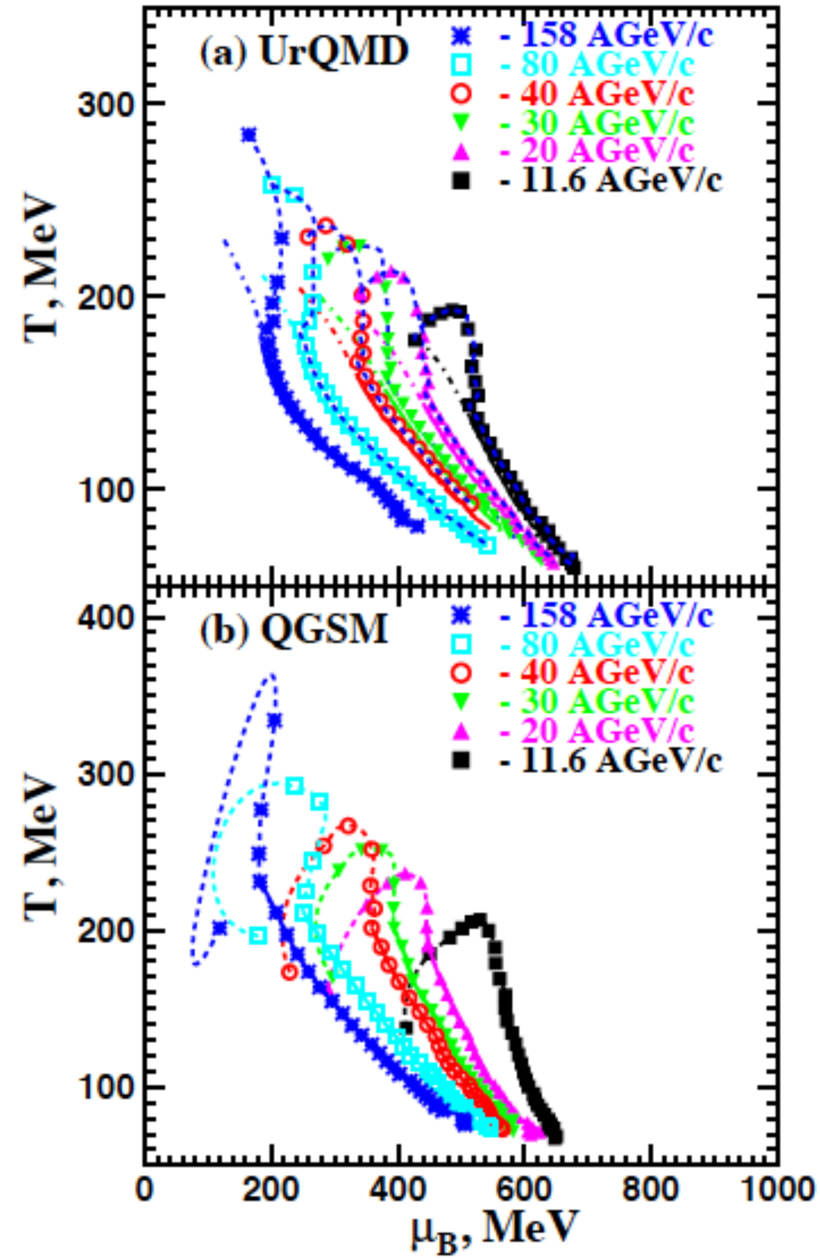

Freeze-out

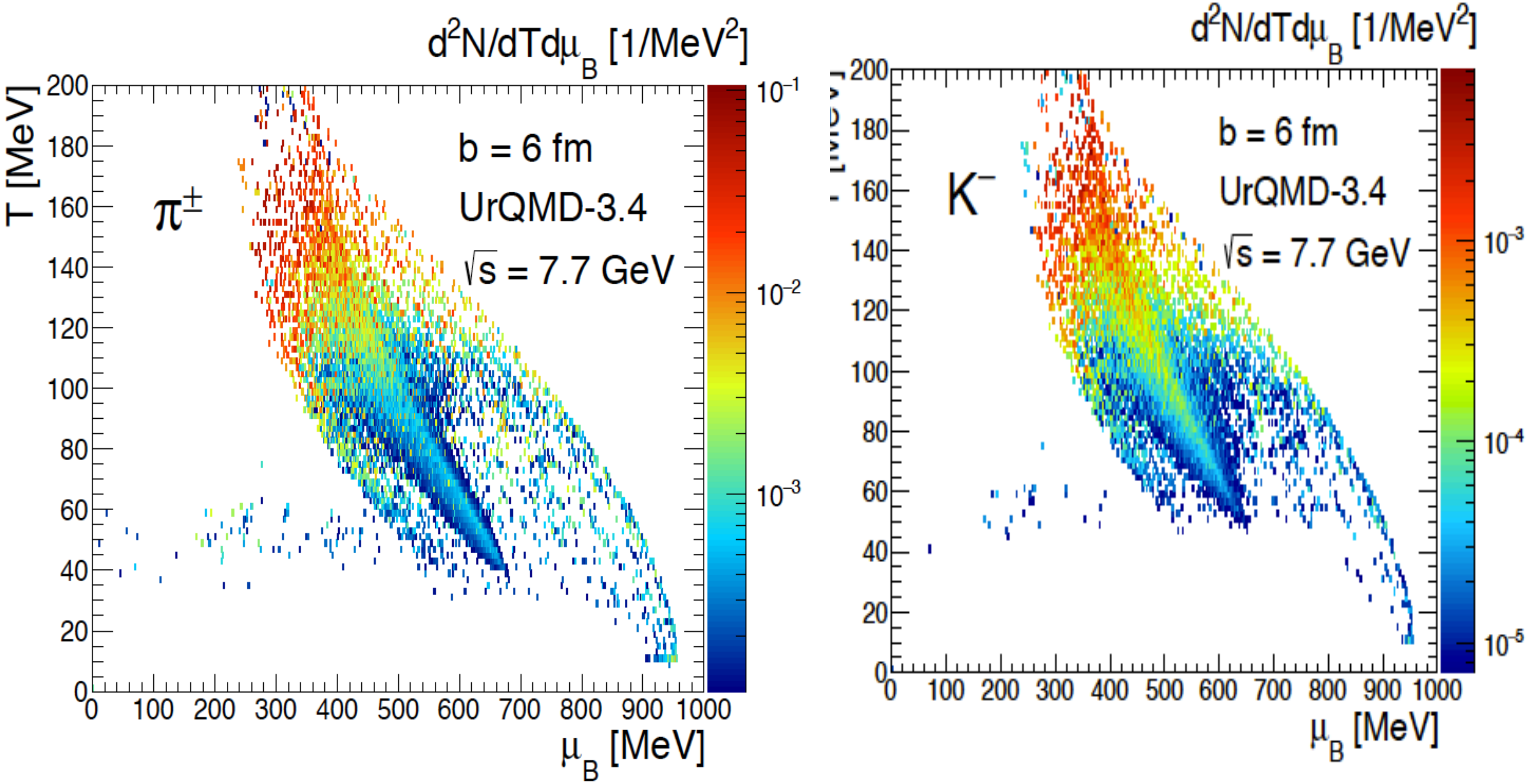

$d^2N/dTd\mu_B$ distribution of the final state hadrons over their formation point in (T, mu_B) plane at $\sqrt{s} = 7.7\ GeV,\ b = 6\ fm$.

Freeze-out

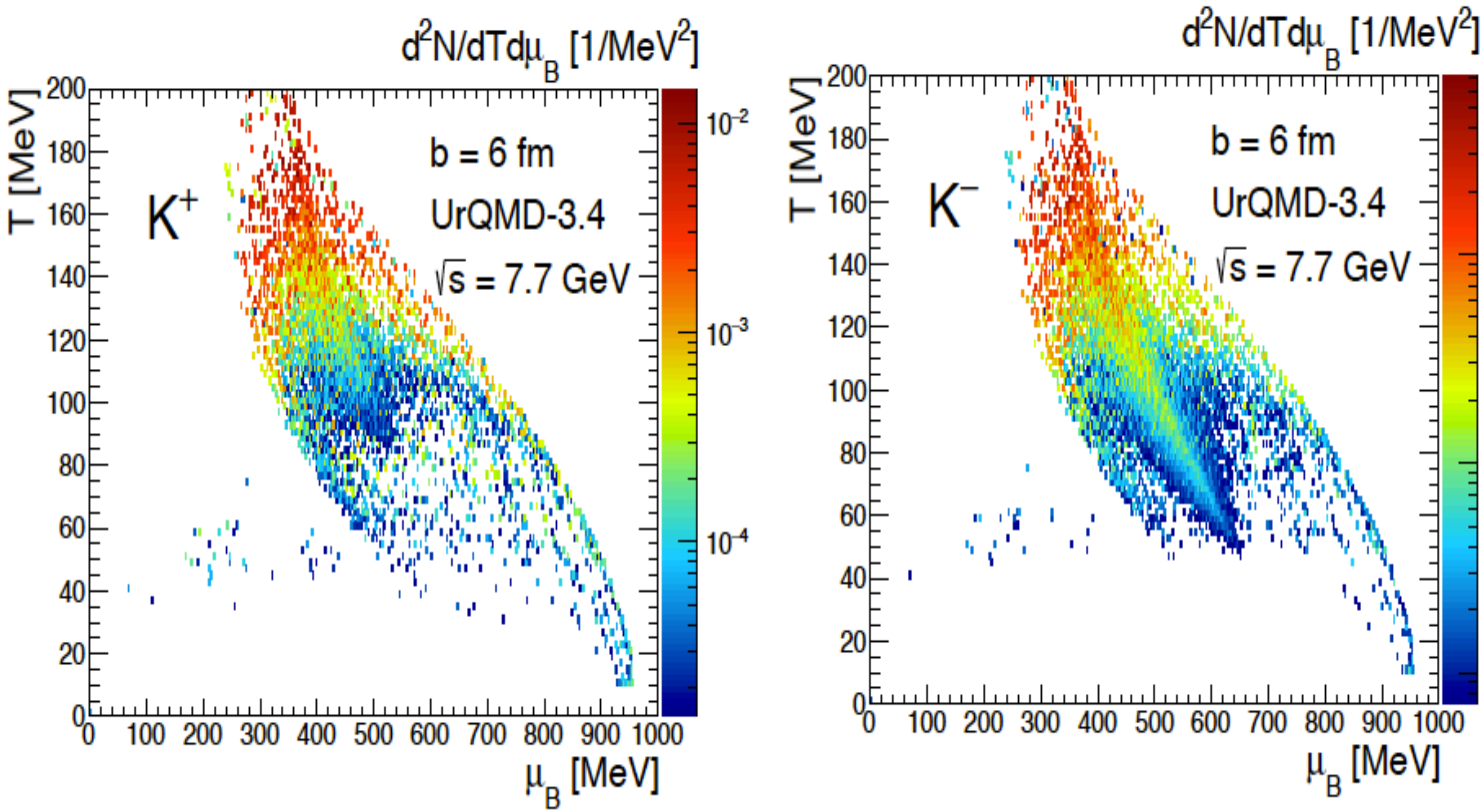

$d^2N/dTd\mu_B$ distribution of the final state hadrons over their formation point in (T, mu_B) plane at $\sqrt{s} = 7.7\ GeV,\ b = 6\ fm$.

Freeze-out

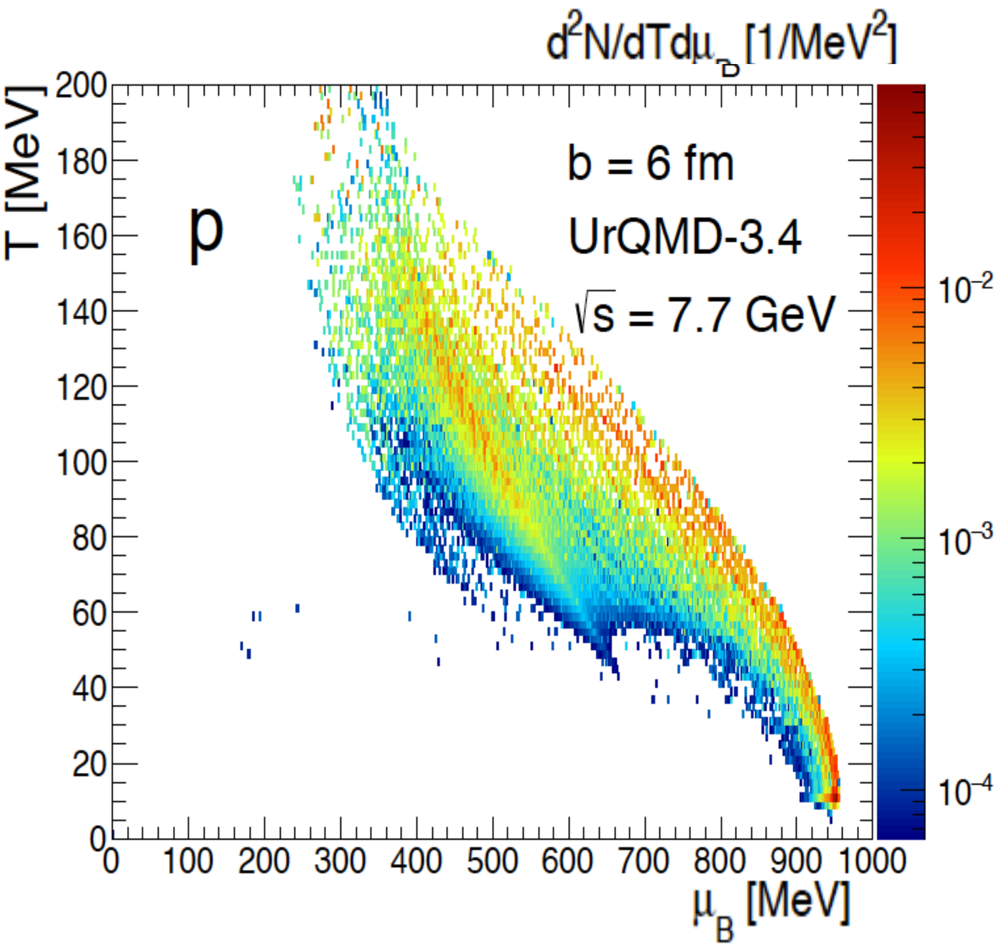

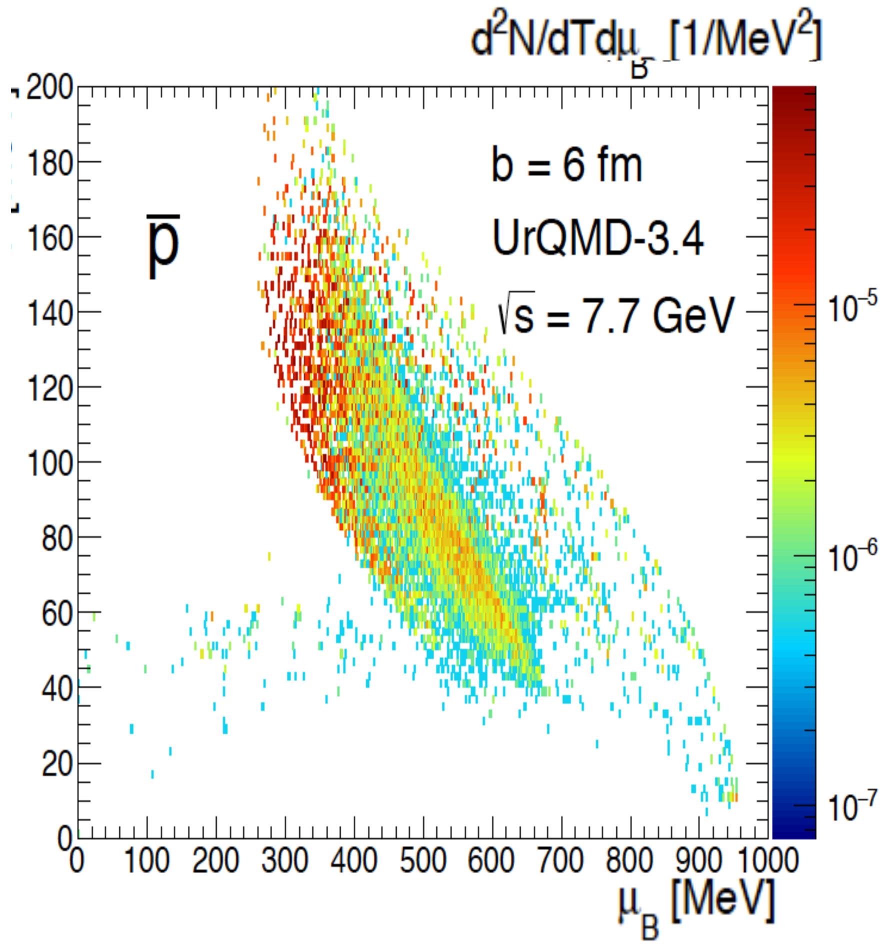

$d^2N/dTd\mu_B$ distribution of the final state hadrons over their formation point in (T, mu_B) plane at $\sqrt{s} = 7.7\ GeV,\ b = 6\ fm.$

Freeze-out

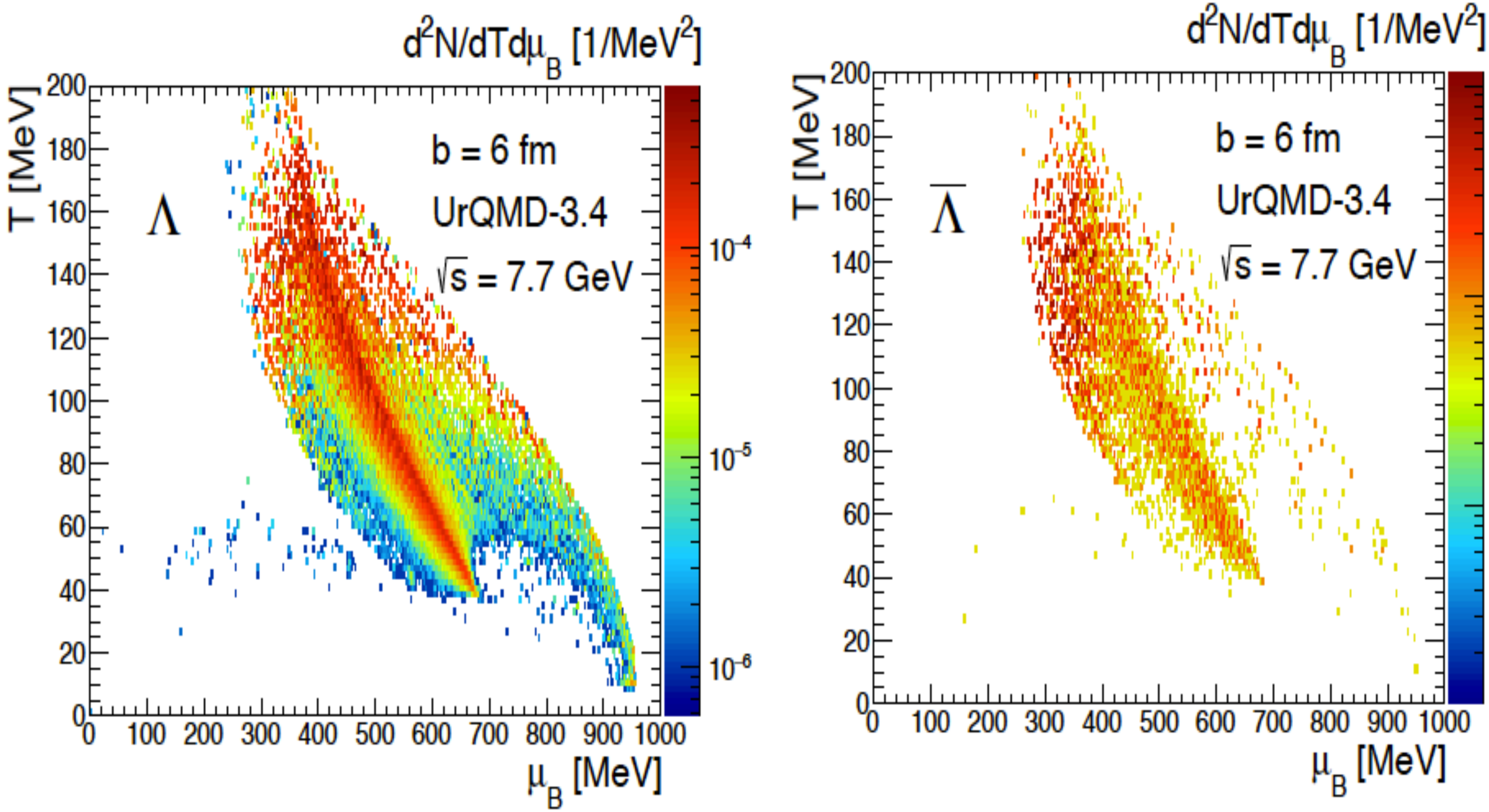

$d^2N/dTd\mu_B$ distribution of the final state hadrons over their formation point in (T, mu_B) plane at $\sqrt{s} = 7.7\ GeV,\ b = 6\ fm.$

Consequences of the different space-time freeze-out:
- Differences in yields in SM

L.Bravina et al, Springer Proceedings in Physics, vol. 250 (2020) p. 215

The difference between average freeze-out and freeze-out for particular species is very large

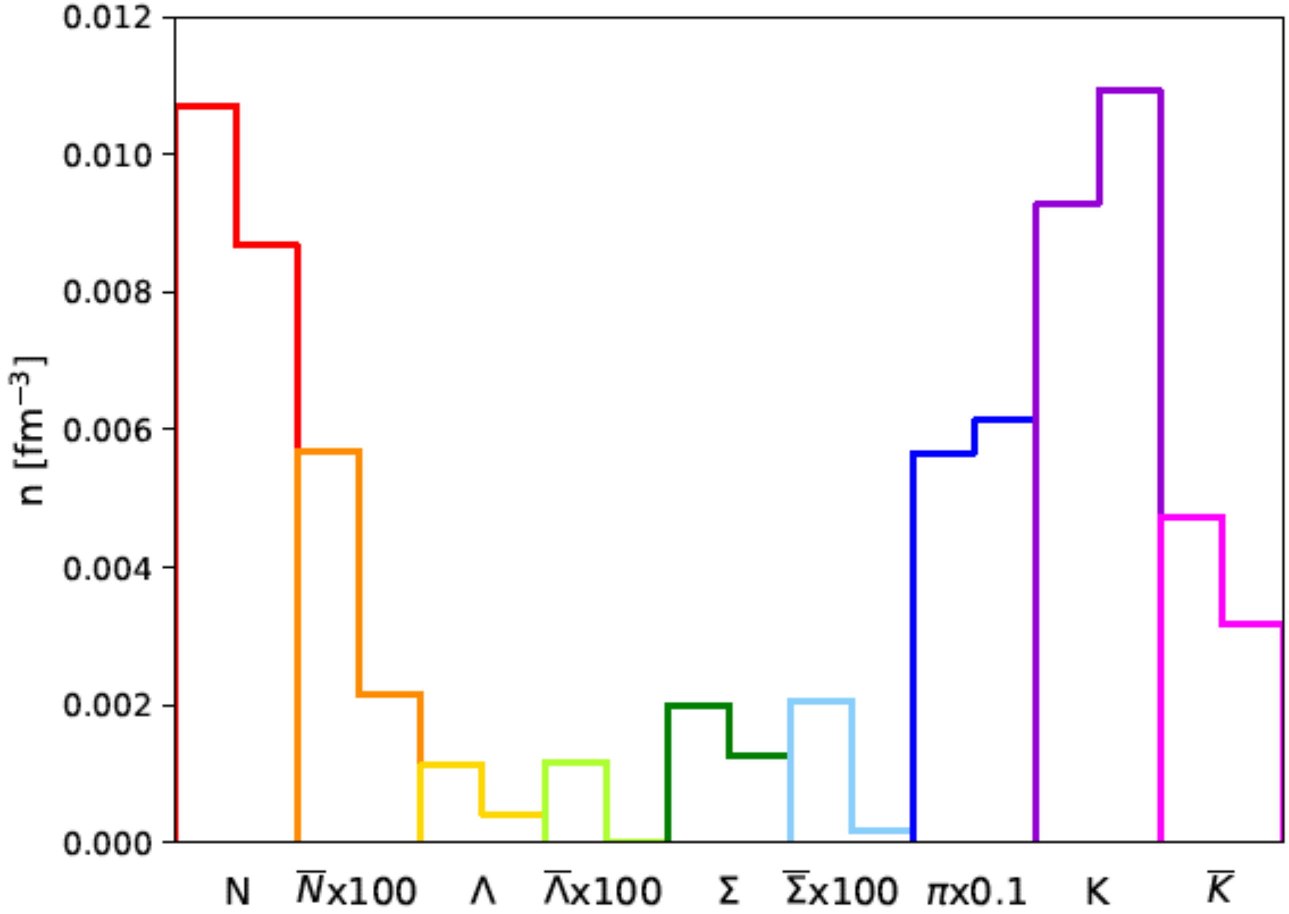

Figure 4: Particle densities at average freezeout coordinates of all particles (left column) and at freezeout coordinates of each particle type (right column) from statmodel; at average freezeout coordinates of all particles (star) and at freezeout coordinates of each particle type (pentagon) from UrQMD. E = 40A GeV.

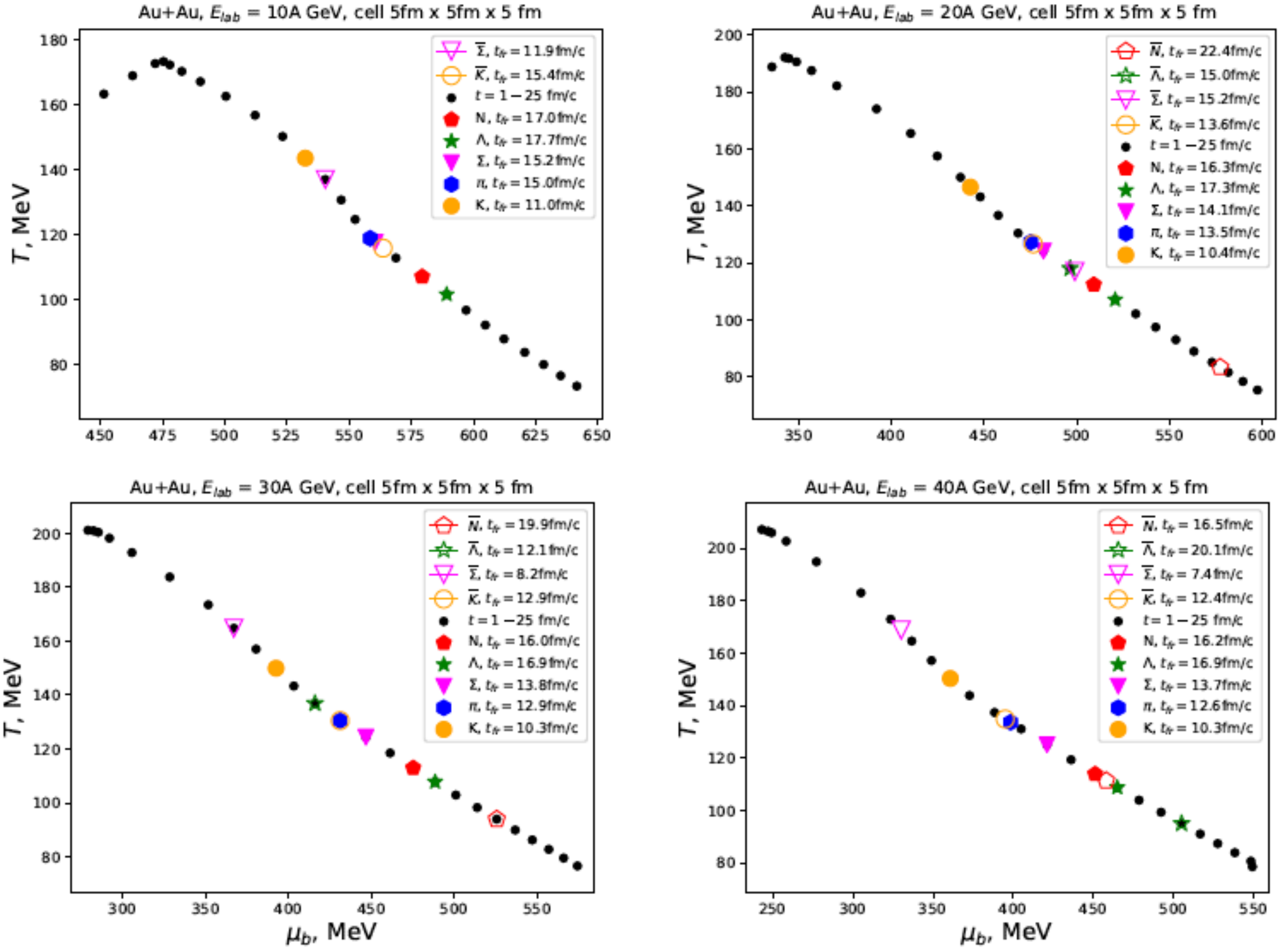

Figure 2: $T(\mu_B)$ in the central cell. Average freezeout times of different particles in the central cell are marked by colored markers.

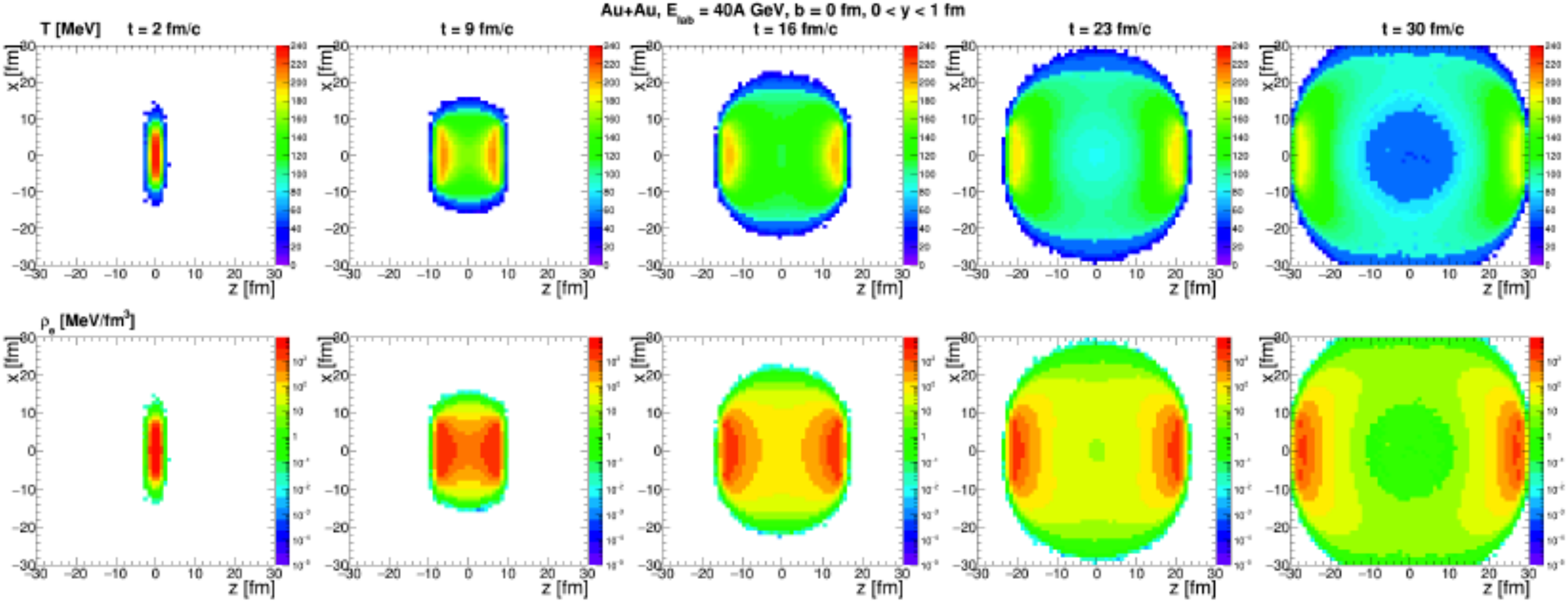

Figure 5: T and ε spatial distributions.

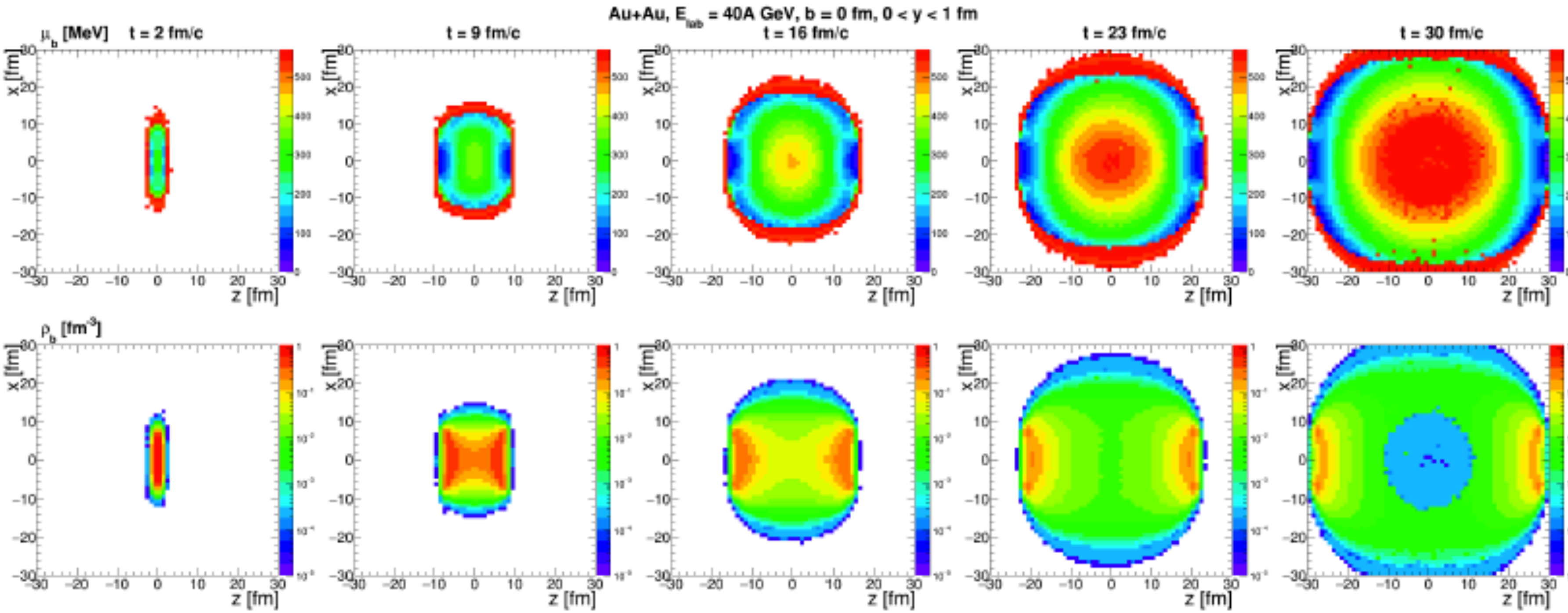

Figure 6: μ_b and ρ_b spatial distributions.

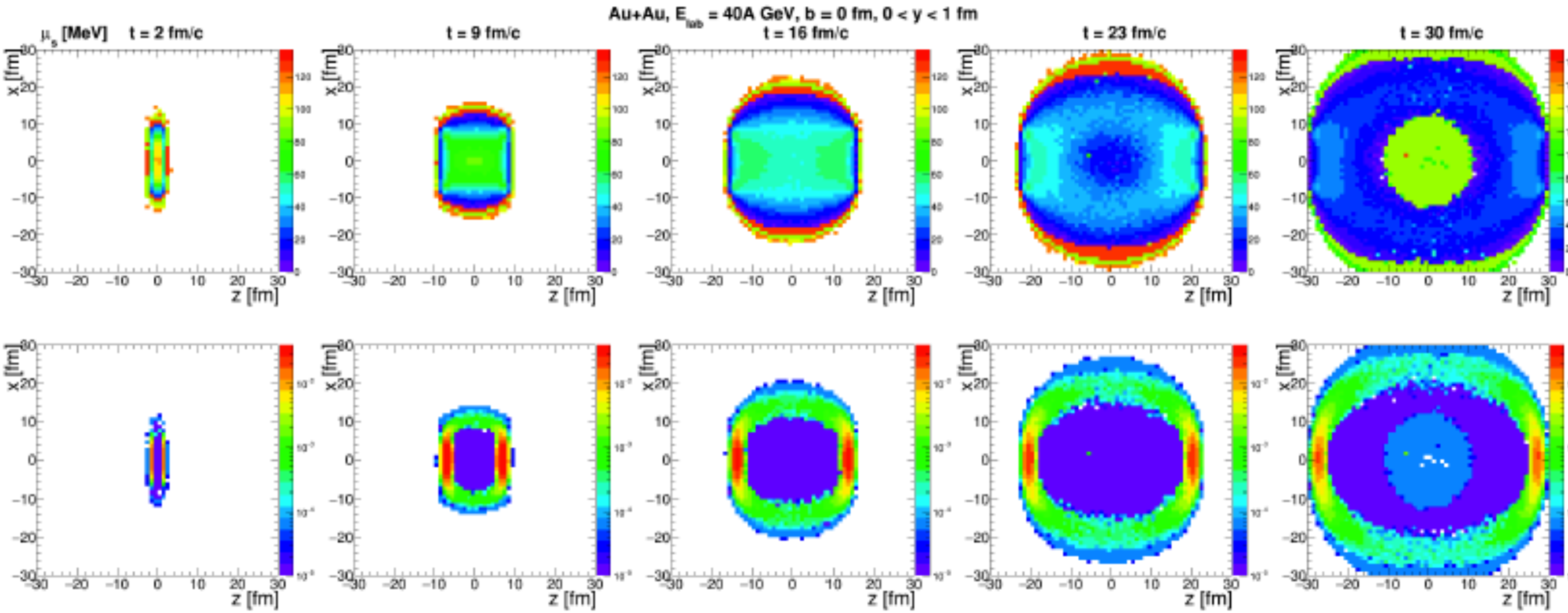

Figure 7: μ_s and ρ_s spatial distributions.

Conequences of the different space-time freeze-out:
- Directed flow

L.B. et al., Universe 5 (2019) 3, 69

Space distribution of Lambdas

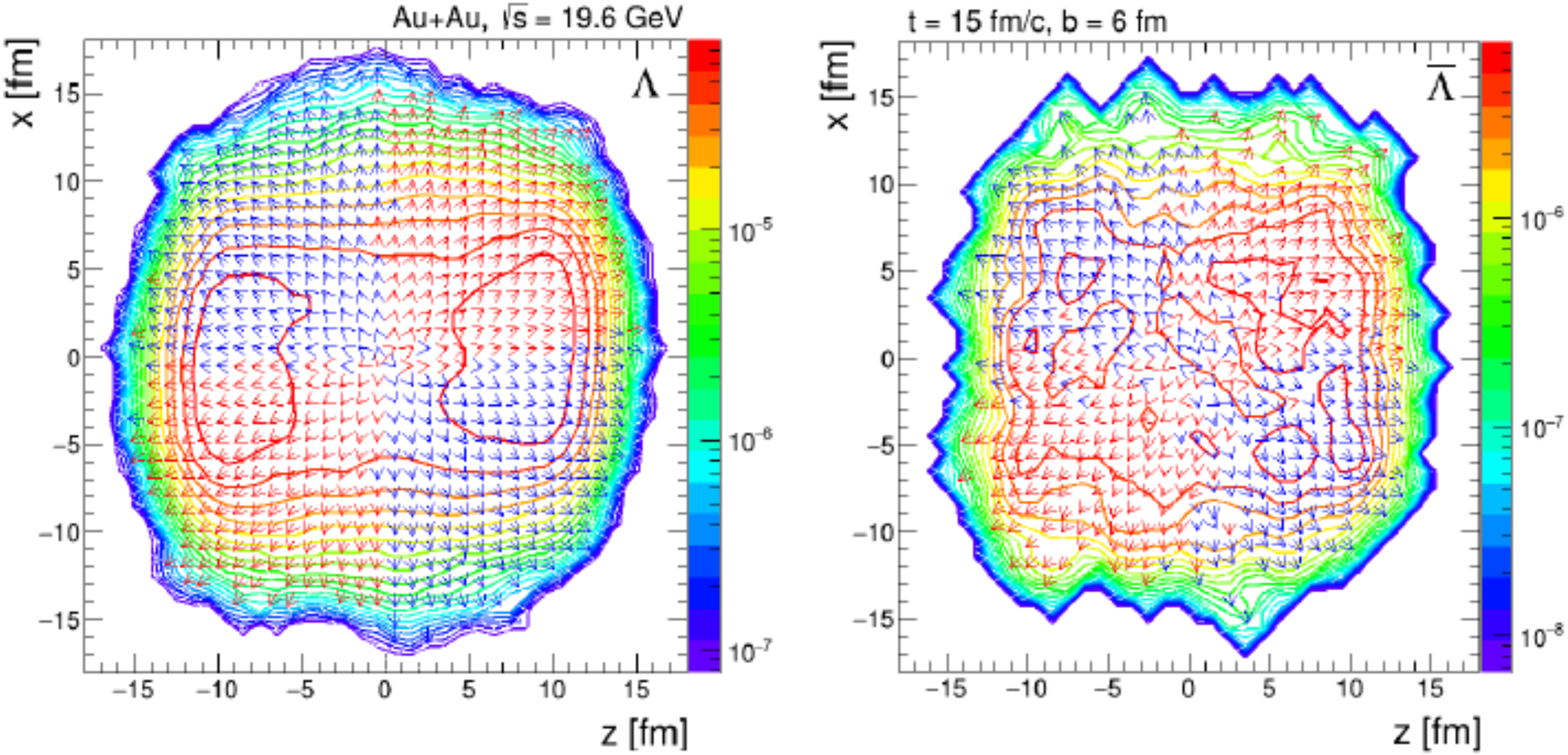

At $\sqrt{s} = 19.6 GeV$ Λ are mostly located near hot and dense regions and $\bar{\Lambda}$ are distributed more uniformly near system center.

Space distribution of Lambdas

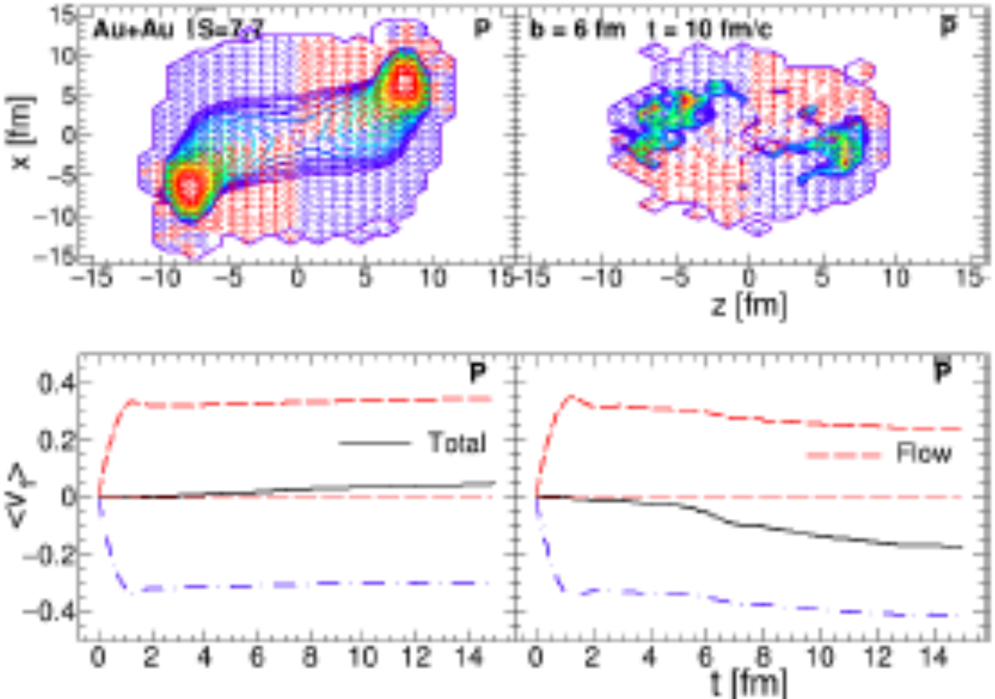

At low energies Λ and $\bar{\Lambda}$ are produced and emitted from the same regions as protons and antiprotons respectively. Λ's are concentrated also near hot and dense spectators, whereas $\bar{\Lambda}$'s are mostly produced in central region.

Mean flow is calculated as:

$$< v_1 >= \int sign(y) v_1(y) \frac{dN^{par}}{dy} dy / \int \frac{dN^{par}}{dy} dy$$

Collective velocities are shown on the picture to demonstrate that particles which have positive product of velocities $v_x v_z$ produce normal component of flow and particles with $v_x v_z < 0$ produce anti-flow component of directed flow. [Bravina et al, EPJ Web of Conferences 191, 05004 (2018)]

Directed flow for Lambdas and kaons

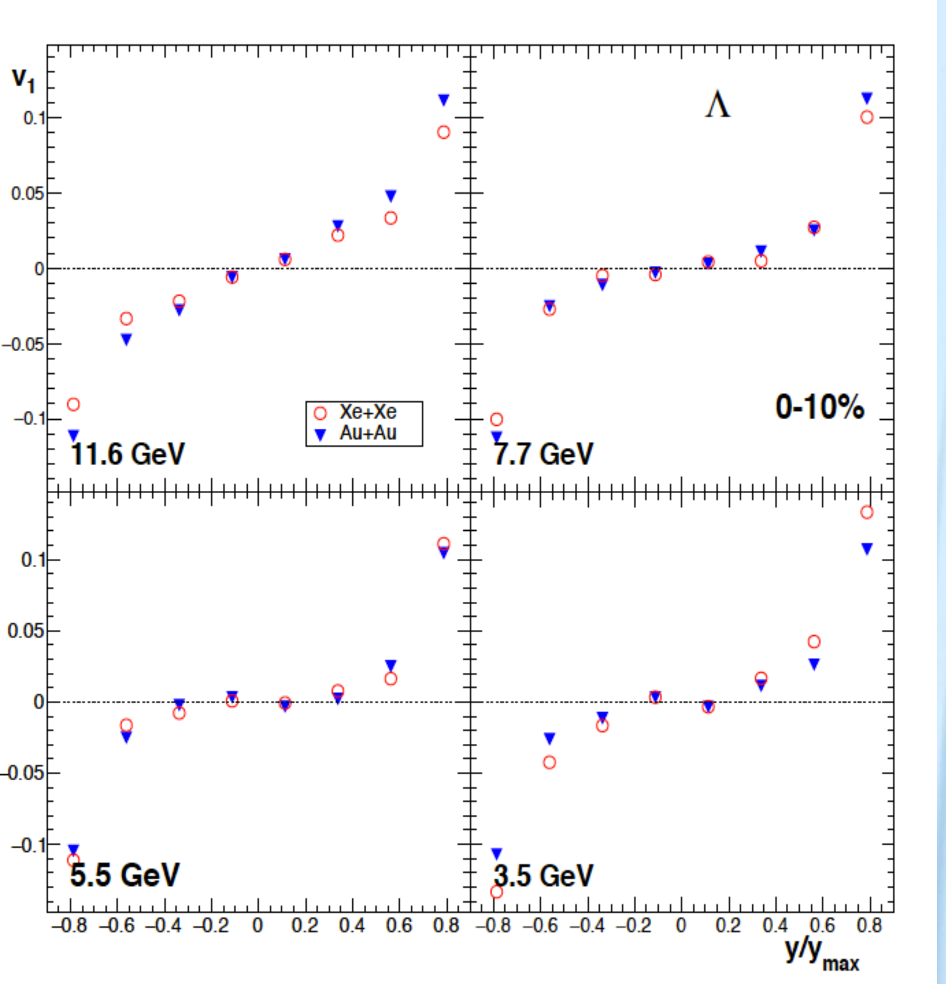

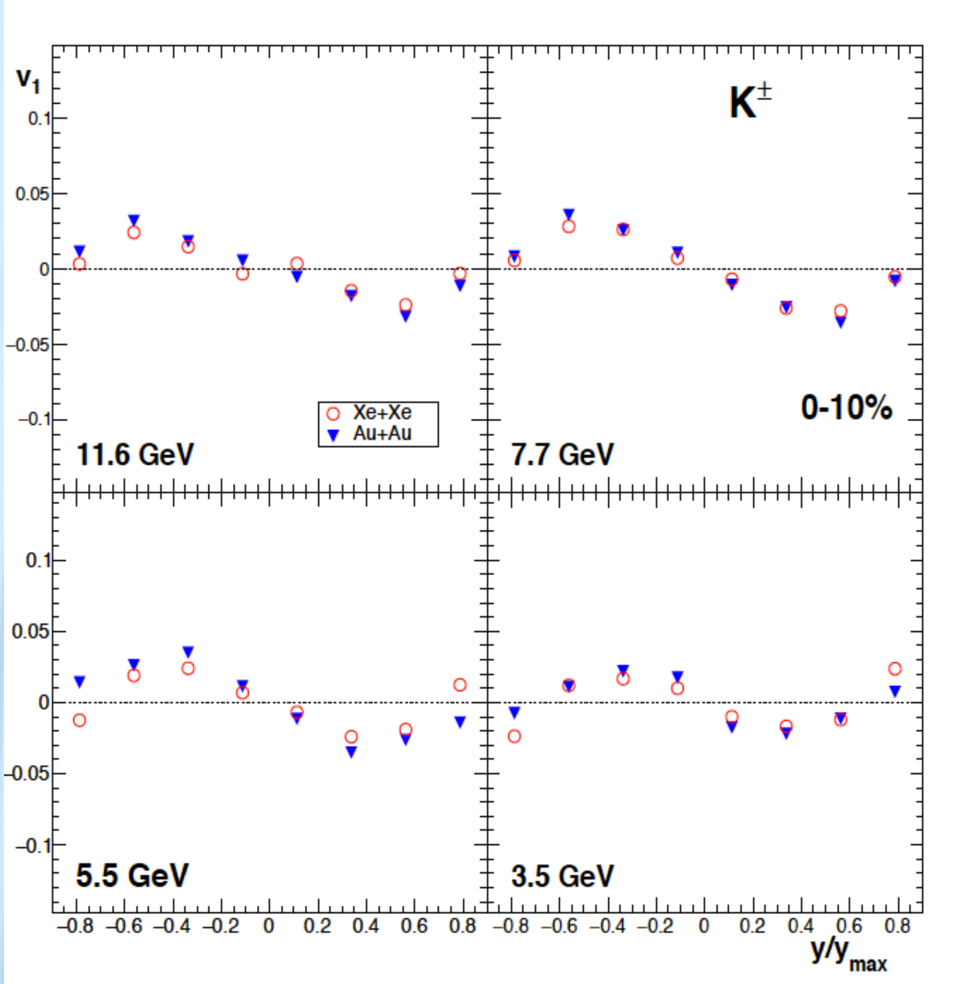

V_1 for Λ changes sign at midrapidity with decreasing collision energy, whereas V_1 for kaons has negative slope (antiflow)

Different slopes of different particles: URQMD and Data

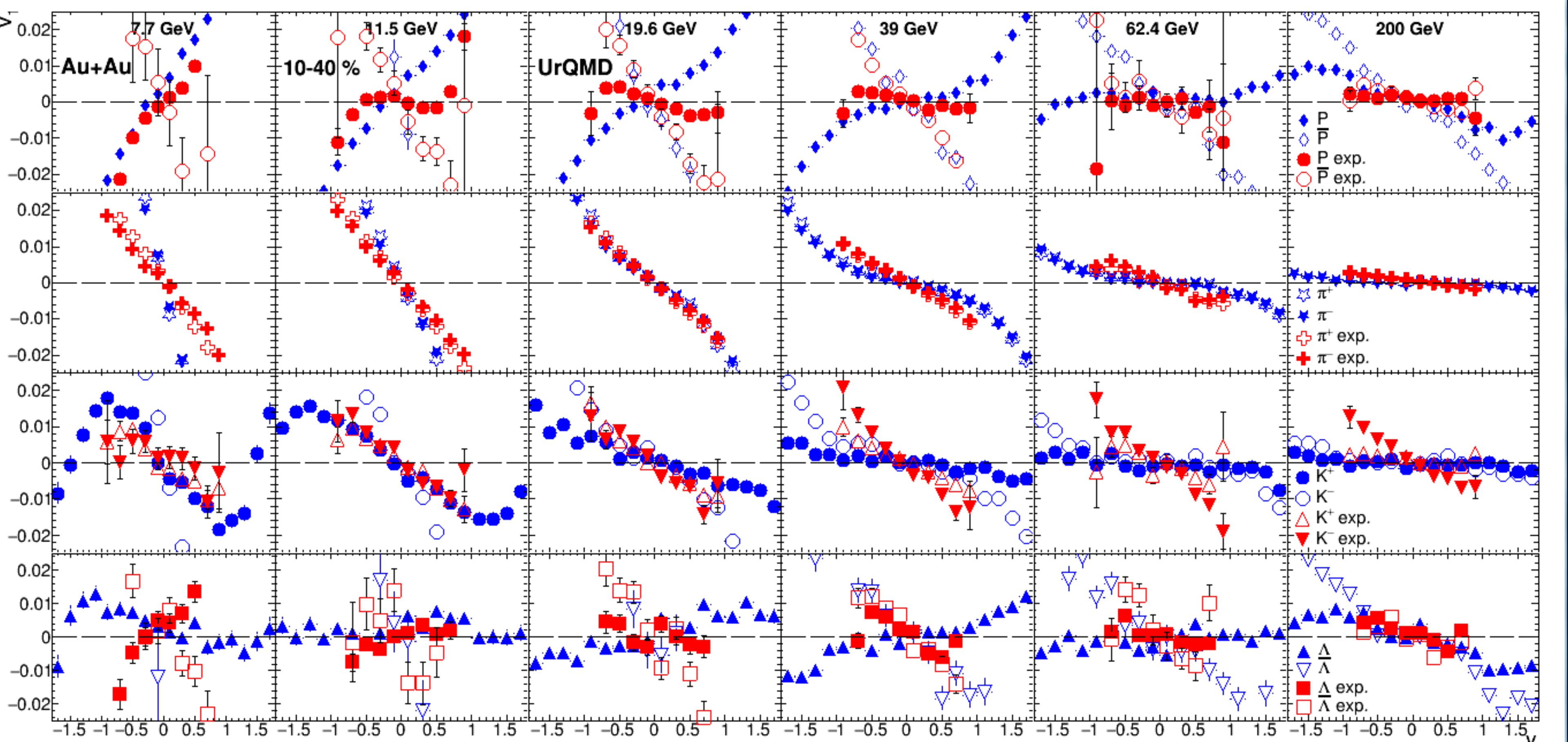

Consequences of the different space-time freeze-out:
- Difference in Polarization for lambdas and antilambdas

O.VITIUK ET AL SPRINGER PROCEEDINGS IN PHYSICS, VOL. 250 (2020) P. 429

O.Vitiuk, L.B., E.Zabrodin, PLB 803 (2020) 135298

Polarization energy dependency

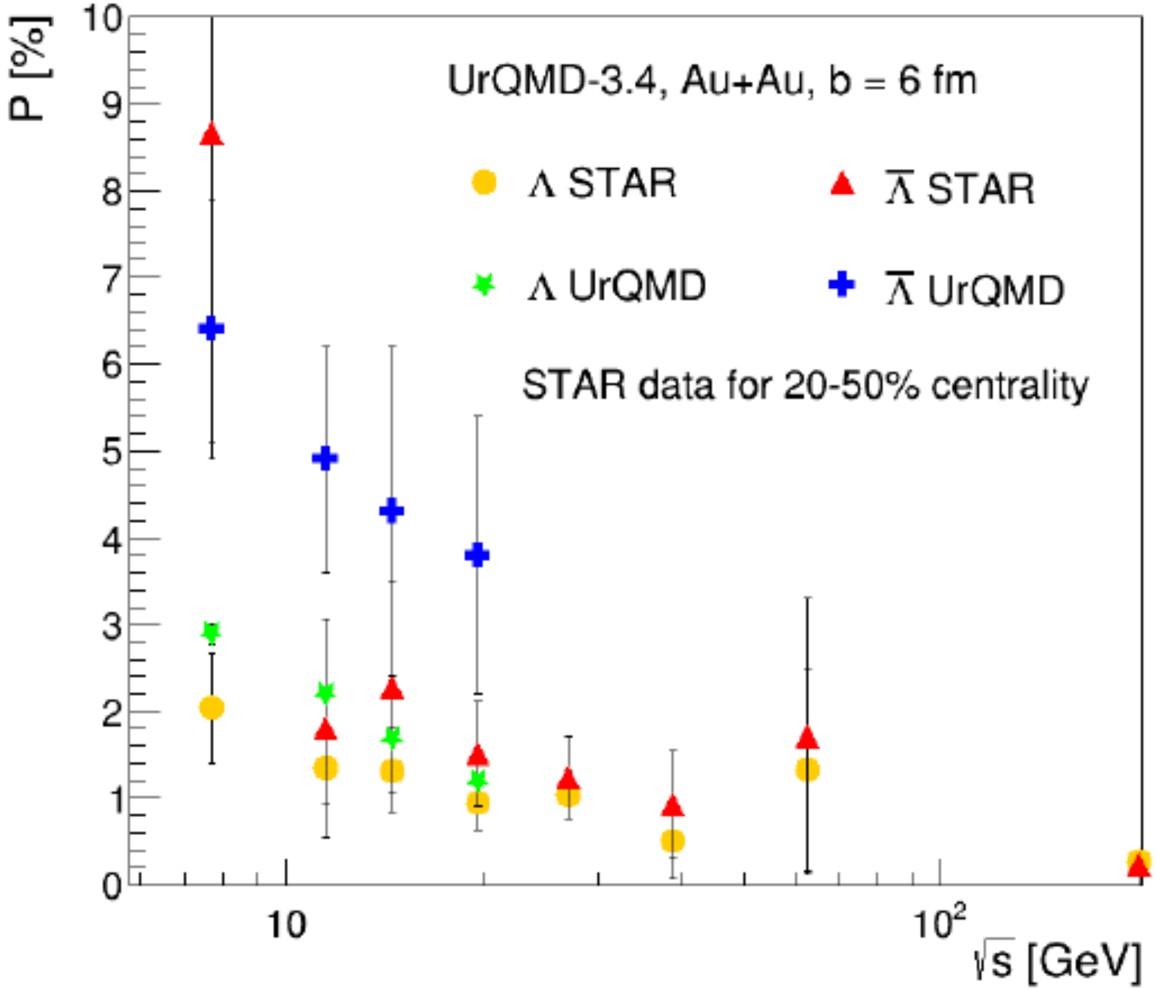

Polarization of Λ and $\bar{\Lambda}$ decreases with energy as in the experiment.
Λ's global polarization agrees well with experimental data. $\bar{\Lambda}$ polarization has right energy dependence.

STAR data from [Phys. Rev. C 98 (2018) 14910]

Freeze-out

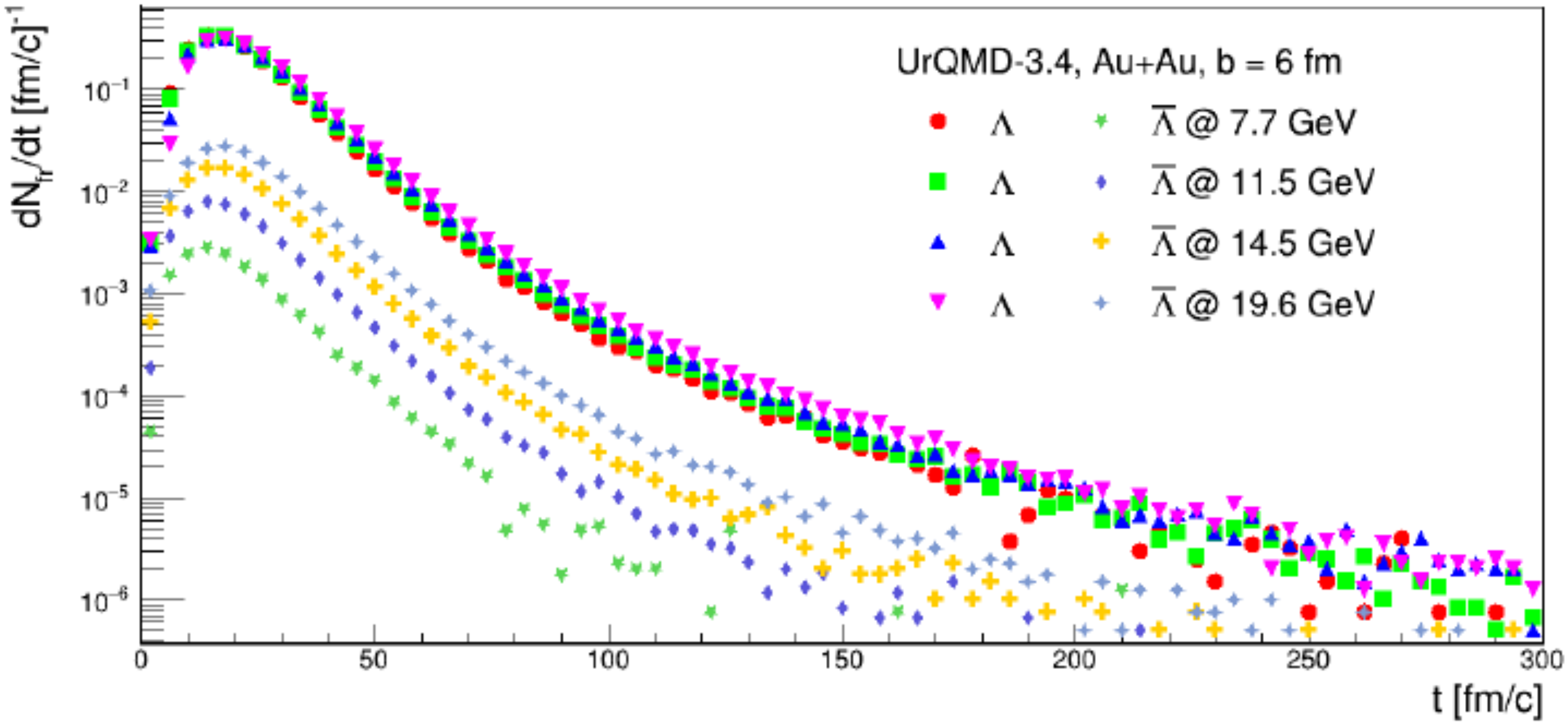

Λ's and $\bar{\Lambda}$'s with $|y| < 1$ and $0.2 < p_t < 3$ GeV/c were analyzed.

$\sqrt{s}$ [GeV]	7.7	11.5	14.5	19.6
Mean freeze-out time Λ [fm/c]	21.3009	21.9568	23.066	24.3462
Mean freeze-out time $\bar{\Lambda}$ [fm/c]	19.7806	21.0302	21.959	23.1288

Proper Temperature

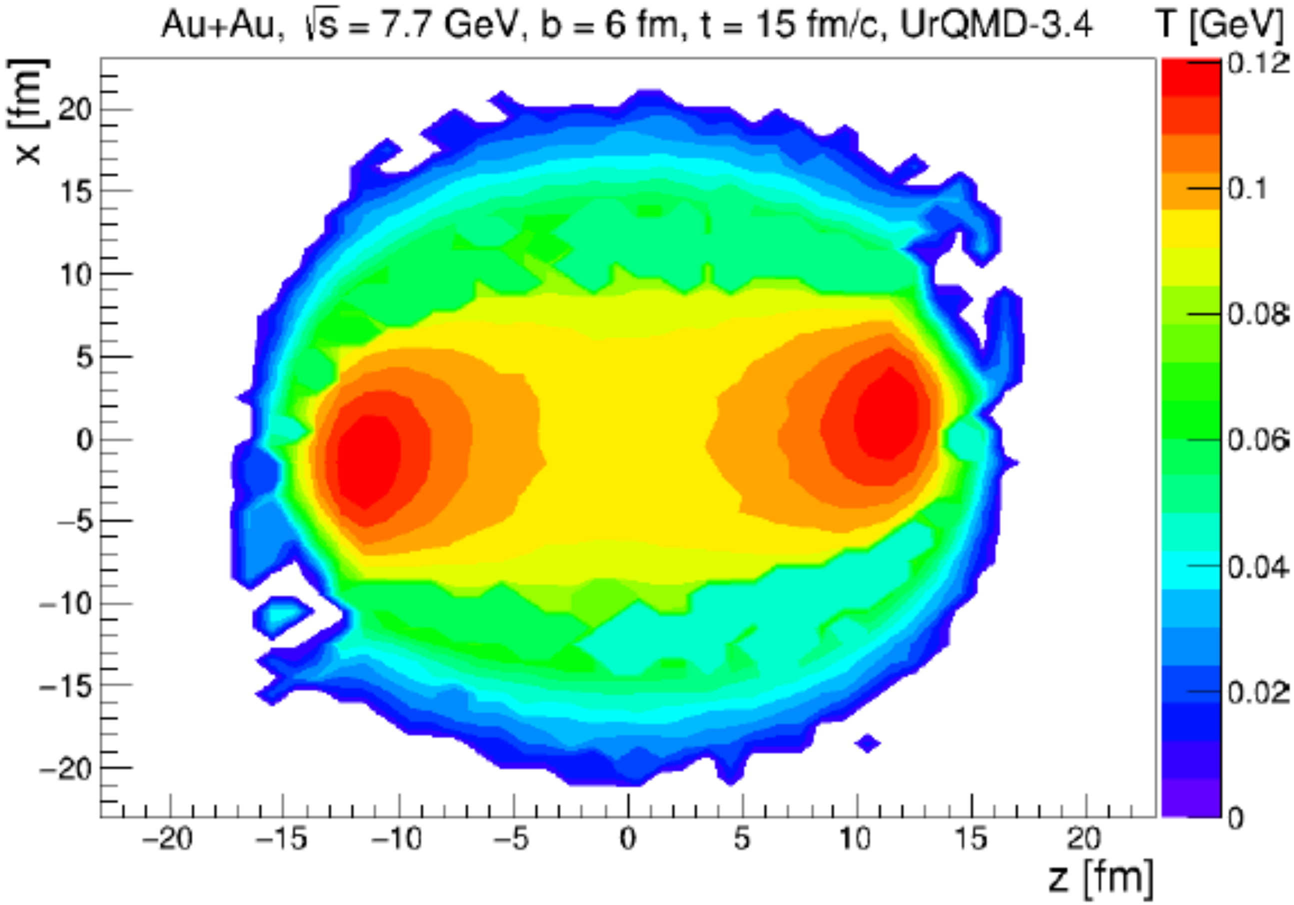

Temperature extracted with statistical model is not uniform. There are two main regions. More hot regions with T $\simeq 100 MeV$ are connected to dense spectators. The other part is related to fireball with temperature $\simeq 60 MeV$.

Thermal vorticity in reaction plane

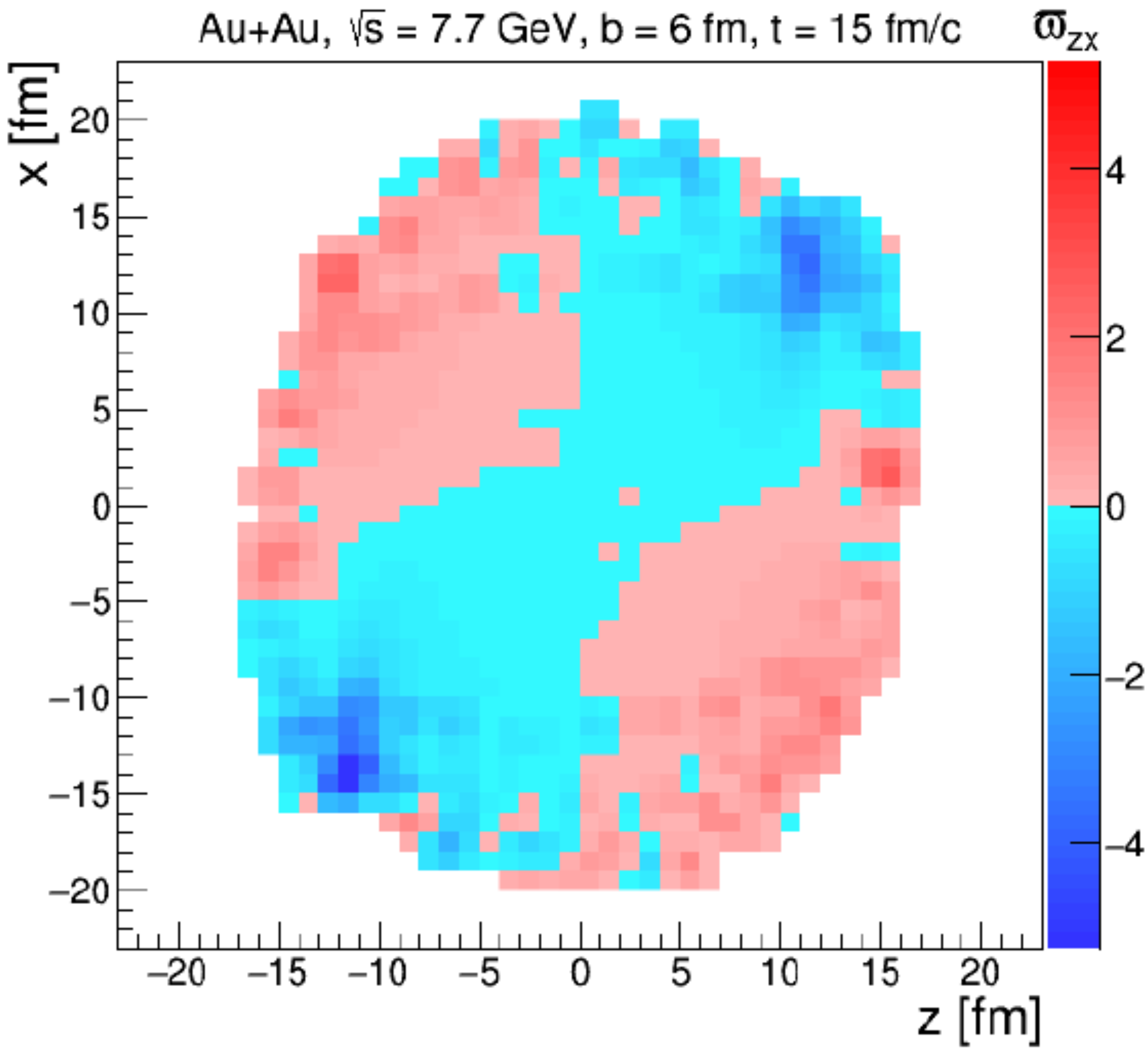

Thermal vorticity component ϖ_{zx} has quadruple-like structure in reaction plane which is stable in time but magnitude decreases due to system expansion. First and third quadrant are connected with central region which has small negative vorticity. This connection part becomes smaller when energy increases.

Polarization time evolution

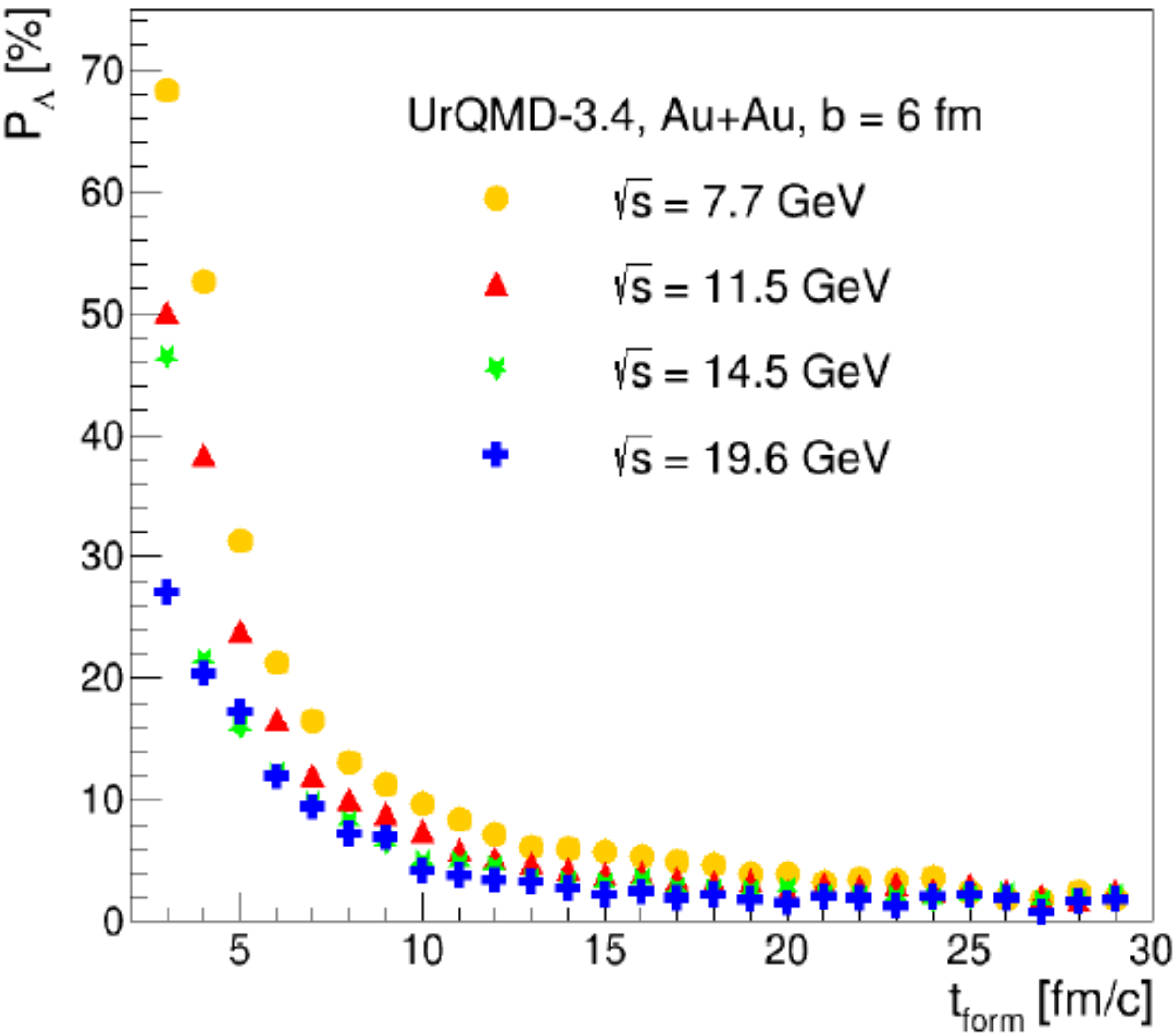

Polarization of Λ hyperon decreases with time. At the beginning lambdas are preferably formed in hot and dense regions with high polarization. But later lambdas are formed uniformly in fireball and average polarization is almost zero.

Polarization energy dependency

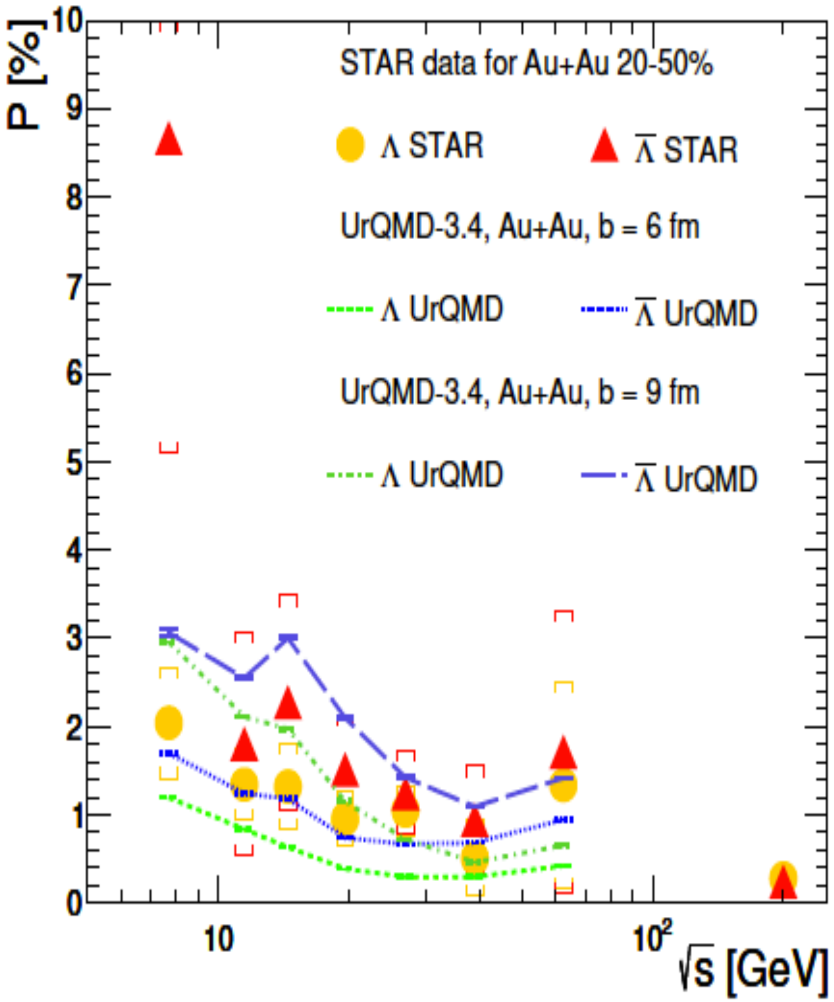

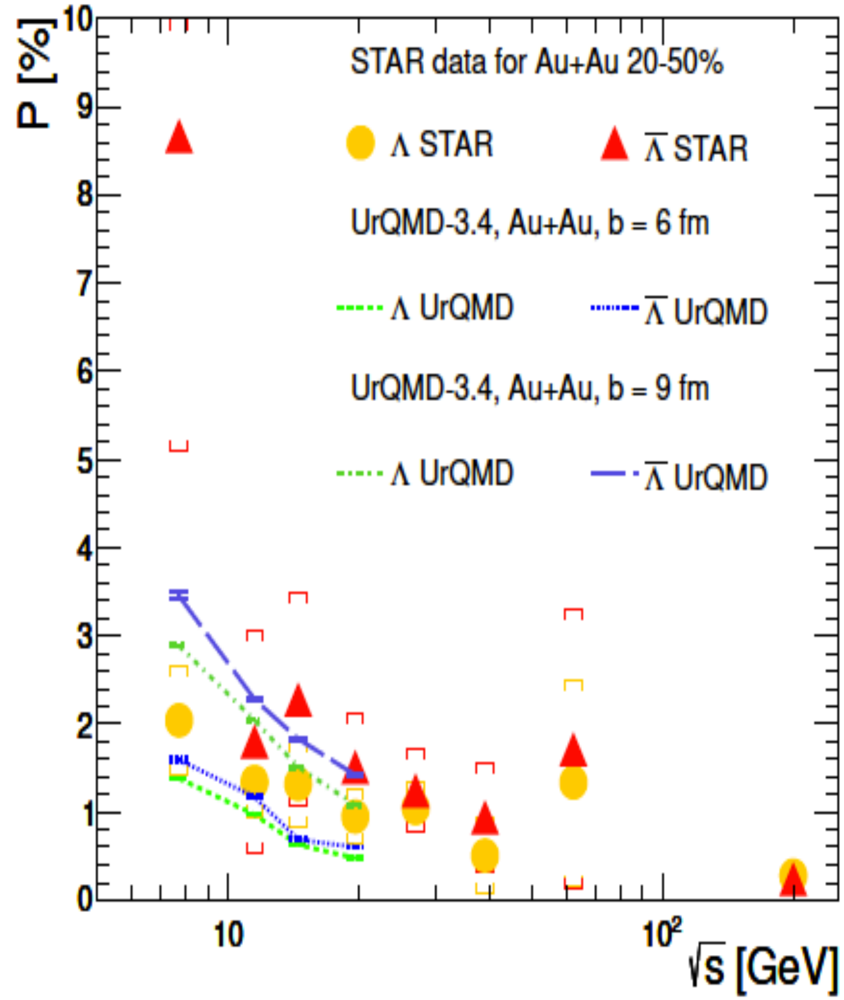

Conclusions

- ***MC models favor chemical equilibration of hot and dense nuclear matter at $t \approx 7$ fm/c***
- ***The EOS has a simple form: P/ε = const (hydro!) even at far-from-equilibrium stage. The speed of sound C^2_s varies from 0.12 (AGS) to 0.14 (40 AGeV), and to 0.15 (SPS & RHIC) => saturation***
- ***In MC models different particles are frozen at different times: K-π-antiΣ-Σ,antip-p-antiΛ-Λ***

and in different space regions with different **T-μ_B-μ_S**

It naturally explanes such effects as **directed flow for p, *Σ, Λ*** **and antiflow for *K-antiΣ-,antip-antiΛ***

and higher polarization for anti-Λ than for Λ at low energies.

IV. Cross-over between phase and space freeze-out (in collaboration with Yu. Sinyukov et al)

Y. Kravchenko(1), L. Bravina(2), E. Khyzhniak(3), G. Nigmatkulov(3), Y. Sinyukov(4), E. Zabrodin(2)

SPATIOTEMPORAL STRUCTURE OF THE PION EMISSION IN AU+AU COLLISIONS AT $\sqrt{s_{NN}}$ = 19.6 GEV IN THE URQMD MODEL

Motivation

Time/hypersurface of pions maximum emission could be analyzed within the two methods.

- The first one utilizes the specific approach for correlation femtoscopy analysis, developed and applied earlier for ultrarelativistic A+A collisions.
- The second one is based on the direct study of the pion kinetic freeze-out in UrQMD.

Main purpose of this research - to examine the consistency of the two methods also at moderate energies of nuclear collisions.

- Were considered Au+Au collisions with energy $\sqrt{s_{NN}} = 19.6\ GeV$
- Selected events with $0 - 5\ \%$ centrality
- Experimental cuts $0.05 < p_t < 1.5\ GeV/c$ and $|\eta| < 0.5$

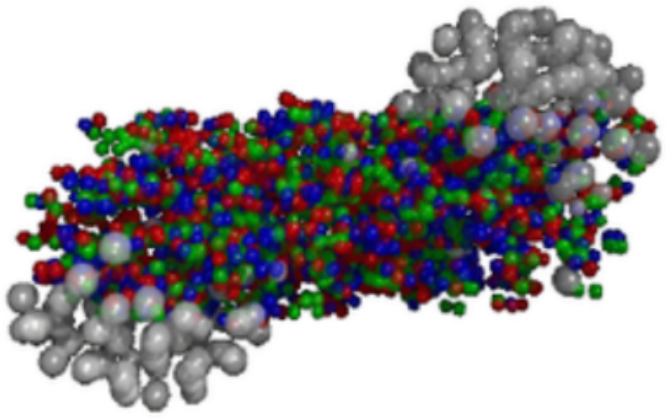

Temperature
from transverse momentum distribution

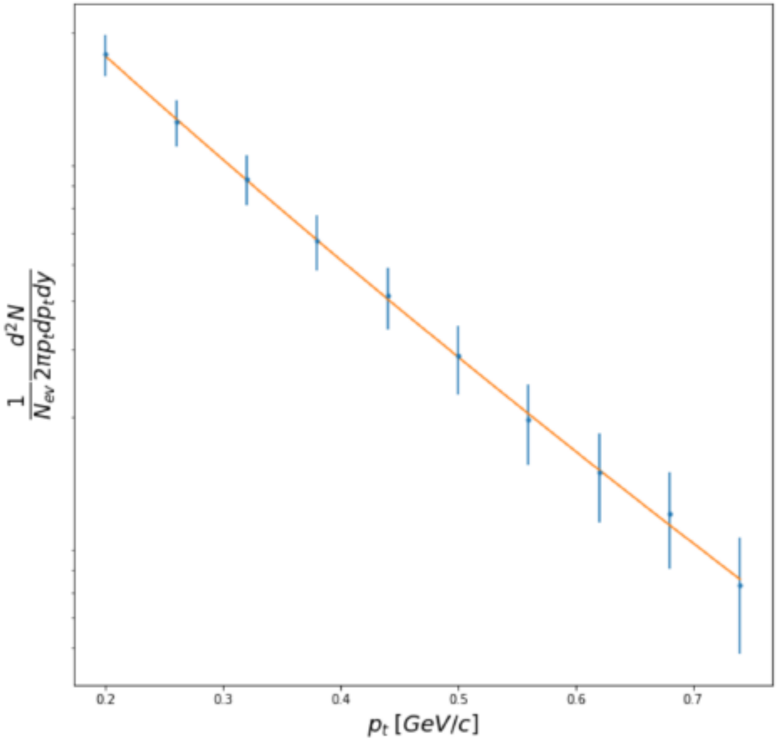

Distribution over p_t in log scale with $y \in [-0.1,\ 0.1]$

$$\frac{p_0 d^3N}{d^3p} = \frac{1}{N_{ev}} \frac{d^2N}{2\pi p_T dp_T dy} \sim e^{-(\frac{m_T}{T}+\alpha)(1-v_T^2)^{1/2}}$$

Where:

$$m_T = \sqrt{m^2 + p_T^2}$$

$$v_T = \frac{k_T}{m_T + T * \alpha}$$

The following temperature was obtained from the fit:

$$\boxed{T = 148\ \pm 1\ MeV}$$

Yu.Sinyukov et al., NPA 946 (2016) 227

Correlation functions

- Charged pions were considered
- Correlation functions built as ratio of distributions with and without weight:

$$C(q_{long}, q_{out}, q_{side}) = \frac{A(q_{long}, q_{out}, q_{side}; w)}{B(q_{long}, q_{out}, q_{side})}$$

$$w = 1 + cos(q \cdot r)$$

q - pair relative 4-momentum,
r - pair relative 4-coordinates
$q_{long}, q_{out}, q_{side}$ - in Bertsch-Pratt parametrization

- Analysed independently pion pairs with $k_T = \frac{|\overrightarrow{p}_{T1} + \overrightarrow{p}_{T2}|}{2}$ in ranges:
[0.05,0.15], [0.15,0.25], [0.25,0.35], [0.35,0.45], [0.45,0.55], [0.55,0.65], [0.65,0.75] GeV/c

The following transformations of relative momentum were applied:

- Lorentz boost into the system of the pair`s center of mass along the Z axis.

- Coordinate rotation according to Bertsch-Pratt parametrization:
  - Long direction - parallel to the beam (z axis)
  - Out direction - parallel to $\overrightarrow{k_T}$
  - Side direction - perpendicular to long and out

Correlation function fit

$$C(q_{long}, q_{out}, q_{side}) = 1 + \lambda \cdot e^{-R_{long}^2 q_{long}^2 - R_{out}^2 q_{out}^2 - R_{side}^2 q_{side}^2}$$

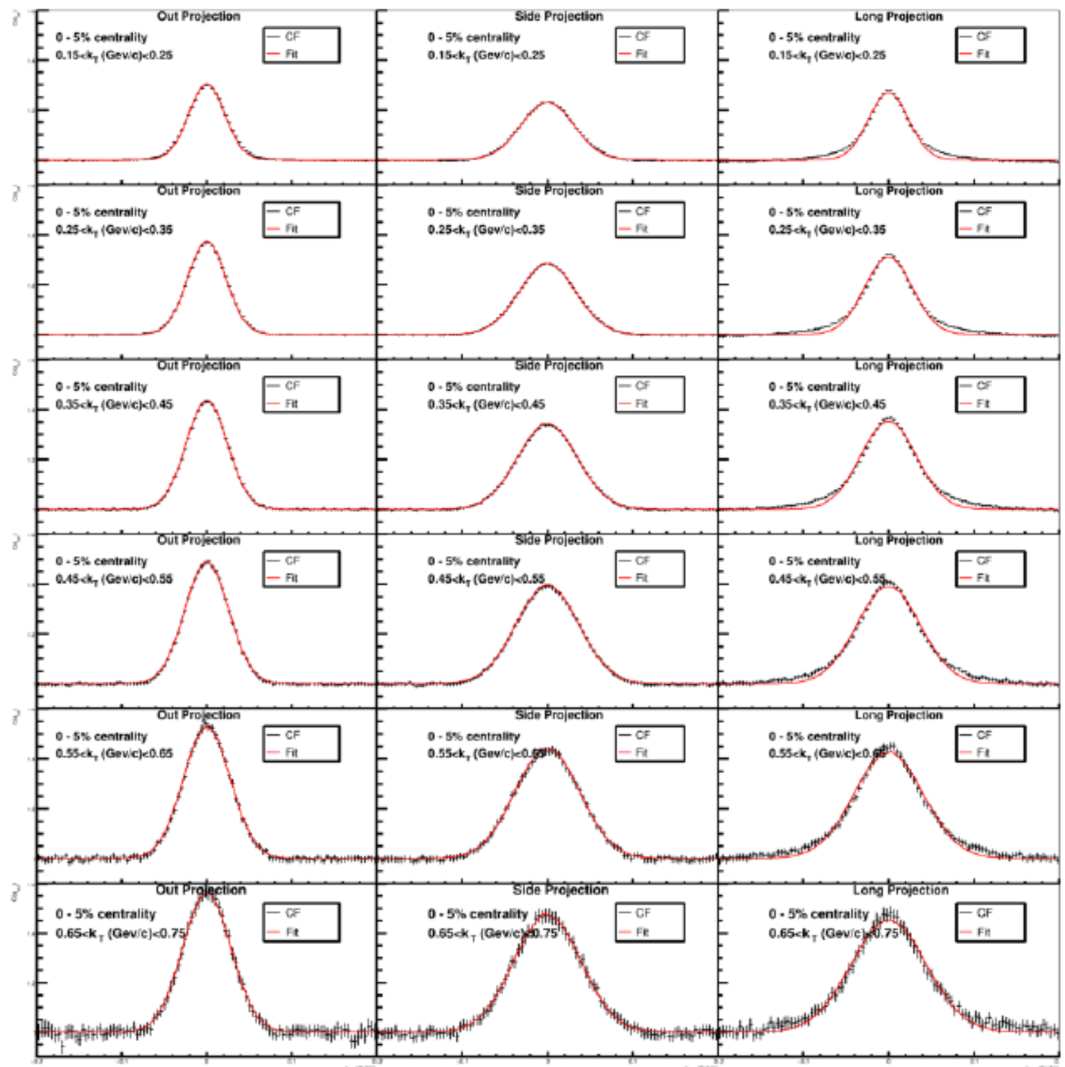
Out Projection
Side Projection
Long Projection
0 - 5% centrality
0.15<k$_T$ (Gev/c)<0.25
0.25<k$_T$ (Gev/c)<0.35
0.35<k$_T$ (Gev/c)<0.45
0.45<k$_T$ (Gev/c)<0.55
0.55<k$_T$ (Gev/c)<0.65
0.65<k$_T$ (Gev/c)<0.75
CF
Fit

m_T dependence of correlation radii

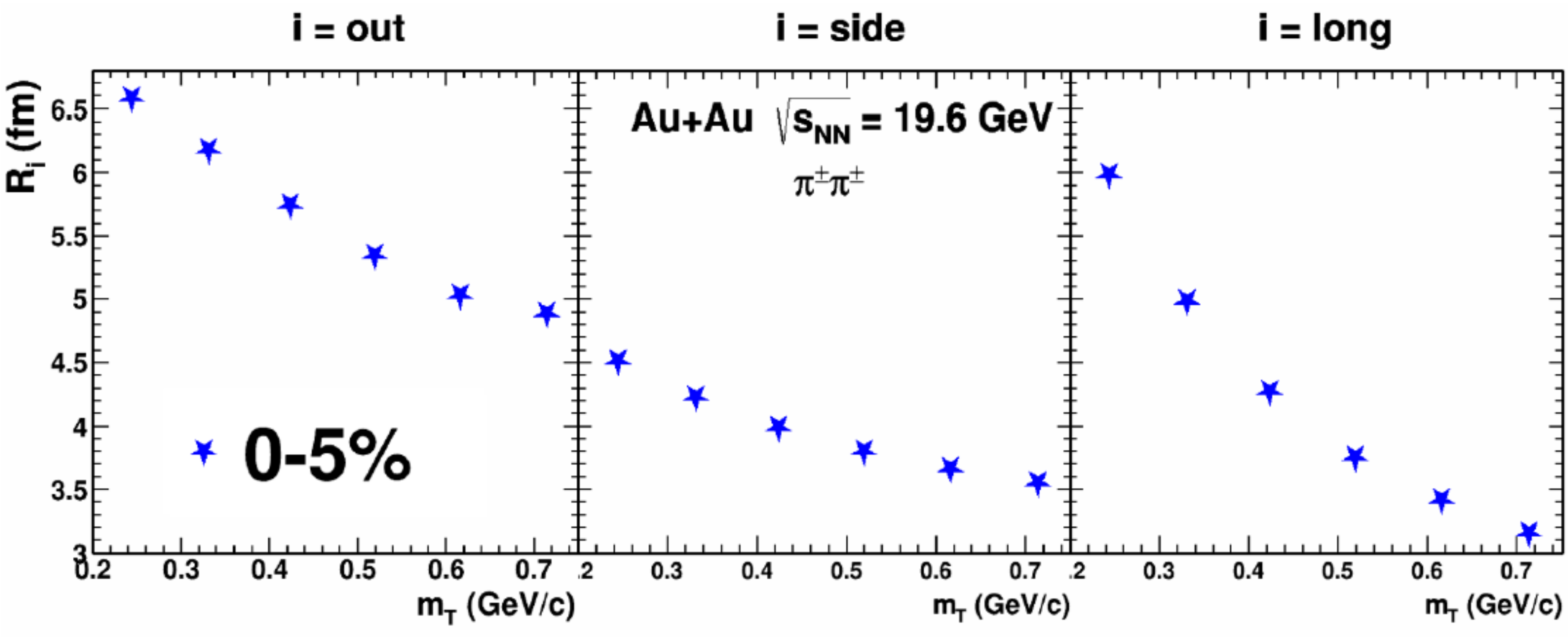

Obtaining τ from R_{long} fit

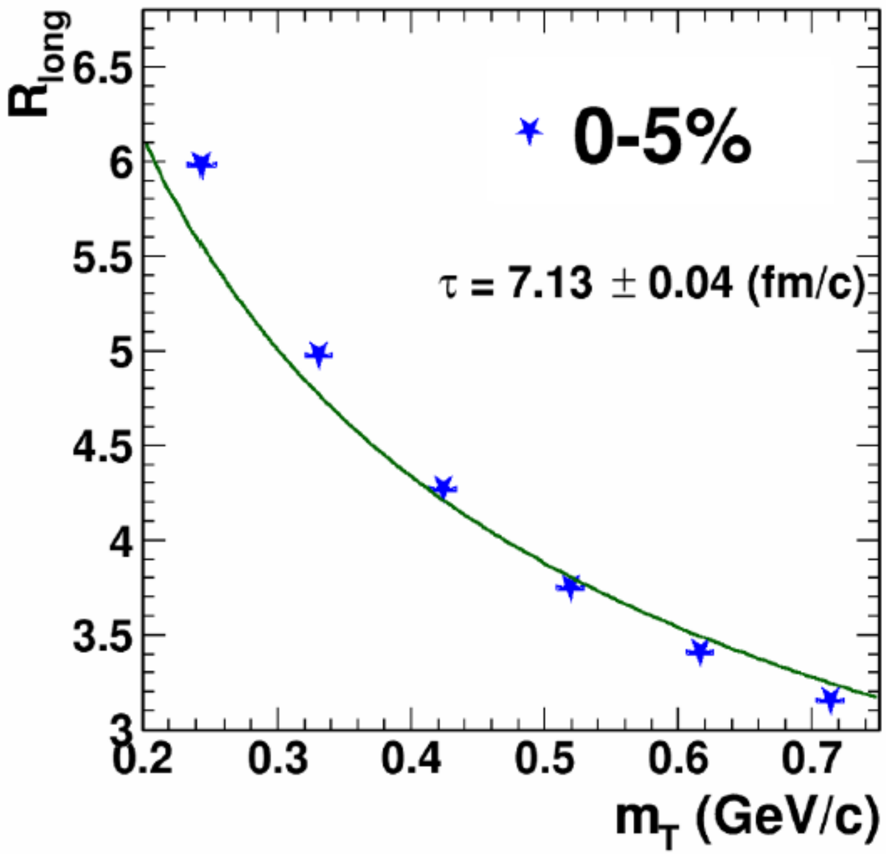

Dependency of R_{long} fitted with:

$$R_{long} = \tau \cdot \sqrt{\frac{T}{m_T}}$$

$$\boxed{\tau = 7.13 \pm 0.04\ fm/c}$$

Obtaining τ from R_{long} fit

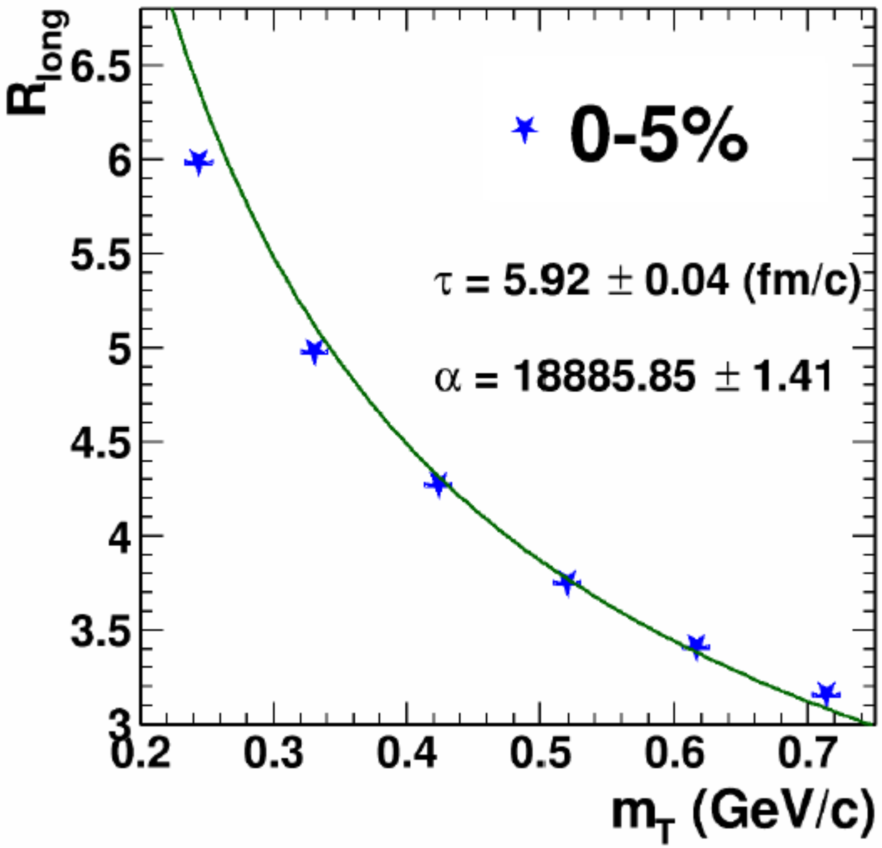

Dependency of R_{long} fitted with:

$$R_{long} = \tau \cdot \lambda\sqrt{1 + \frac{3}{2}\lambda^2}$$

where:

$$\lambda^2 = \frac{T}{m_T}\sqrt{1 - v_T^2}$$ - homogeneity length in longitudinal direction

$$v_T = \frac{k_T}{m_T + \alpha T}$$ - transverse velocity in the saddle point

$$\boxed{\tau = 5.92 \pm 0.04\ fm/c}$$

Yu.Sinyukov et al., NPA 946 (2016) 227

Emission function distribution

The second approach is based on a direct analysis of the last collision points. In UrQMD full information about last collision points is available, that allows studying the spatiotemporal structure of emission function straightforwardly.

Considered distribution of π^+ kinetic freeze-out:

$$\frac{dN^2}{r_T \cdot d\tau dr_T}$$

Where:

$$\tau = \sqrt{t^2 - z^2}$$

$$r_T = \sqrt{r_x^2 + r_y^2}$$

With the following cuts:

Time-space rapidity: $|\frac{1}{2} \cdot ln\frac{t+z}{t-z}| < 0.5$

Momentum rapidity: $|\frac{1}{2} \cdot ln\frac{E+p_z}{E-p_z}| < 0.5$

Distributions built separately for p_T in ranges:
[0,0.1], [0.1,0.2], [0.2,0.3], [0.3,0.4], [0.4,0.5], [0.5,0.6], [0.6,0.7], [0.7,0.8], [0.8,0.9]

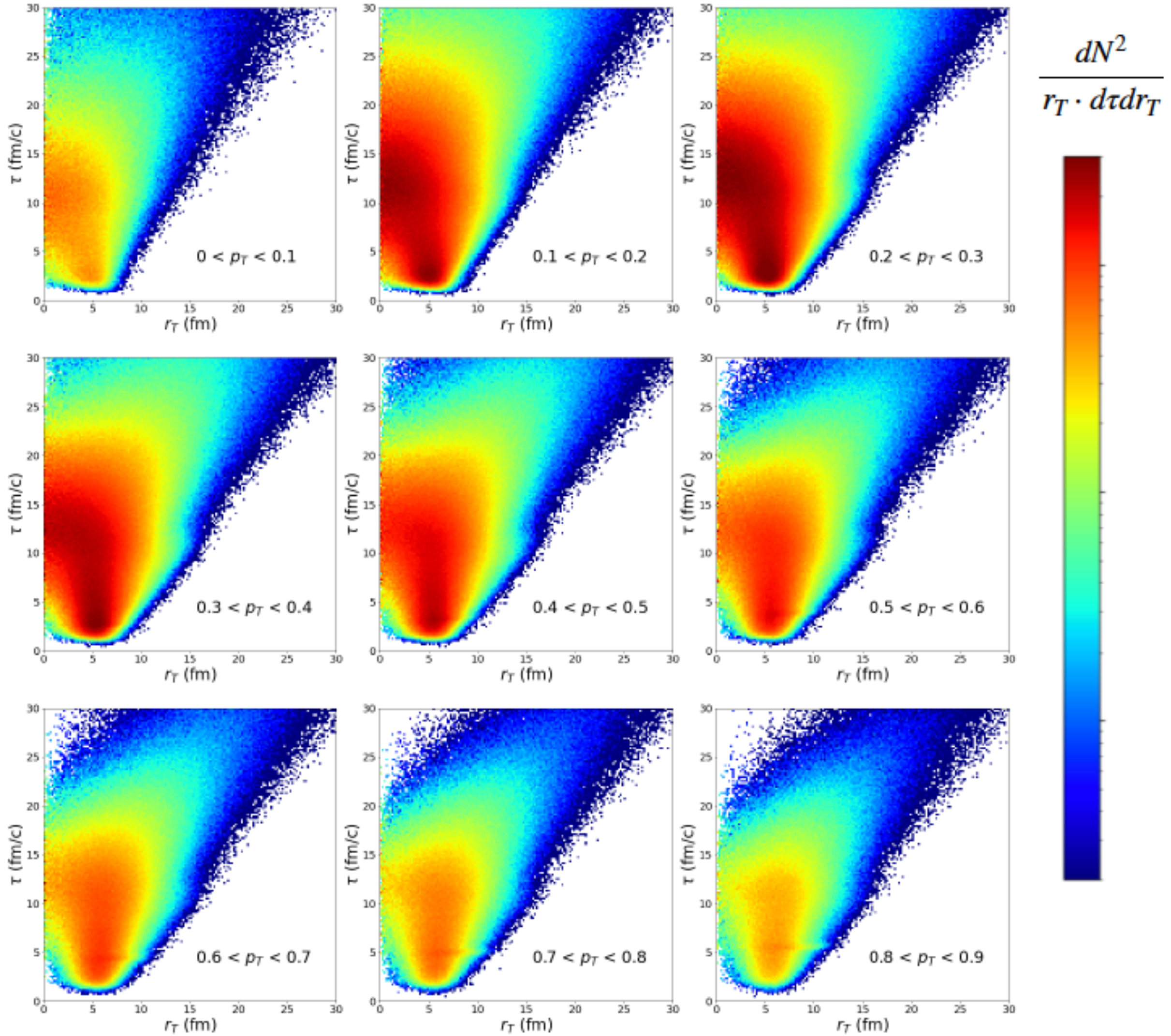
$0 < p_T < 0.1$
$0.1 < p_T < 0.2$
$0.2 < p_T < 0.3$
$0.3 < p_T < 0.4$
$0.4 < p_T < 0.5$
$0.5 < p_T < 0.6$
$0.6 < p_T < 0.7$
$0.7 < p_T < 0.8$
$0.8 < p_T < 0.9$
τ (fm/c)
r_T (fm)
$\frac{dN^2}{r_T \cdot d\tau dr_T}$

To the accordance with asymptotic formulas, high-p_T will be considered further.

In the area of $p_T > 0.4$ GeV/c maximum absolute value is observed in the interval of [0.6, 0.7] GeV/c

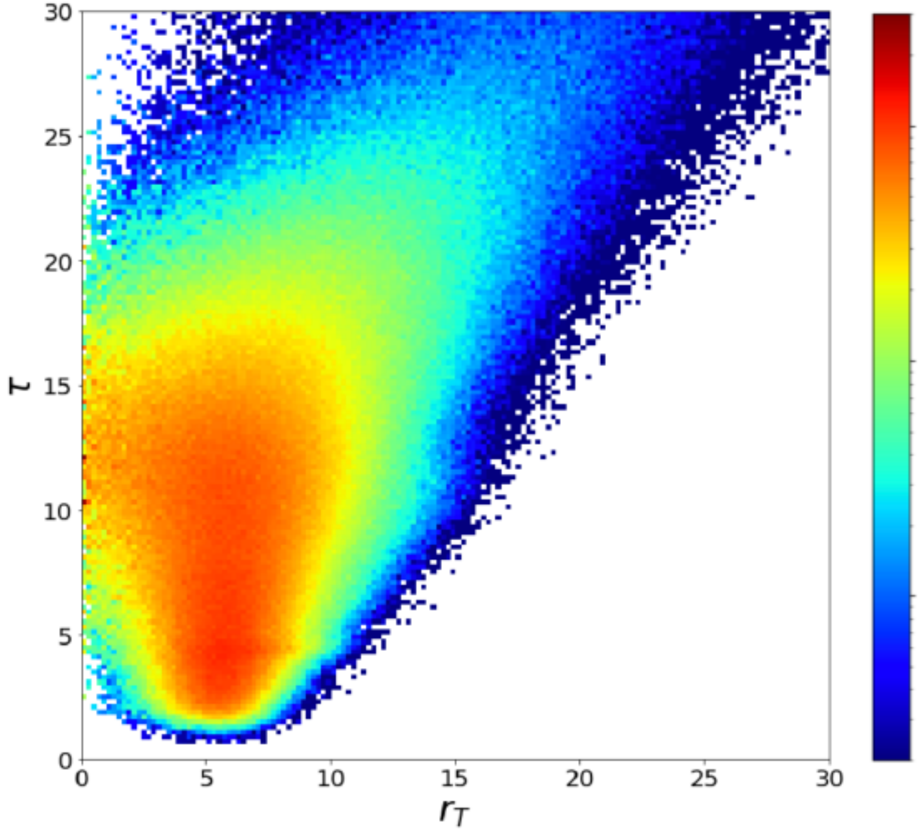

Maximum emission, τ_{max}, could be obtained from the fit:

$$g(\tau) \sim e^{-\frac{(\tau - \tau_{max})^2}{2 \cdot d^2}}$$

where d - emission duration

To move to the distribution over τ, the r_T integration interval has to be selected

Interval over r_T is centered around the point of distribution maximum value

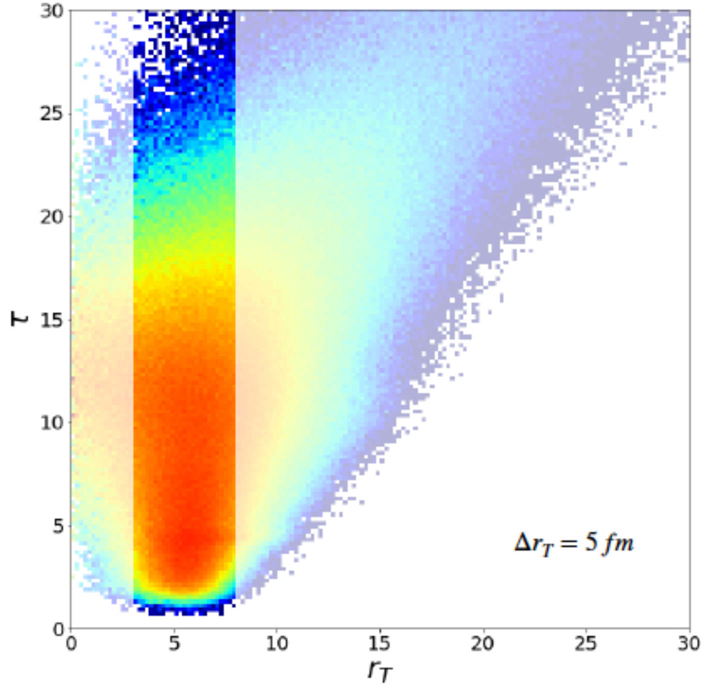

The 10% and 30% of points were truncated from the left and right distribution edge correspondingly, due to asymmetry of the distribution

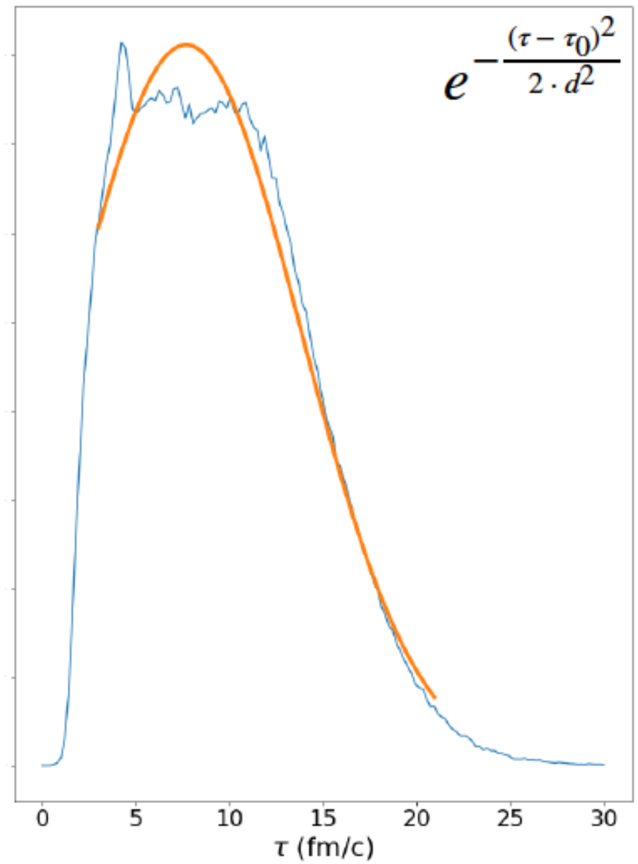

Different width of r_T regions were considered for extraction of τ.

r_T variation defines the uncertainty of the final value:

$$\boxed{\tau = 7.03 \pm 0.88\ fm/c}$$

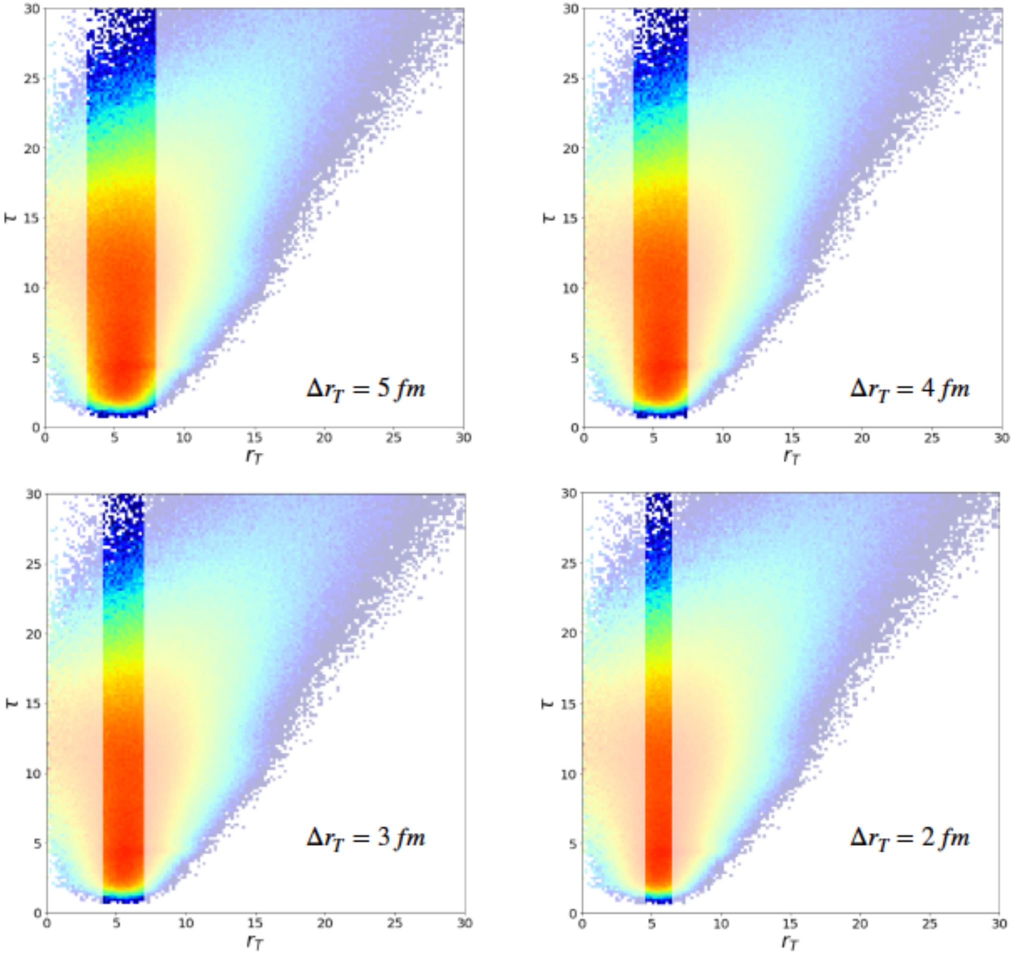

Comparison

Maximum emission time from correlation femtoscopy:

Fitting $R_{long} = \tau \cdot \sqrt{\frac{T}{m_T}}$

$$\boxed{\tau = 7.13 \pm 0.04\ fm/c}$$

Fitting R_{long} accordingly to Yu.Sinyukov et al., NPA 946 (2016) 227

$$\boxed{\tau = 5.92 \pm 0.04\ fm/c}$$

Maximum emission time from distribution of emission function:

$$\boxed{\tau = 7.03 \pm 0.88\ fm/c}$$

Conclusions

To compare approaches to pions emission analysis at moderate energies of nuclear collisions, Au+Au collisions at $\sqrt{s_{NN}} = 19.6$ GeV in the UrQMD model were considered.

- Temperature was obtained from the spectrum over p_T
- Correlation function in Bertsch-Pratt parametrization was built
- τ was extracted from $R_{long}(m_T)$ dependency
- Kinetic freeze-out distribution was considered directly and τ obtained

Correlation femtoscopy approach has shown consistency with straightforward kinetic freeze-out analysis

3FD-Hydro and polarization byYu.B. Ivanov

3-Fluid Dynamics (3FD)

Target-like fluid: $\partial_\mu J_t^\mu = 0$ $\quad \partial_\mu T_t^{\mu\nu} = -F_{tp}^\nu + F_{ft}^\nu$

Leading particles carry bar. charge $\quad$ exchange/emission

Projectile-like fluid: $\partial_\mu J_p^\mu = 0,$ $\quad \partial_\mu T_p^{\mu\nu} = -F_{pt}^\nu + F_{fp}^\nu$

Fireball fluid: $J_f^\mu = 0,$ $\quad \partial_\mu T_f^{\mu\nu} = F_{pt}^\nu + F_{tp}^\nu - F_{fp}^\nu - F_{ft}^\nu$

Baryon-free fluid $\quad$ Source term $\quad$ Exchange

The source term is delayed due to a formation time τ

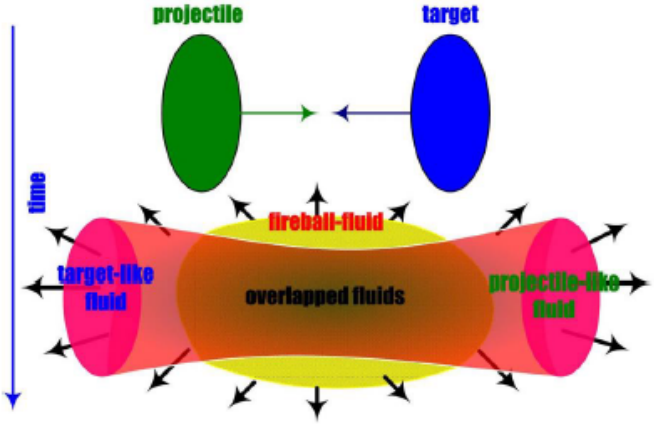

Total energy-momentum conservation:

$$\partial_\mu (T_p^{\mu\nu} + T_t^{\mu\nu} + T_f^{\mu\nu}) = 0$$

Ivanov, Russkikh, Toneev, PRC 73, 044904 (2006)

Physical Input

- ✓ Equation of State
- ✓ Friction
- ✓ Freeze-out energy density $\varepsilon_{frz} = 0.4$ GeV/fm^3

Calculations of polarization at NICA energies

Only few calculations at $\sqrt{s_{NN}} <$ 7.7 GeV

✓Within thermodynamic approach by *Becattini et al.*

Deng, Huang, Ma, Zhang, PRC 101, 064908 (2020) [UrQMD, mean vorticity] [Shanghai]

Ivanov, et al., PRC 100, 014908 (2019), PRC 102, 024916 (2020) [3FD model] [Dubna]

✓Within axial-vortical-effect approach *[Sorin&Teryaev, PRC 95, 011902 (2017)]*

Baznat, Gudima, Sorin, Teryaev, PRC 97, 041902 (2018) [QGSM model] [Dubna]

Ivanov, 2006.14328 [nucl-th] [3FD model] [Dubna]

Equilibration at NICA energies

Longitudinal and transverse pressure
in the center of colliding nuclei

Ivanov, Soldatov, PRC C 101, 024915 (2020)

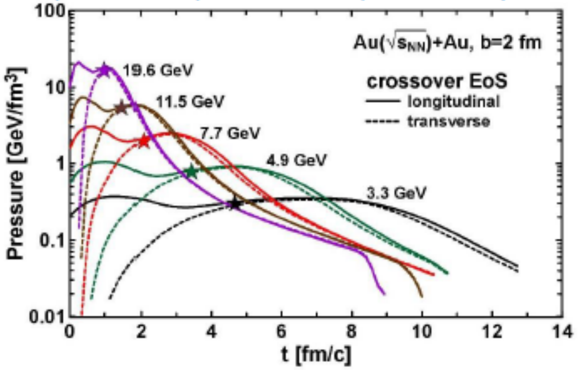

Mechanical equilibration time is
comparatively long

Freeze-out is mechanically equilibrium.
This of prime importance for the models.

Ivanov, Soldatov, EPJ A 52 (2016) 12, 367

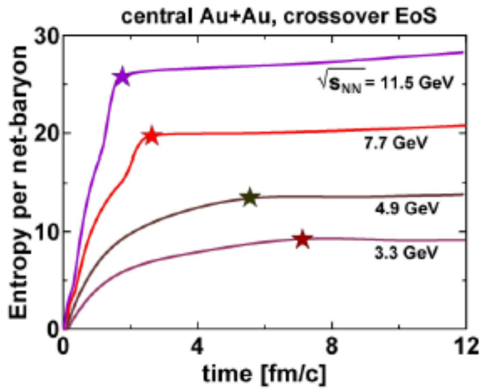

Chemical equilibration (and hence thermalization)
takes longer

Thermalization at NICA energies

Other models result in similar thermalization times

Bravina et al., PRC 78, 014907 (2008); De et al., PRC 94, 054901 (2016);
Khvorostukhin, Toneev, Phys.Part.Nucl.Lett. 14 (2017), 9; Teslyk et al., PRC 101, 014904 (2020)

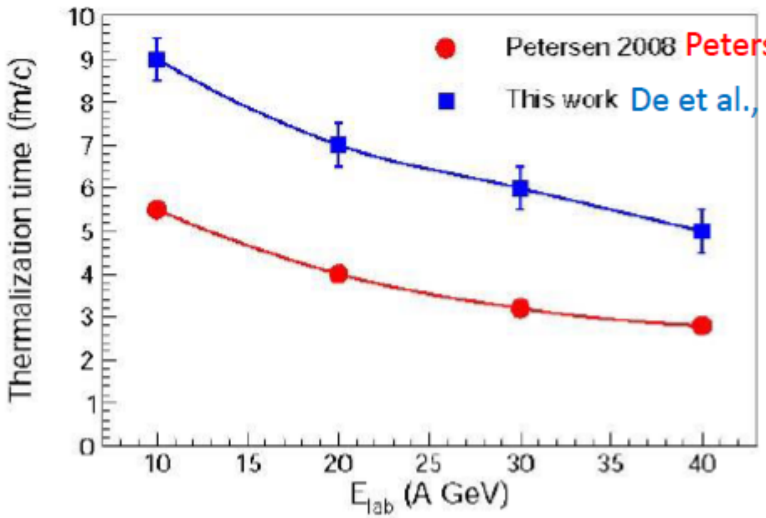

Petersen et al., PRC 78, 044901 (2008) [twice overlap time]

De et al., PRC 94, 054901 (2016) [UrQMD]

For comparison:
Mechanical Equilibration at 10 A GeV
$\approx$ 3.5 fm/c

The system is thermalized at the freeze-out stage, although it can be reached right before the freeze-out

Thermodynamic approach

Relativistic Thermal Vorticity

$$\varpi_{\mu\nu} = \frac{1}{2}(\partial_\nu \hat{\beta}_\mu - \partial_\mu \hat{\beta}_\nu),$$

where $\hat{\beta}_\mu = \hbar \beta_\mu$ and $\beta_\mu = u_\nu / T$ with $T =$ the local temperature.

ϖ is related to **mean spin vector, $\Pi^\mu(p)$, of a spin 1/2 particle** in a relativistic fluid [F. Becattini, et al., Annals Phys. **338**, 32 (2013)]

$$\Pi^\mu(p) = \frac{1}{8m} \frac{\int_\Sigma \mathrm{d}\Sigma_\lambda p^\lambda n_F(1 - n_F)\, p_\sigma \epsilon^{\mu\nu\rho\sigma} \partial_\nu \hat{\beta}_\rho}{\int_\Sigma \Sigma_\lambda p^\lambda\, n_F},$$

n_F = Fermi-Dirac distribution function,
integration over the freeze-out hypersurface Σ.

Axial vortical effect (AVE)

Axial current

$$J_5{}^{\nu}(x) = -N_c\left(\frac{\mu^2}{2\pi^2} + \kappa\frac{T^2}{6}\right)\epsilon^{\nu\alpha\beta\gamma}u_\alpha\omega_{\beta\gamma}$$

induced by vorticity

$$\omega_{\mu\nu} = \frac{1}{2}(\partial_\nu u_\mu - \partial_\mu u_\nu)$$

Vilenkin, PRD 20, 1807 (1979); 21, 2260 (1980).

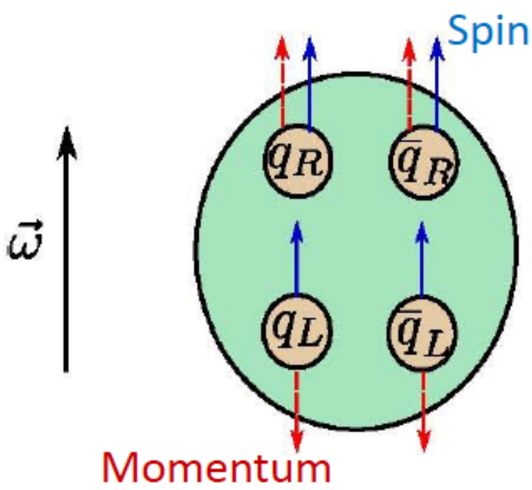

Gao, et al., PRL 109 (2012) 232301

$\frac{\mu^2}{2\pi^2}$ = axial anomaly term is topologically protected

$\kappa\frac{T^2}{6}$ = holographic gravitational anomaly

Landsteiner, Megias, Melgar, Pena-Benitez, JHEP 1109, 121 (2011) [Gauge-gravity correspondence]

Lattice QCD results in $\kappa = 0$ in confined phase and $\kappa \leq 0.1$ in deconfined phase

[Braguta, et al., PRD 88, 071501 (2013); 89, 074510 (2014)]

AVE polarization

Assuming axial-charge conservation at hadronization

$$P_{\Lambda} = \int d^3x \, (J_{5s}{}^0/u_y) \, /(N_{\Lambda} + N_{\bar{K}^*})$$

$$P_{\bar{\Lambda}} = \int d^3x \, (J_{5s}{}^0/u_y) \, /(N_{\bar{\Lambda}} + N_{K^*})$$

u_y results from boost to the local rest frame of the matter

Sorin and Teryaev, PRC 95, 011902 (2017)

In principle, an alternative assumption is possible.

Coalescence-like hadronization: quarks coalesce into hadrons, keeping their polarization.

Polarization increases with $\sqrt{s_{NN}}$ decrease

AVE approach predicts higher polarization at low energies than **thermodyn. one**

Baznat, Gudima, Sorin, Teryaev, PRC 97, 041902 (2018)

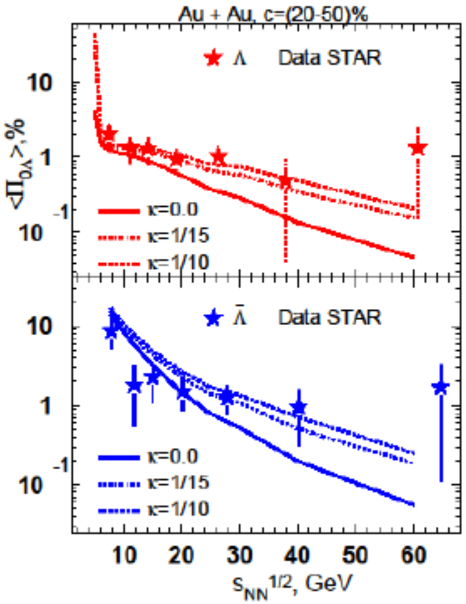

Ivanov, 2006.14328

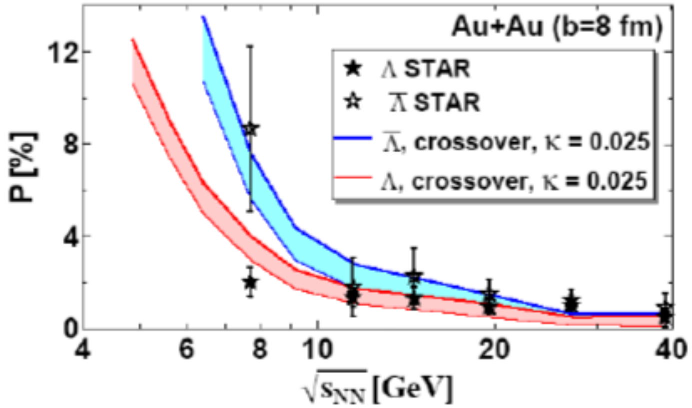

Ivanov, Soldatov, PRC 102, 024916 (2020)

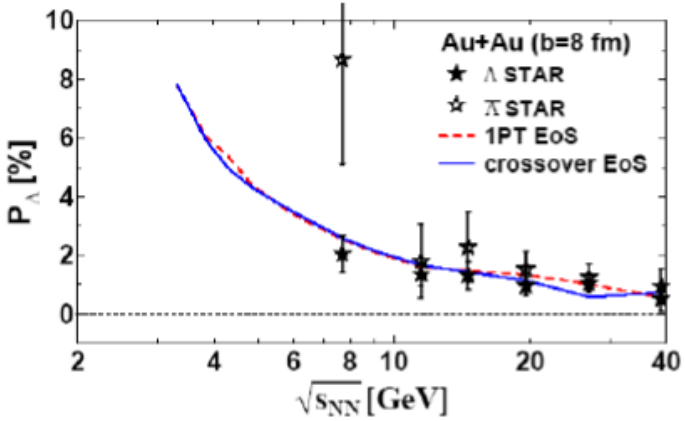

NICA data will distinguish between AVE and thermodynamic predictions

Λ -- $\bar{\Lambda}$ polarization splitting (1)

In the standard thermodynamic approach this splitting is either very small

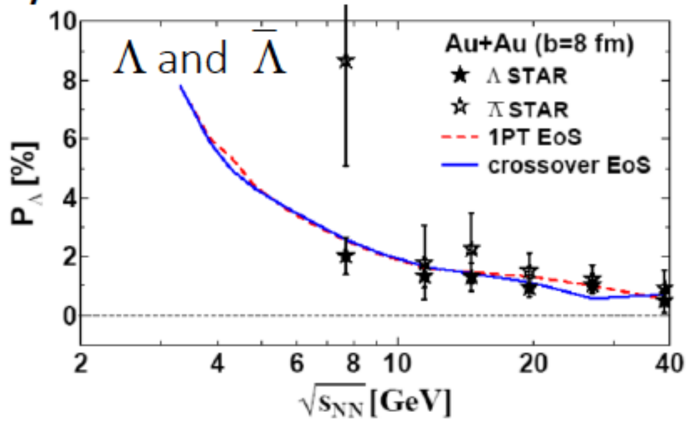

or simply small, if different freeze-out for Λ and $\bar{\Lambda}$ is taken into account,

Vitiuk, Bravina and Zabrodin, Phys. Lett. B 803, 135298 (2020)

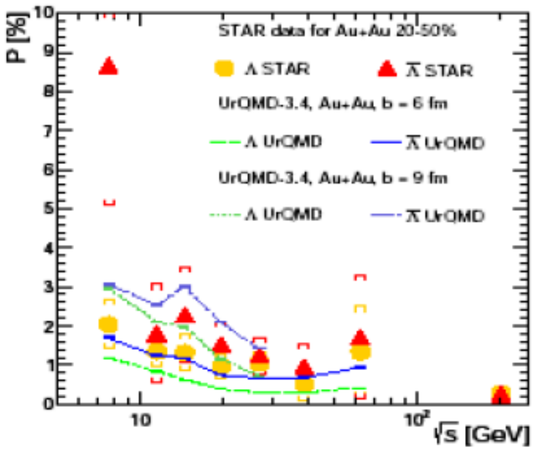

while exp. difference is large at 7.7 GeV, although error bars for $\bar{\Lambda}$ are also large.

Λ -- $\bar{\Lambda}$ polarization splitting (2)

A possible reason: presence of a strong electro-magnetic field:

$$\varpi_{\rho\sigma} \rightarrow \varpi_{\rho\sigma} + \frac{\mu}{S} F_{\rho\sigma}$$

Becattini, et al. PRC 95, 054902 (2017)

Still open question:

if required strong magnetic field is generated at freeze-out?

Discussion in [Becattini and Lisa, arXiv:2003.03640]

Λ -- $\bar{\Lambda}$ polarization splitting (3)

Interaction mediated by massive vector and scalar bosons (Walecka-like model)

Csernai, Kapusta, Welle, PRC 99, 021901 (2019)

This is a dynamical (rather than thermodynamical) mechanism: polarization itself should differ from the thermodynamical one.

Xie, Chen, Csernai, arXiv:1912.00209

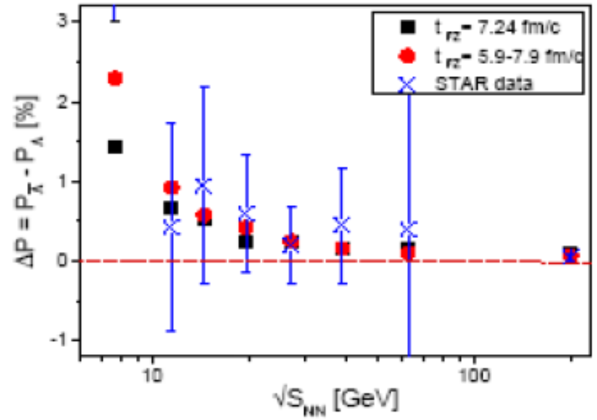

Glauber: More Λ's than $\bar{\Lambda}$'s are produced in corona.

Assumption: Polarization in corona is negligible.

Ayala, et al., arXiv:2003.13757, PLB accepted

Also a completely dynamical (rather than thermodynamical) mechanism

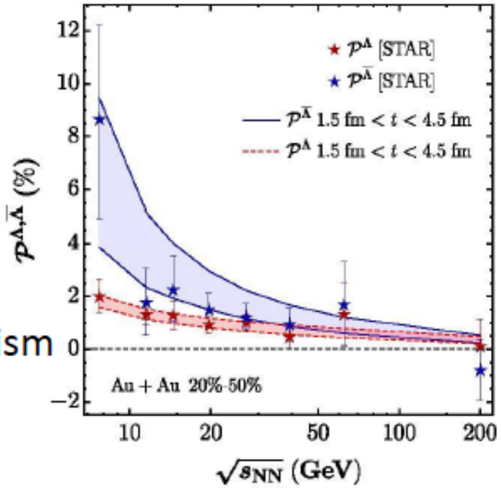

Λ -- $\bar{\Lambda}$ polarization splitting (4)

AVE approach naturally predicts the Λ -- $\bar{\Lambda}$ polarization splitting

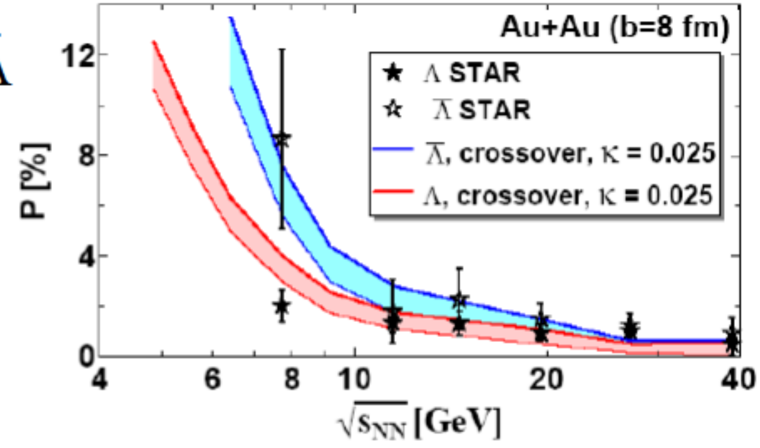

Measurements at NICA can refine the data at 7.7 GeV and extend them down to 5 GeV

and thus clarify the nature of the Λ -- $\bar{\Lambda}$ polarization splitting

Fixed-target experiments

Ivanov, et al., PRC 100, 014908 (2019), Phys.Atom.Nucl. 83, 179 (2020)

BM@N at JINR, CBM at FAIR, STAR FXT, HADES

Rapidity dependence of polarization is still under debates
[Becattini and Lisa, arXiv:2003.03640]

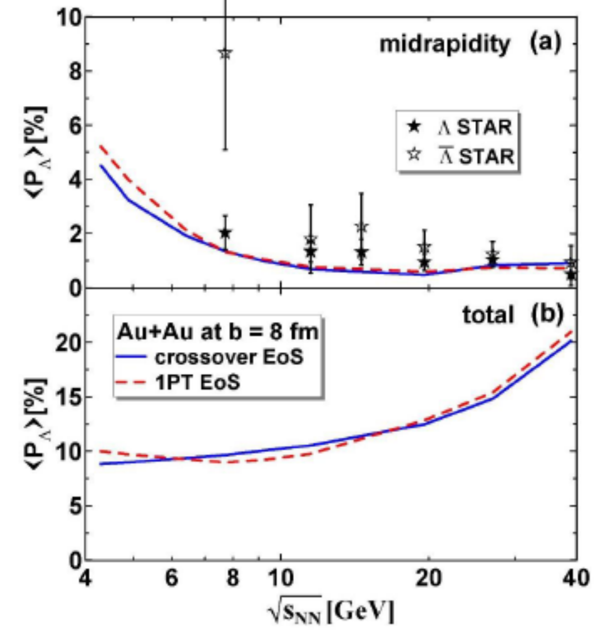

3FD: **total Λ polarization (i.e. averaged over all rapidities)** increases with collision energy rise, in contrast to **midrapidity polarization**.

In means
- ✓ Λ polarization in target fragmentation region is higher than the midrapidity one
- ✓ It increases with collision energy rise

It would be interesting to check these predictions

Summary

✓NICA data will distinguish between AVE and thermodynamic predictions

✓Measurements at NICA can clarify the nature of the Λ -- $\bar{\Lambda}$ splitting

✓Measurements of local longitudinal Λ polarization are also possible at $\sqrt{s_{NN}} \geq$ 6 GeV

✓Polarization measurements at NICA are planned in 2025

✓Fixed-target experiments will clarify rapidity dependence of the polarization

Conclusions

- *MC models favor chemical equilibration of hot and dense nuclear matter at $t \approx 7$ fm/c*
- *The **EOS** has a simple form: $P/\varepsilon = const$ **(hydro!) even at far-from-equilibrium stage.** The speed of sound C^2_s varies from 0.12 (AGS) to 0.14 (40 AGeV), and to 0.15 (SPS & RHIC) => saturation*
- *In MC models different particles are frozen at different times: K-π-antiΣ-Σ,antip-p-antiΛ-Λ*

and in different space regions with different **T-μ_B-μ_S**

It naturally explanes such effects as **directed flow for p, *Σ, Λ* and antiflow for *K-antiΣ-,antip-antiΛ***

and higher polarization for anti-Λ than for Λ at low energies.

PUBLICATIONS FOR 2019-2020

- L. Bravina – 21 publications, ca 10 talks
- Yu. Ivanov - 8 publications, ca 10 talks
- M. Baznat – 5 publications
- E. Zabrodin – 15 publications, ca 10 talks

Chemical Freeze-out

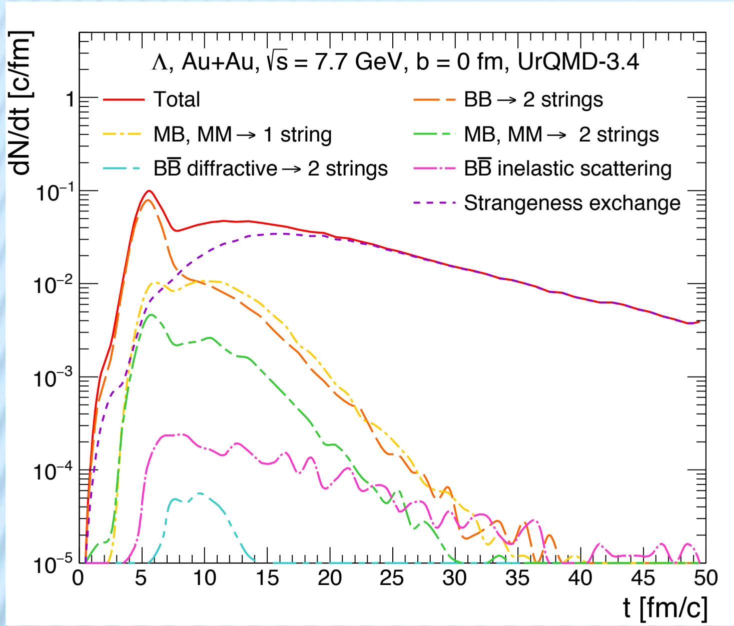

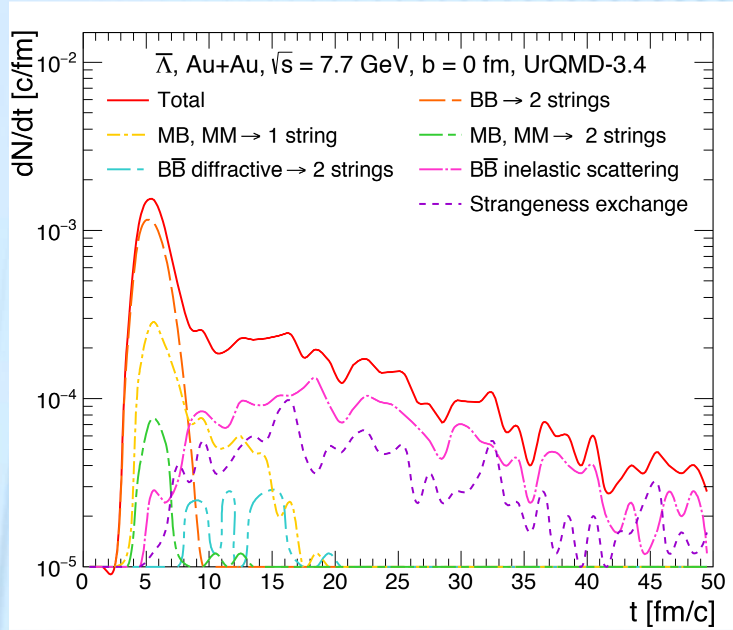

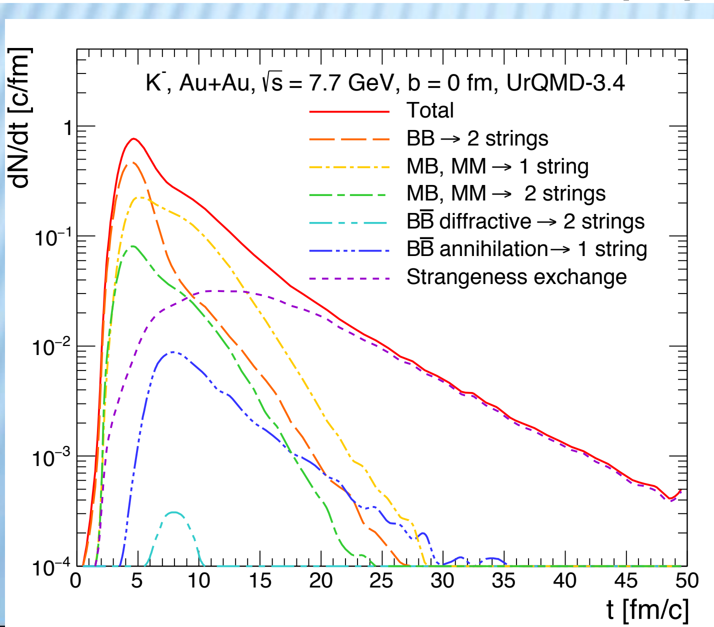

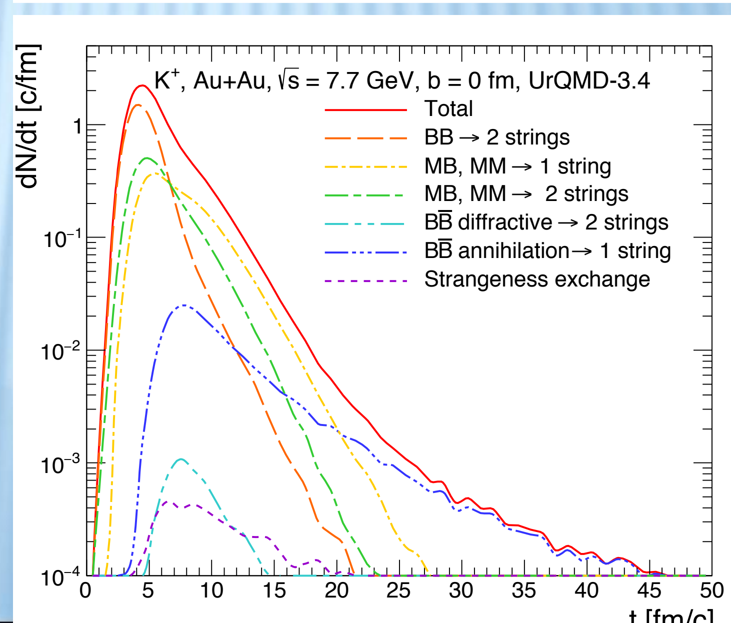

Chemical Freeze-out of pions at b=6 fm

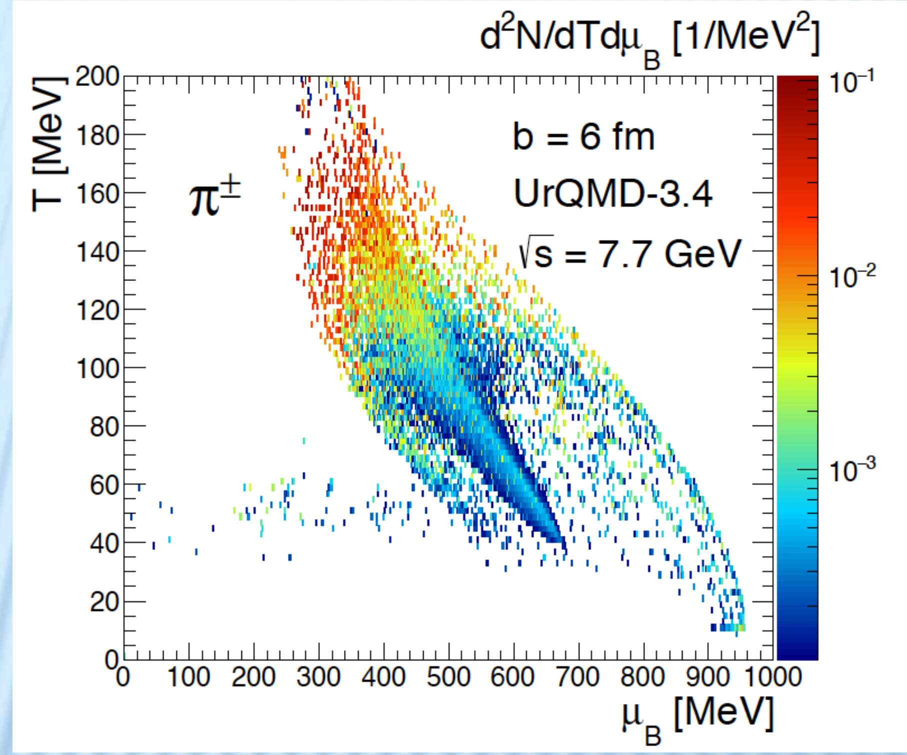

BOX: HAGEDORN-LIKE LIMITING TEMPERATURE

M.Belkacem et al., PRC 58, 1727 (1998)

HSD

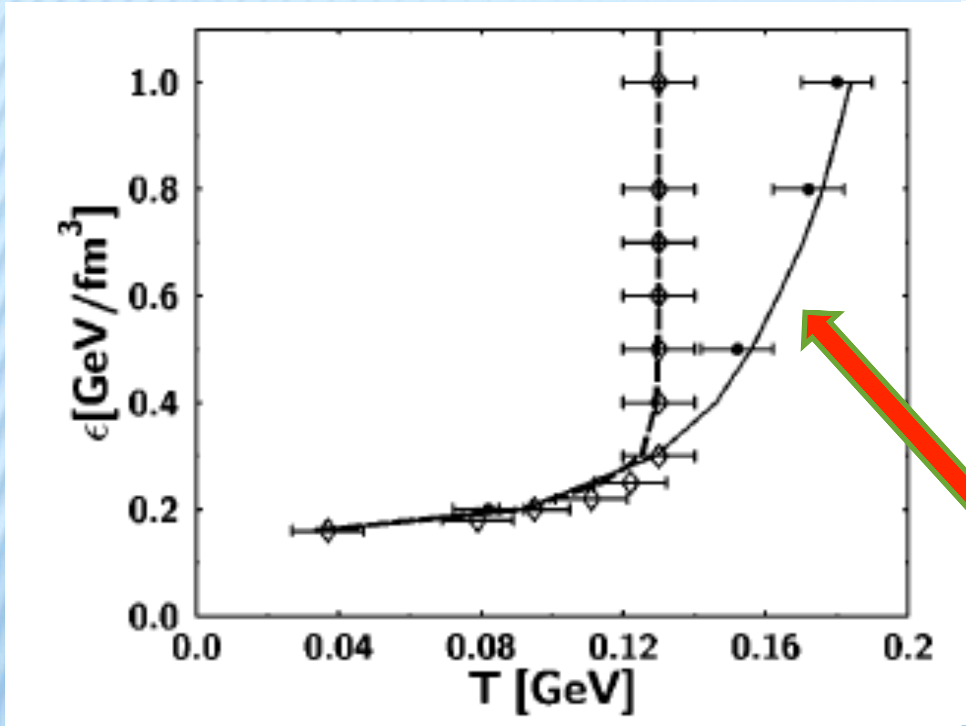

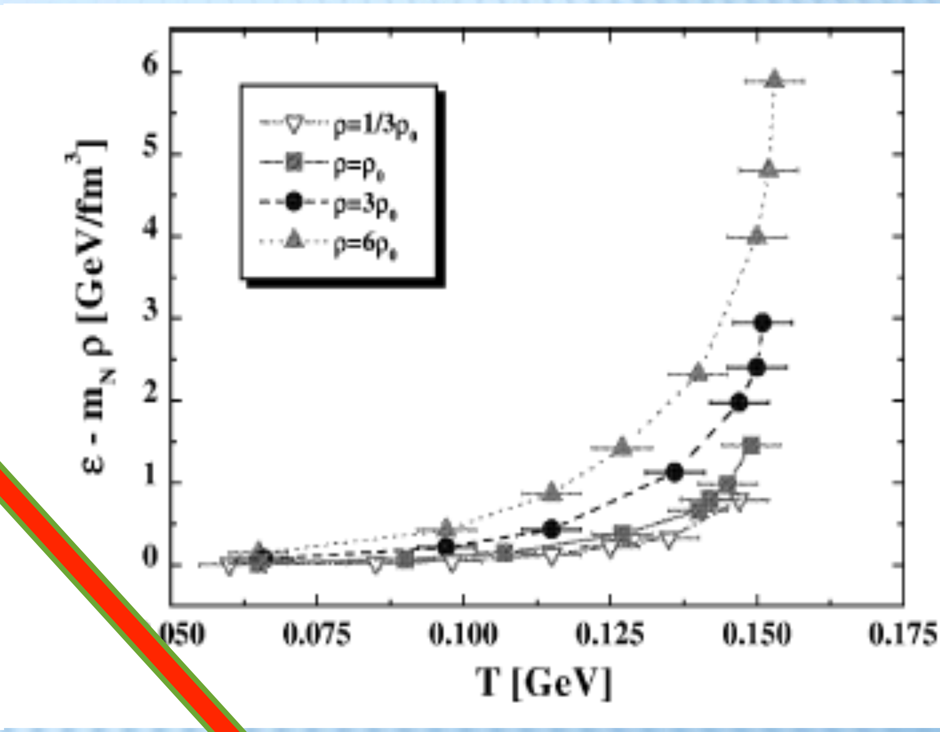

E.Bratkovskaya et al., NPA 675, 661 (2000)

UrQMD

A rapid rise of T at low ε and saturation at high energy densities. Saturation temperature depends on number of resonances in the model. W/o strings and many-N decays – no limiting T is observed.

Au+Au, E_{lab}=20A GeV, b = 0 fm, all space

	All y						$\|y\| < 1$					
	t, fm/c	$\|x\|, \|y\|$, fm	$\|z\|$, fm	T, MeV	μ_b, MeV	μ_s, MeV	t, fm/c	$\|x\|, \|y\|$, fm	$\|z\|$, fm	T, MeV	μ_b, MeV	μ_s, MeV
All	18.2	4.8	8.4	120.8	396.0	57.9	17.7	5.2	6.3	112.0	419.9	55.2
p	21.0	4.9	10.0	113.1	406.5	51.0	19.9	5.2	6.9	105.2	447.6	47.2
$\overline{p}$	20.0	6.4	9.5	110.3	390.0	51.1	18.2	7.0	6.4	110.2	406.8	52.9
Λ	26.0	5.9	11.2	93.9	481.9	34.0	25.0	6.1	8.6	90.7	488.4	48.5
$\overline{\Lambda}$	25.0	7.1	11.5	98.7	435.9	50.8	23.7	7.5	8.7	95.5	463.2	41.4
Σ	21.3	4.9	9.0	106.4	444.0	51.8	20.7	5.1	7.0	103.8	444.9	49.0
$\overline{\Sigma}$	21.1	6.2	9.4	107.1	409.4	45.5	20.1	6.6	7.3	106.0	429.6	43.1
π	16.9	4.8	7.8	121.6	394.8	66.1	16.6	5.1	6.0	115.6	397.7	55.0
K	15.1	4.0	6.3	131.8	374.8	68.0	14.8	4.2	4.9	120.6	416.2	59.6
$\overline{K}$	20.3	5.3	8.8	110.5	419.1	44.7	19.7	5.6	6.8	105.2	447.6	47.2

Table 2: Average coordinates of freezeout and T, μ_b, μ_s at this coordinates.

Au+Au, E_{lab}=30A GeV, b = 0 fm, all space

	All y						$\|y\| < 1$					
	t, fm/c	$\|x\|,\|y\|$, fm	$\|z\|$, fm	T, MeV	μ_b, MeV	μ_s, MeV	t, fm/c	$\|x\|,\|y\|$, fm	$\|z\|$, fm	T, MeV	μ_b, MeV	μ_s, MeV
All	18.6	5.0	9.7	120.1	370.0	42.9	17.6	5.3	6.8	113.2	393.4	47.9
p	22.3	5.1	12.0	115.5	355.4	35.5	20.3	5.4	7.5	108.8	404.4	52.3
$\overline{p}$	20.7	6.6	10.7	111.4	373.6	38.0	18.4	7.2	6.7	107.9	363.1	33.8
Λ	27.2	6.0	13.3	97.4	428.9	39.1	25.5	6.3	9.4	93.2	464.7	39.7
$\overline{\Lambda}$	26.1	7.3	12.9	97.9	420.0	35.7	24.1	7.8	9.1	96.9	431.4	34.6
Σ	22.3	5.1	10.7	109.4	392.4	37.1	21.2	5.3	7.7	104.0	427.5	45.3
$\overline{\Sigma}$	22.0	6.4	10.9	107.0	397.3	36.7	20.3	6.8	7.6	107.6	399.5	37.5
π	17.4	4.9	9.0	126.9	343.5	42.2	16.6	5.3	6.6	116.3	375.0	43.1
K	15.9	4.1	7.6	127.2	344.8	46.4	15.2	4.4	5.5	124.9	362.4	56.3
$\overline{K}$	20.5	5.3	9.8	114.4	380.6	50.1	19.3	5.6	7.2	112.1	393.3	49.7

Table 3: Average coordinates of freezeout and T, μ_b, μ_s at this coordinates.

Au+Au, E_{lab}=40A GeV, b = 0 fm, all space

	All y						$\|y\| < 1$					
	t, fm/c	$\|x\|,\|y\|$, fm	$\|z\|$, fm	T, MeV	μ_b, MeV	μ_s, MeV	t, fm/c	$\|x\|,\|y\|$, fm	$\|z\|$, fm	T, MeV	μ_b, MeV	μ_s, MeV
All	19.1	5.0	10.6	122.7	321.6	41.3	17.7	5.4	7.2	116.5	358.8	41.6
p	23.4	5.2	13.6	115.8	343.2	37.8	20.7	5.5	7.9	105.2	403.5	37.8
$\overline{p}$	21.5	6.7	11.5	114.9	340.4	32.7	18.8	7.2	7.0	109.0	351.8	33.6
Λ	28.3	6.2	14.9	96.2	423.3	20.2	25.9	6.5	10.0	91.0	459.3	33.3
$\overline{\Lambda}$	27.0	7.4	14.0	96.8	413.7	30.7	24.5	7.9	9.4	95.4	423.0	31.8
Σ	23.1	5.2	12.0	107.8	391.3	25.4	21.6	5.5	8.2	102.9	416.3	37.2
$\overline{\Sigma}$	22.7	6.4	11.8	107.8	380.0	28.7	20.7	6.9	7.9	103.6	402.3	42.6
π	17.8	5.0	9.8	125.6	323.4	39.1	16.7	5.4	6.9	117.5	359.8	40.5
K	16.6	4.3	8.6	126.3	332.3	42.1	15.5	4.5	5.9	120.2	371.5	52.8
$\overline{K}$	20.7	5.4	10.6	113.6	359.6	30.6	19.3	5.7	7.5	111.9	379.5	34.9

Table 4: Average coordinates of freezeout and T, μ_b, μ_s at this coordinates.

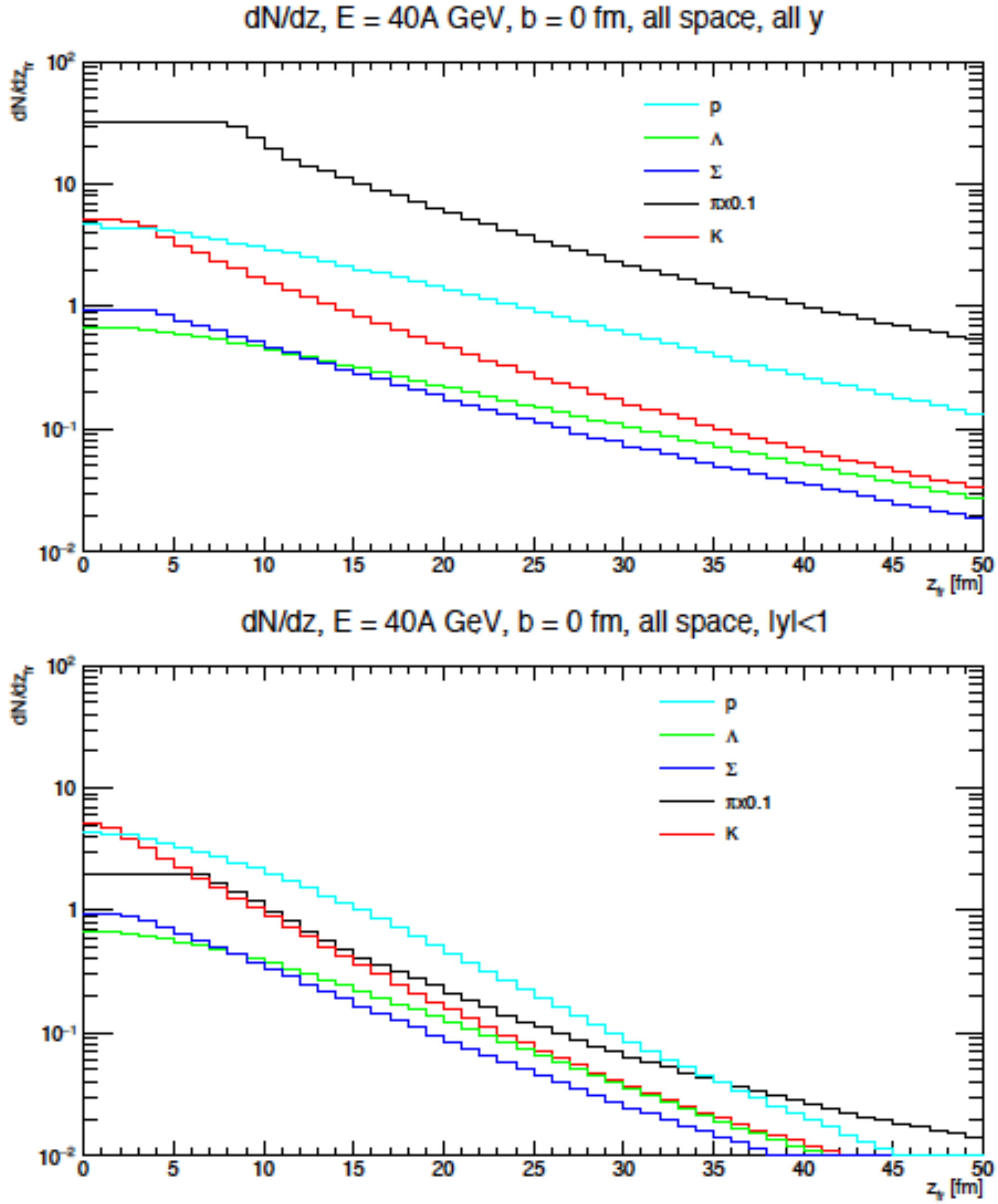

Figure 5: dN/dz for protons, lambdas, sigmas, pions and kaons for all rapidities (top figure) and for $|y| < 1$ (bottom figure). One can see that there are much more particles with large z for all rapidities, than for $|y| < 1$.

Single-particle method for extraction T-μB-μS

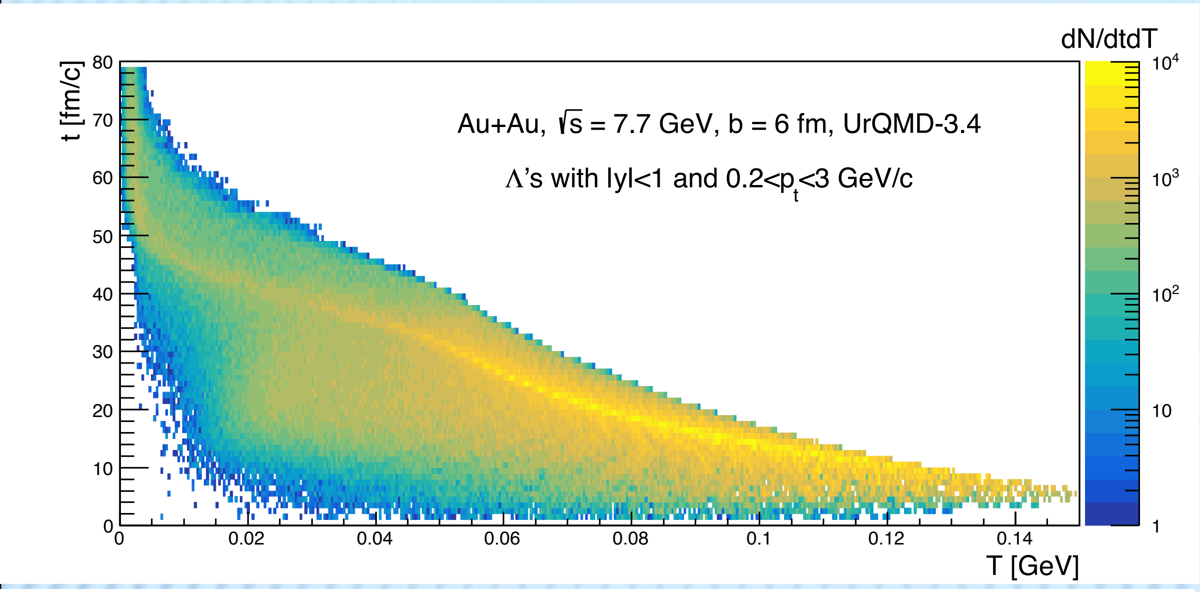

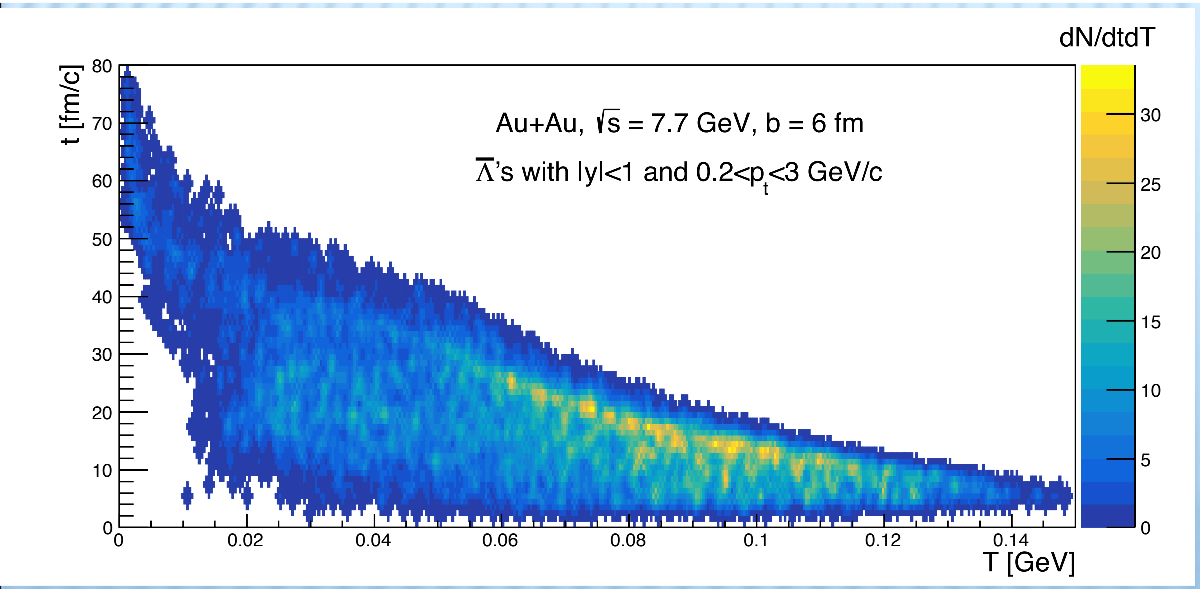

gives more precise estimation of average T-μ_B-μ_S

Thermal Approach

In local thermal equilibrium, the ensemble average of the spin vector for spin-1/2 fermions with four-momentum p at space-time point x is obtained from the statistical-hydrodynamical model as well as the Wigner function approach and reads

$$S^\mu(x,p) = -\frac{1}{8m}(1-n_F)\,\epsilon^{\mu\nu\rho\sigma} p_\nu \varpi_{\rho\sigma}(x),$$

where the thermal vorticity tensor is given by

$$\varpi_{\mu\nu} = \frac{1}{2}\left(\partial_\nu \beta_\mu - \partial_\mu \beta_\nu\right),$$

with $\beta^\mu = u^\mu/T$ being the inverse-temperature four-velocity. The number density of Λ's is very small so that we can make the approximation $1 - n_F \simeq 1$ Therefore:

$$S^\mu(x,p) = -\frac{1}{8m}\epsilon^{\mu\nu\rho\sigma} p_\nu \varpi_{\rho\sigma}(x).$$

By decomposing the thermal vorticity into the following components,

$$\boldsymbol{\varpi}_T = (\varpi_{0x}, \varpi_{0y}, \varpi_{0z}) = \frac{1}{2}\left[\nabla\left(\frac{\gamma}{T}\right) + \partial_t\left(\frac{\gamma\mathbf{v}}{T}\right)\right],$$

$$\boldsymbol{\varpi}_S = (\varpi_{yz}, \varpi_{zx}, \varpi_{xy}) = \frac{1}{2}\nabla\times\left(\frac{\gamma\mathbf{v}}{T}\right),$$

Equation can be rewritten as

$$S^0(x,p) = \frac{1}{4m}\mathbf{p}\cdot\boldsymbol{\varpi}_S, \quad \mathbf{S}(x,p) = \frac{1}{4m}\left(E_p\boldsymbol{\varpi}_S + \mathbf{p}\times\boldsymbol{\varpi}_T\right),$$

where E_p, $\mathbf{p}$, m are the Λ's energy, momentum, and mass, respectively.The spin vector of Λ in its rest frame is denoted as $S^{*\mu} = (0, \mathbf{S}^*)$ and is related to the same quantity in the c.m. frame by a Lorentz boost. Finally:

$$P = \frac{\langle \mathbf{S}^* \rangle \cdot \mathbf{J}}{|\langle \mathbf{S}^* \rangle||\mathbf{J}|},$$

[F. Becattini et al, Phys. Rev. C 95, 054902 (2017)]

UrQMD

- Represents a Monte Carlo method for the time evolution of the various phase space densities of particle species.
- Based on the covariant propagation of all hadrons on classical trajectories, stochastic binary scatterings, resonance and string formation with their subsequent decay.
- Provides the solution of the relativistic Boltzmann equation.
- The collision criterion (black disk approximation): $d < d_0 = \sqrt{\sigma_{tot}(\sqrt{s}, \text{type})/\pi}$
- 55 baryons and 32 mesons are included. All antiparticles and isospin-projected states are implemented.
- Cross sections are taken from PDG.
- Resonances are implemented in Breit–Wigner form.

[S. A. Bass et al, Prog. Part. Nucl. Phys. 41 (1998) 255-369,
M. Bleicher et al, J. Phys. G: Nucl. Part. Phys. 25 (1999) 1859-1896]

Emission of Λ and $\bar{\Lambda}$

At $\sqrt{s} = 19.6 GeV$ Λ and $\bar{\Lambda}$ are also mainly emitted from regions with small negative vorticity, but distributions are more symmetric and wide. Thus mean values of ϖ_{zx} for Λ and $\bar{\Lambda}$ drop ($\simeq -0.009$ and $\simeq -0.011$ respectively).

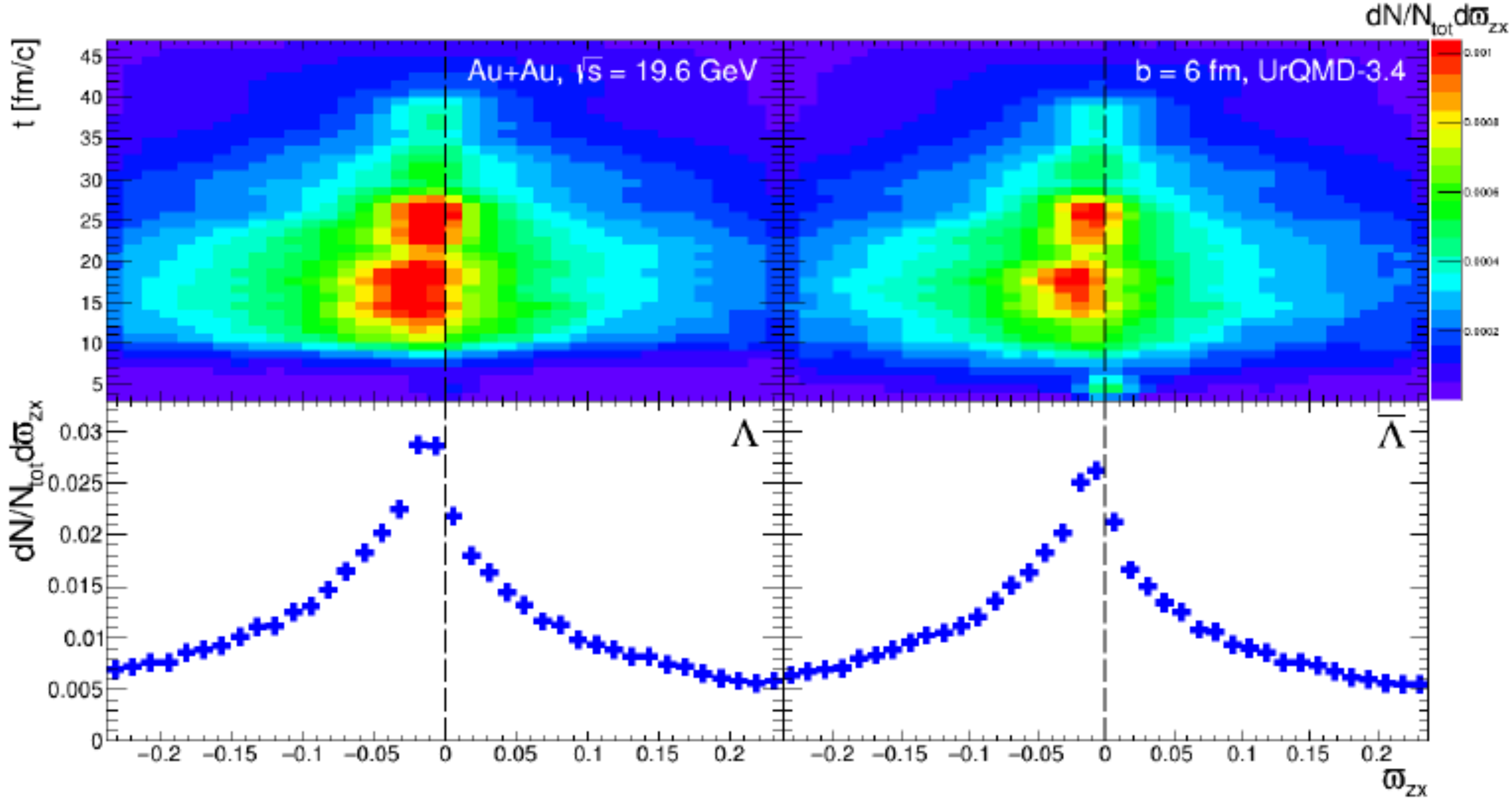

Statistical model

Input from UrQMD:

$$\varepsilon_{UrQMD} = \frac{1}{V}\sum_i E_i$$
$$\rho B_{UrQMD} = \frac{1}{V}\sum_i B_i$$
$$\rho S_{UrQMD} = \frac{1}{V}\sum_i S_i$$

Stat. Physics:

$$\varepsilon_{stat} = \sum_i \varepsilon_i(T, \mu_B, \mu_S)$$
$$\rho B_{stat} = \sum_i B_i n_i(T, \mu_B, \mu_S)$$
$$\rho S_{stat} = \sum_i S_i n_i(T, \mu_B, \mu_S)$$

$$\chi^2 = \frac{(\varepsilon_{UrQMD} - \varepsilon_{stat})^2}{\sigma_\varepsilon^2} + \frac{(\rho B_{UrQMD} - \rho B_{stat})^2}{\sigma_{\rho B}^2} + \frac{(\rho S_{UrQMD} - \rho S_{stat})^2}{\sigma_{\rho S}^2}$$

Minuit2 numerical minimizer

Output:

T, μ_B, μ_S

[L. Bravina et al, Phys. Rev. C60 (1999) 024904]